UNIVERSITY OF CALIFORNIA, SAN DIEGO

Towards a Fluid-Structure-Growth and Remodeling Framework to Simulate Vein Graft Failure Post Coronary Artery Bypass Surgery

A Dissertation submitted in partial satisfaction of the
requirements for the degree
Doctor of Philosophy

in

Engineering Sciences with a Specialization in Multi-Scale Biology

by

Abhay Bangalore Ramachandra

Committee in charge:

Professor Juan C. del Alamo, Chair
Professor Alison L. Marsden, Co-Chair
Professor Andrew M. Kahn
Professor Andrew D. McCulloch
Professor Geert W. Schmid-Schoenbein
Professor Daniel M. Tartakovsky

2017

The Dissertation of Abhay Bangalore Ramachandra is approved, and it is acceptable in quality and form for publication on microfilm and electronically:

_____

_____

_____

_____

_____

Co-Chair

_____

Chair

University of California, San Diego

2017

DEDICATION

To my parents:

Vijayalakshmi B. R. and Dr. Ramachandra B. C.

EPIGRAPH

"The human body is the temple of God."

– Upanishads

" our 'Physick' and 'Anatomy' have embraced such infinite varieties of being, have laid open such new worlds in time and space, have grappled, not unsuccessfully, with such complex problems, that the eyes of Vesalius and of Harvey might be dazzled by the sight of the tree that has grown out of their grain of mustard seed."

– Thomas Huxley

Nature seems to operate always according to an original plan, from which she departs with regret and whose traces we come across everywhere.

–D'Azyr

TABLE OF CONTENTS

Signature Page iii

Dedication iv

Epigraph v

Table of Contents vi

List of Figures viii

List of Tables x

Acknowledgements xi

Vita xiv

Abstract of the Dissertation xv

Chapter 1 Introduction 1
1.1 Anatomy and Physiology 3
1.2 Pathophysiology 4
1.3 Two-pronged approach 6
1.3.1 Quantify Mechanical Stimuli on Bypass Grafts in Patient-Specific Geometries 7
1.3.2 Continuum Mechanics Based Models of Growth and Remodeling 9

Chapter 2 Methods 12
2.1 Patient-Specific Modeling and Simulations 12
2.1.1 Simulation Methodology 15
2.1.2 Statistical Analysis 25
2.2 Growth and Remodeling Framework 25
2.2.1 Active behaviour 28
2.2.2 Mass production and degradation functions 29
2.2.3 Active Smooth Muscle 32
2.2.4 Step and gradual load 35
2.3 Optimization 38
2.3.1 The Surrogate Management Framework 38
2.3.2 Cost function 40

Chapter 3 Patient-Specific Simulations of Coronary Bypass Graft Surgeries 42
3.1 Patient Population . . . 42
3.2 Preprocessing and Simulations . . . 43
3.3 Postprocessing and Clinically Relevant Indices . . . 46
3.4 Results . . . 49
3.5 Discussion . . . 51
3.5.1 Augmenting clinical practice with non-invasive modeling tools . . . 52
3.5.2 Quantification and role of mechanical stimuli . . . 54
3.6 Limitations . . . 58
3.7 Acknowledgements . . . 61

Chapter 4 Growth and Remodeling Simulations in a Vein Graft . . . 62
4.1 Material characterization of native vein . . . 62
4.1.1 Parameter estimation and bounds . . . 67
4.2 Altered Pressure . . . 69
4.2.1 Numerical Experiment 1 . . . 70
4.3 Altered Pressure and Flow . . . 73
4.3.1 Numerical Experiment 2: Moderate load . . . 74
4.3.2 Numerical Experiment 3: Combined loads (moderate to severe) . . . 75
4.3.3 Step versus Gradual loading . . . 78
4.4 Discussion . . . 82
4.5 Limitations . . . 92
4.6 Acknowledgements . . . 95

Chapter 5 Future work . . . 97
5.1 Translational Outlook . . . 98
5.1.1 Patient-Specific Simulations . . . 98
5.1.2 Growth and Remodeling . . . 101
5.2 Frameworks are general enough for multiple clinical applications . . . 102
5.3 Coupled Fluid-Structure-Growth (FSG) models to risk stratify patients . . . 103
5.4 Acknowledgements . . . 105

Bibliography . . . 108

LIST OF FIGURES

Figure 2.1: Simulation methodology for coronary artery bypass graft (CABG) patients in SimVascular (www.simvascular.org) 16
Figure 2.2: Schema of a G&R framework illustrating the configurations of a vessel (i.e., constrained mixture) and its constituents at instant $s = 0$, without hemodynamic perturbations, and at G&R time s, with hemodynamic perturbation. 35
Figure 2.3: Illustration of (a) a step increase in pressure and (b) a gradual increase in pressure, both illustrated for $\gamma = 2$. 37
Figure 2.4: Flowchart of the Surrogate Management Framework (SMF) used for identifying the optimal parameter set for vein G&R 40

Figure 3.1: Youngs modulus (MPa) distribution in a cohort of patient-specific coronary artery bypass graft (CABG) models. 44
Figure 3.2: CABG simulation tuning pipeline 45
Figure 3.3: Representative solution fields in the patient-specific cohort. Top - time averaged wall shear stress (dyn/cm^2), bottom - displacement (cm) field near peak systole 51
Figure 3.4: Representative pressure, flow, wall shear stress, A_{athero} , and strain values during a cardiac cycle in a venous and an arterial graft from patient 2. 52
Figure 3.5: Box plot summary of normalized time averaged wall shear stress (TAWSS), oscillatory shear index (OSI), atheroprone area (A_{athero}), and wall strain in the arterial and venous grafts. 53
Figure 3.6: Frequency distribution of A_{athero} by different WSS thresholds, averaged across all venous and arterial grafts in the cohort. The averaged A_{athero} regions in arterial grafts are consistently lower than the venous values, regardless of the WSS cutoff value. 54
Figure 3.7: Summary of diameter and tortuosity of grafts in the cohort. The venous graft diameters were significantly larger than the arterial graft diameters (p = 0.005*). The differences in tortuosity were not significant (p = ns). 55

Figure 4.1: Biaxial stress - stretch data (dashed lines) for a mouse vena cava and the associated best-fits achieved in the parameter estimation : (a) $\sigma_\theta - \lambda_\theta$, (b) $\sigma_z - \lambda_\theta$. 66
Figure 4.2: Framework demonstrating a general approach for parameter estimation and simulating adaptation in a blood vessel. Parameter estimation is accomplished in several serial steps and optimization is used to accelerate the process. 68
Figure 4.3: Summary of (a) radius and (b) thickness evolution with time for K_1^k & $K_2^k \leq 20$ and $G_h^m \leq 1.8$. The radius curves are within a 10% deviation. The arrows indicate the thickness for an ideal adaptation. 71

Figure 4.4: Evolution of radius and thickness for a moderate perturbation in load, $\gamma = 1.5$ (fold pressure increase) and $\epsilon = 1.1$ (fold flow increase). 75
Figure 4.5: Failed points in $\gamma - \epsilon$ load space, where γ is the fold increase in pressure above homeostatic and ϵ is fold increase in flow. 'X'- indicates a failed simulation and '.' indicates a simulation that successfully converged. 76
Figure 4.6: Changes in adaptive capacity with different values of smooth muscle tone - $K^{act} = 1/20day^{-1}$ (control, left panel) and $K^{act} = 1/3day^{-1}$ (right panel). 77
Figure 4.7: Interpolated surface plot of cost function as a function of $\gamma - \epsilon$ loads, with a modified vasomotor evolution rate of $K^{act} = 1/3day^{-1}$. 78
Figure 4.8: Failed simulations in the $\gamma - \epsilon$ load space for four scenarios of loading- a) step pressure and flow (control), b) step pressure and gradual flow, c) gradual pressure and step flow, and d) gradual pressure and gradual flow. 80
Figure 4.9: Failed simulations in the $\gamma - \epsilon$ load space for four scenarios of loading- a) step pressure and flow (control), b) step pressure and gradual flow, c) gradual pressure and step flow, and d) gradual pressure and gradual flow. 81
Figure 4.10: Predicted evolution of radius and thickness for an optimized set of parameters from a geometric cost function based optimization for a modest hemodynamic perturbation ($\gamma = 1, \epsilon = 1.1$) - notice the non-physiological immediate increase in thickness. 89

Figure 5.1: Patient-specific model from CT scan of a patient who had undergone CABG surgery with venous grafts in Y configuration (left); Sequential (middle) and 2 single graft (right) - virtual modifications of the graft geometry. 100
Figure 5.2: Illustrative result showing the TAWSS distribution in the original geometry (left) and the modified geometries (middle and right). . 100
Figure 5.3: FSI simulations and models coupled with models of Growth and Remodeling can inform risk stratification guidelines in CABG models. 106

LIST OF TABLES

Table 3.1: Summary of patients used in study with non-invasive clinical measurements and details of grafts. 43
Table 3.2: Summary of non-invasive clinical measurements, population averaged targets from literature and respective quantities from simulations. 49

Table 4.1: Material coefficients estimated from the biaxial test, using the SMF algorithm 65
Table 4.2: Parameters for G&R optimization and their prescribed bounds . . 69
Table 4.3: Parameters used in G&R simulations. 73

ACKNOWLEDGEMENTS

I want to thank my advisor Prof. Alison Marsden for her guidance and support through the course of my PhD. I also want to thank her for giving me a problem that kept me captivated through the course of my PhD and a lab / peer group that was a pleasure to work with.

I had the opportunity to collaborate with Prof. Andrew Kahn, School of Medicine, UC San Diego and Prof. Jay Humphrey, Department of Biomedical Engineering, Yale University for my work. They have been amazing mentors and I have benefitted tremendously from their expertise in their respective fields.

I want to thank my committee members Prof. Juan Carlos del Alamo, Prof. Andrew McCulloch, Prof. Geert Schmid-Schoenbein and Prof. Daniel Tartakovsky for their inputs during the course of my PhD. I was also fortunate to have them all as course instructors and have learnt from them, in several different forms, inside and outside the classroom. I want to acknowledge the insights from a variety of computational classes from Prof. Yuri Bazilevs in Structural Engineering. Special thanks to Prof. del Alamo for being my primary advisor at UCSD during my final 18 months of PhD and Prof. Padmini Rangamani for her administrative help.

I am not sure a work this interdisciplinary in nature would've been possible without the good ecosystem at UCSD and Stanford. Programs such as Interfaces at UCSD helped me get a good footing in disciplines that were alien to me. I had the pleasure of working with a talented peer group which included Weiguang Yang, Sethuraman Sankaran, Dibyendu Sengupta, Jessica Oakes, Christopher Long, Mahdi E. Moghadam, Matt Bockmann, Ethan Kung, Shahrouz Alimo, Daniele Schiavazzi, Justin Tran, Noelia Grande-Gutierrez, Aekaansh Verma, Hongzhi Lan, Vijay Vedula, Jessica Shang, Gabriel Maher, Casey Fleeter, Nicole Schiavone, Chris Jensen, Ju Liu, Christopher Chu, Melody Dong and Richard Hsiao. Special thanks to Sethuraman

Sankaran for being a mentor, a very patient one, during my initial years of PhD.

Simvascular open source software was a critical component of my thesis and I want to thank the Simvascular 2.0 team - Hongzhi Lan, Adam Updegrove, Daniele Schiavazzi, Nathan Wilson, Prof. Shawn Shadden, and Prof. Alison Marsden for keeping the software functional through a turbulent reorganization process.

This work was supported by an MAE Department Fellowship to Abhay B. Ramachandra, an NIH grant (NIH R01-RHL123689A), NSF CAREER Award OCI-1150184, and a Burroughs Wellcome Fund Career Award at the Scientific Interface to Alison L. Marsden. Computational resources were provided by a grant to Alison Marsden (TG-CTS130034) through the Extreme Science and Engineering Discovery Environment (XSEDE). This dissertation has resulted in the following papers that have been published, submitted or is being prepared for publication.

Chapter 3, in full, is a reprint of the material as it appears in "Patient-Specific Simulations Reveal Significant Differences in Mechanical Stimuli in Venous and Arterial Coronary Grafts", *Journal of Cardiovascular Translational Research*, 9:279290, 2016. Authors are Ramachandra, A. B., Kahn, A., & Marsden, A. L.. The dissertation author was the primary investigator and author of this paper.

Chapter 4, in part, is a reprint of the material as it appears in " Computational simulation of the adaptive capacity of vein grafts in response to increased pressure", *Journal of Biomechanical Engineering*, 137(3), 2015. Authors are Ramachandra, A. B., Sankaran, S., Humphrey, J. D., & Marsden, A. L. The dissertation author was the primary investigator and author of this paper.

Chapter 4, in part, has been submitted for publication of the material as it may appear in " Gradual loading ameliorates maladaptation in computational simulations of vein graft growth and remodeling", *submitted* and is under review. Authors are Ramachandra, A. B., Humphrey, J. D., & Marsden, A. L. The dissertation author

was the primary investigator and author of this paper.

Chapter 5, in part is currently being prepared for submission for publication of the material. Authors are Ramachandra, A. B., Jensen, C. W., Chu, C., Boyd, J., Kahn, A. M. & Marsden, A. L. The dissertation author was the primary investigator and author of this paper.

The Center for Biomechanics corridor at UCSD and the Biodesign corridor at Stanford were fun and made my graduate school enjoyable. Indian student association activities and UCSD Recreation classes provided a positive distraction from work. I will single out Siddhartha Nath, and my house mates Viraj Deshpande, Amol Patwardhan and Sieuwerd Gaastra, from my list of friends at UCSD, for making this journey pleasant.

Finally, I want to thank my grandparents (K. V. Savithri and D. S. Nagaraj, and B. C. Lalithamma and Dr. B. R. Chandrashekar), my immediate and extended family for their support in various forms through the course of my education. My parents, Vijayalakshmi and Dr. Ramachandra, and my brother, Sujay, have provided unconditional support and encouragement for my education. This journey would've probably not happened without them.

VITA

2004-2008	B. Tech. in Mechanical Engineering, National Institute of Technology Karnataka, Surathkal, India
2009-2011	M. S. in Mechanical Engineering, Carnegie Mellon, Pittsburgh, PA
2011-2017	Ph. D. in Engineering Sciences with a Specialization in Multi-Scale Biology, University of California, San Diego, CA

PUBLICATIONS

Ramachandra, A. B., Sankaran, S., Humphrey, J. D., & Marsden, A. L., " Computational simulation of the adaptive capacity of vein grafts in response to increased pressure", *Journal of Biomechanical Engineering*, 137(3), 2015

Ramachandra, A. B., Kahn, A., & Marsden, A. L., " Patient-Specific Simulations Reveal Significant Differences in Mechanical Stimuli in Venous and Arterial Coronary Grafts", *Journal of Cardiovascular Translational Research*, 9:279290, 2016

Tran, J. S., Schiavazzi, D., Ramachandra, A. B., Kahn, A. M. & Marsden, A. L., "Automated tuning for parameter identification and uncertainty quantification in multi-scale coronary simulations.", *Computers & Fluids*(2016).

Ramachandra, A. B., Humphrey, J. D., & Marsden, A. L., " Gradual loading ameliorates maladaptation in computational simulations of vein graft growth and remodeling", *submitted*

Ramachandra, A. B., Jensen, C. W., Chu, C., Boyd, J., Kahn, A. M. & Marsden, A. L., "Virtual evaluation of surgical revascularization techniques in coronary artery bypass surgery, *in preparation*

ABSTRACT OF THE DISSERTATION

Towards a Fluid-Structure-Growth and Remodeling Framework to Simulate Vein Graft Failure Post Coronary Artery Bypass Surgery

by

Abhay Bangalore Ramachandra

Doctor of Philosophy in Engineering Sciences with a Specialization in Multi-Scale Biology

University of California, San Diego, 2017

Professor Juan C. del Alamo, Chair
Professor Alison L. Marsden, Co-Chair

Vein graft maladaptation, leading to poor long-term patency, is a serious clinical problem in patients receiving coronary artery bypass grafts (CABGs). Mechanics is known to play a key role as a stimulus contributing towards vein graft failure. Mechanical stimuli are key to understanding disease progression and clinically observed differences in failure rates between arterial and venous grafts following coronary artery bypass graft surgery. But little has been done to quantify the mechanics in these grafts and its effects on long-term outcomes on grafts. Hence, one of the goals of this the-

sis was to quantify mechanical stimuli acting on the grafts and the other goal was to develop continuum mechanics based models of growth and remodeling (G&R) to simulate long-term adaptation.

We quantify biologically relevant mechanical stimuli, not available from standard imaging, in patient-specific simulations incorporating non-invasive clinical data. We couple computational fluid dynamics with closed-loop circulatory physiology models to quantify biologically relevant indices, including wall shear, oscillatory shear, and wall strain. We account for vessel-specific material properties in simulating vessel wall deformation. Wall shear was significantly lower and atheroprone area significantly higher in venous compared to arterial grafts. Wall strain in venous grafts was significantly lower than in arterial grafts while no significant difference was observed in oscillatory shear index. Simulations demonstrate significant differences in mechanical stimuli acting on venous vs. arterial grafts, in line with clinically observed graft failure rates, offering a promising avenue for stratifying patients at risk for graft failure.

We also propose a computational model of venous adaptation to altered hemodynamics based on a constrained mixture theory of G&R. We identify constitutive parameters that optimally match biaxial data from a mouse vena cava, then numerically subject the vein to altered hemodynamic conditions and quantify the extent of adaptation. We identify constitutive relations and parameters that enable adaptations for a moderate perturbation in hemodynamics. We then fix these relations and parameters, and subject the vein to a range of combined loads (pressure and flow), from moderate to severe, and identify plausible mechanisms of adaptation versus maladaptation. We also explore the beneficial effects of a gradual increase in load on adaptation.

Chapter 1

Introduction

Coronaries are blood vessels that supply oxygen rich blood to the walls of the heart. As people age, these arteries get diseased, often in the form of plaque build up on the vessel walls, developing into acquired coronary artery disease (CAD). The plaque is the result of a complex interaction between cells in the vessel wall, blood, and the exchange of molecular messages between them. Previously considered a cholesterol storage disease, in the light of recent research, CAD is now being viewed as an inflammatory disorder leading to atherosclerosis.[1] The plaque can rupture and block blood flow through the coronary arteries causing a heart attack (myocardial infarction), or the plaque can harden and narrow, obstructing blood perfusion to myocardium, leading to ischemia.

Myriad treatments exist for CAD including lifestyle changes such as diet and exercise, medication, percutaneous coronary intervention (PCI), and coronary artery bypass graft surgery (CABG). Severe versions of the disease are treated with either

PCI or CABG. The choice between CABG and PCI comes with numerous trade offs, weighing the advantages of a less invasive procedure against risks of restenosis, and potential differences in long-term outcomes. PCI has been increasing over the past decade and has clear advantages for focal stenosis, and high-risk patients who are not surgical candidates. CABG will remain necessary due to inability of PCI to treat diffuse and multi-vessel CAD. Most patients with CAD need multivessel revascularization and clinical trials have consistently shown that post-CABG outcomes are as good as or often better than those with percutaneous intervention (PCI).[2,3] CABG is known to have superior long-term reduction in mortality and myocardial infarctions, and reductions in repeat revascularizations, compared to PCI, in patients with multivessel disease. To date, CABG is established as the most effective treatment for symptomatic multivessel disease.[4]

Approximately 400,000 patients undergo CABG surgeries in the United States alone to relieve angina, reperfuse ischemic myocardium and to relieve or perfuse left ventricle dysfunction. Flow to the ischemic region in the myocardium is restored by bypassing the stenosed or occluded region with a graft. Classic bypass grafts typically employ an end-to-side anastomosis at the proximal end, to the aorta, and an end-to-side anastomosis at the distal end, to a native coronary artery, distal to a stenosis or an occlusion. Arterial, venous and synthetic grafts, in the order of preference, are the grafts of choice for a CABG. While arterial grafts offer superior patency rates, they are limited in availability. Hence, more than 70% of CABG surgeries use autologous venous grafts. Despite advances in surgical techniques and

post-surgical management, only 60% of vein grafts remain patent and 50% remain free of significant stenosis after 10 years, and event-free survival is as low as 40% after 12 years.[5] Late stenosis and vein graft occlusion, which account for the majority of adverse events, are primarily due to recurrent atherosclerosis.[5] Vein graft occlusion is associated with worse long-term outcomes,[6] and once grafts become completely occluded, they typically are not amenable to percutaneous intervention. In addition, repeat revascularization with percutaneous and surgical methods is associated with increased morbidity and mortality.[7] Thus, vein graft failure continues to pose a significant clinical challenge and economic healthcare burden.

1.1 Anatomy and Physiology

Arteries and veins serve very different functions; the former are high pressure, high flow conduits whereas, the latter are low pressure, low flow conduits with high capacitance. Compared to an artery a vein has a larger, thinner, less firmly anchored subendothelium, more permeable intima, poorly defined internal elastic membrane, thinner media, absent elastic lamella, fewer smooth muscle in media-widely separated by collagen, and valves. Physiologically, a vein is relatively inelastic at arterial pressures, has lower lipolysis capacity, has more active synthesis and rapid uptake of lipids, lower production of prostacyclin, is more sensitive to vasoconstrictors and less sensitive to vasodilators, compared to an artery. It is not surprising, therefore, that arteries and veins have very different structure and properties.[8,9] Indeed,

there should be little expectation that a vein should behave like an artery when transplanted to an arterial environment. With a bias against vasodilation, lower production of anti-thrombotic/vasodilatory prostacyclin, an inclination to more rapidly uptake and synthesize lipids, the vein seems to have an inherent physiological bias towards atherosclerosis in an arterial environment.

1.2 Pathophysiology

Vein graft failure is defined as complete occlusion, stenosis of 70% or more, or extensive conduit narrowing on coronary angiography. Vein graft failure can lead to recurrence of angina or myocardial infarction and significant morbidity and mortality. The mechanisms of long-term failure differ between arterial and venous grafts following CABG surgery. Arterial graft failure results primarily from fibroinitimal hyperplasia at the site of anastomosis.[10] Vein graft failure can be predominantly classified into the following categories - thrombosis during the acute period (<1 month), intimal hyperplasia during the first few months, wall thickening during the intermediate period (1 to 12 months), and atherosclerosis in the long-term (3-5 years). An interested reader is referred to Cox et al. for an excellent review on pathogenesis of the saphenous vein graft.[8] A few pertinent aspects are discussed in the following paragraphs.

Multiple factors contribute to the underlying pathophysiology of vein graft failure, and it is best understood by looking at the causal factors in a chronological

order. Surgical harvesting leads to a loss of vaso vasorum and hence an increase in oxidative stress. Presurgical treatment (such as overdistension prior to implantation) and tissue handling could cause vascular injury, including cell damage and endothelial dysfunction. Suturing, during implantation, could further damage the vessel walls. Post implantation, although the denuded endothelial layers are covered by migrating endothelial cells in the first four weeks, endothelial functionality may be delayed for up to 6 months post surgery.[11] Dysfunctional or damaged endothelial linings promote procoagulant activity and, coupled with inflammation (due to above mentioned insults), could trigger a coagulation cascade, leading to short-term failure due to thrombosis, which accounts for $\approx 10\%$ of failures in vein grafts. The release of surgical clamps at the time of graft implantation suddenly subjects the veins to arterial pressures and flows. The severe change in flow and pressure alters the stress state (predominantly circumferential and shear, plausibly axial too) in the vessel triggering a remodeling response. The first 4 weeks of adaptation are characterized by a proliferation of cells in the intima, and virtually all grafts show intimal hyperplasia (IH) in the first four weeks.[8,12,13]

Cell proliferation in vein grafts is in response to an increase in hemodynamic load, possibly due to release of growth factors and a phenotype switch in a few wall constituents (e.g. smooth muscle).[14] Cell proliferation is also accompanied by cell migration into the intima and signs of atherosclerosis are seen as early as 6 months in a few vein grafts. It is hypothesized that IH is a major cause of graft alteration in the intermediate period and could create conditions conducive to long term atherosclerosis.

The intermediate period of remodeling is characterized by proliferation in the intima and scarring of media, with smooth muscle replaced by collagen bundles. In the later period, 1-5 years post implantation, there is a decrease in intimal proliferation and an increase in medial hypertrophy.

The predisposing factors and process of atheroma formation in vein graft failure are similar to native vessels. Monocytes penetrate the intimal wall, become macrophages, form foam cells and lay a foundation for the formation of atherosclerotic plaque. Subsequently, there is an increase in adhesion of leukocytes and platelets and increased expression of adhesion molecules, ultimately leading to atherosclerosis.[12] Atherosclerotic plaque and its rupture are the primary mechanisms of occlusion / stenosis in vein grafts. There is substantial evidence relating hemodynamic loads to vein graft remodeling.[15–18] Understanding the kinetics of these (mal)adaptative processes could be facilitated by a computational model that relates macroscopic hemodynamic quantities and structural adaptations to underlying cellular mechanisms, thus providing a mechanobiological understanding of vein adaptation versus maladaptation or failure.[8,12,13]

1.3 Two-pronged approach

Over the past few decades a lot has been done to understand and address the issue of vein graft failure, but much remains to be done.[12] Mechanical stimuli are known to contribute to vein graft failure, and comprehending their role is key to

understanding disease progression and clinically observed differences between arterial and venous grafts following CABG. We take a two-pronged approach to understand vein graft failure from a mechanobiological perspective - first, using computational fluid dynamics coupled with closed loop models of circulation, we quantify biologically relevant mechanical stimuli, not available from standard imaging, in patient-specific simulations incorporating non-invasive clinical data. Second, to understand how mechanics affects vein graft (mal)adaptation we extend an existing continuum mechanics-based constrained mixture model of arterial growth and remodeling (G&R) to a vein and identify plausible mechanisms of adaptation versus maladaptation.

1.3.1 Quantify Mechanical Stimuli on Bypass Grafts in Patient-Specific Geometries

Hemodynamics and wall biomechanics, influencing the behavior of the endothelial lining and regulation, as well as turnover and degradation of wall constituents such as fibroblasts and smooth muscle, play a key role as mechanobiological stimuli contributing to vein graft failure and disease progression.[19,20] However, biologically relevant indices, including wall shear stress (WSS), oscillatory shear index (OSI) and wall strain, are not currently attainable via standard clinical measurement modalities. In addition, the prediction of post-surgical disease progression using vascular growth and remodeling (G&R) methods[21,22] will require these mechanical stimuli as inputs. Without these data it will likely be impossible to make patient-specific simulation-based predictions of risk of graft failure to risk stratify patients. Non-

invasive quantification of mechanical stimuli is therefore a crucial first step towards improved understanding of the differential success rates of arterial vs. venous grafts. Image-based patient-specific computational fluid dynamic (CFD) simulations now offer a non-invasive means to quantify temporally and spatially resolved hemodynamics and wall mechanics quantities of clinical relevance. We present a novel closed-loop multiscale CABG simulation framework that can predict local hemodynamics and wall mechanics using non-invasive clinical data. This framework includes fluid structure interaction with appropriate arterial and graft material properties. The major objective of this work is to apply this framework to simulate graft hemodynamics and wall mechanics in patient-specific CABG geometries, and characterize differences in indices of mechanical stimuli between arterial and venous grafts. We hypothesized that patient-specific simulations would reveal significant differences in key mechanical stimuli that may predispose vein grafts to increased atherosclerosis progression. Specifically, motivated by clinical observations that venous grafts fail more often than arterial grafts, and that low shear and high oscillatory flow are correlated with atheroprone regions, we hypothesized that shear would be lower in venous grafts while atheroprone area would be larger than in arterial grafts. We also hypothesized that wall strain in venous and arterial grafts would be significantly different.

1.3.2 Continuum Mechanics Based Models of Growth and Remodeling

Our growing understanding of molecular-level and tissue-level changes in the vessel needs to be placed within the context of a macroscopic changes in radius, thickness and stiffness. A constrained mixture theory of growth and remodeling (G&R) that models cell-mediated responses of arteries to altered chemo-mechanical stimuli has provided insights into normal responses to injury, adaptation, and disease progression.[23–26] This theory incorporates cellular information phenomenologically within fundamental constitutive relations in a continuum context. Motivated by the robust performance of arterial G&R models, the current work extends this approach to vein grafts. Although previous arterial applications of the G&R framework have been restricted to moderate changes in blood pressure and flow, application to vein grafts necessitates extension to far larger changes in hemodynamic loads than previously investigated. Hence, in extending previous arterial models to vein grafts, one must identify and evaluate a new set of G&R model parameters, not just parameters for native wall properties, and plausibly new constitutive laws. Since it is intractable to find these parameter sets by brute force, we propose a novel use of optimization to formulate a parameter identification problem in the context of G&R. This is in contrast to common uses of optimization in the context of empirical curve fitting to experimental data. The proposed optimization framework accelerates the problem sufficiently to render it computationally tractable.

As a first step in the development of a G&R model for vein grafts, this work focuses on the response of a vein to increased pressure and the associated intermediate period of wall thickening (1 to 12 months). This approach is motivated by prior studies that show medial thickening to associate best with increased intramural circumferential stress or strain.[27] There is also evidence that circumferential stress plays a primary role and wall shear stress a secondary role in determining overall vein graft dimensions,[17] though shear stress likely controls neointimal formation.[28] Adaptation to a sustained change in hemodynamic loading is known to be biphasic, with acute changes countered by an adjustment of vascular tone followed by a chronic remodeling process spanning weeks to months.[29] We hypothesize that acute changes influence the long-term adaptive capacity of venous grafts. To evaluate this hypothesis, we then extend venous G&R theory to model the adaptive response to both altered pressure and flow.

Toward this end, we first identify constitutive parameters for a normal mouse vena cava based on published experimental data from pressure-diameter and axial force-length tests.[30] We then identify through optimization the set of G&R parameters that comes closest to achieving homeostatic conditions, given slight perturbations from normal hemodynamic loading, using difference from homeostatic values of stress as an objective function. Using these parameters, we numerically subject the vein to increasingly higher hemodynamic loads and assess the extent of its adaptation, within a biologically reasonable set of bounds for G&R parameters. We then explore possible physiological constraints that lead to maladaptation by numerically quantifying

adaptations under different loads. Finally, we test the hypothesis that a gradual, rather than a step, change in load will lessen such maladaptations. We submit that the proposed computational model forms a basis for guiding mechanobiological experiments and can help provide new insights into the causes, effects, and mechanisms of vein graft G&R, and thereby may be used to guide mechanobiological studies or the design of new clinical methods.

Chapter 2

Methods

2.1 Patient-Specific Modeling and Simulations

Hemodynamics and mechanics play a critical role in the functioning of the cardiovascular system and influence biology across multiple temporal and spatial scales. Thus, quantifying mechanical stimuli in an in vivo setting is an essential step in understanding their role in vascular health and disease. Modeling hemodynamics in isolation is insufficient as it fails to capture the subtle relationship between local geometry and global hemodynamics. Hence there is a pressing need for models of circulation that can capture the interplay between mechanics and biology across multiple scales of space and time. Amongst existing approaches patient-specific modeling has held promise as a tool to non-invasively quantify these stimuli at an organ scale and lend themselves naturally to coupling with other physiological models at tissue or cellular scales, thus providing the much required multi-scale approach to un-

derstanding vascular systems. Advances in imaging methods, which provide detailed anatomy, and computing has made patient-specific simulations a tractable problem.[31] While good resolution of images and computing power are necessary ingredients for patient-specific simulations, challenges associated with model construction, boundary conditions, material properties, accurate solutions of non-linear equations in finite time, numerical coupling issues, and lack of good physiological models have impeded the translation of these technologies into the clinic as predictive tools or as apparatus to quantify mechanical stimuli in a non-invasive setting. One of the overarching goals of this thesis is to address some of these issues within the context of a CABG patient-specific simulation.

Recent advances in multiscale modeling[31–37] now permit physiologically realistic simulations in patient-specific coronary geometries avoiding prior limitations of idealized geometries, rigid walls, non-physiologic boundary conditions etc. Some of the earlier efforts in patient-specific coronary modeling have constructed models of the epicardial coronaries from medical images and have coupled them with lumped parameter networks (LPN), to unveil relationships between local flow and global hemodynamics. Kim et al.[35] analytically coupled LPN models of the heart, systemic circulation and coronary circulation with a patient-specific model of the coronaries. Sengupta et al.[38,39] numerically coupled the lumped parameter network (LPN) to the 3D domain, in an open-loop setting, to simulate hemodynamics in patients with Kawasaki disease. Building on an implicit modular numerical 0D-3D coupling scheme,[34] Sankaran et al.[37] proposed a numerically coupled closed-loop framework for

patient-specific rigid wall CABG simulations. The closed-loop formulation proposed by Sankaran et al. not only mimics the human circulation but, due to numerical coupling, naturally lends itself to tuning the boundary conditions to match invasive and non-invasive measurements from the clinic. Rigid wall simulations do not provide accurate pressure fields and cannot predict strains, hence there is a need for deformable wall simulations. While wall deformation has been examined extensively in simulations of cerebral and abdominal aortic aneurysms, there has been little work in patient-specific coronary artery simulations with fluid-structure interaction (FSI),[35] and none using models with appropriate wall properties for different graft types. One cannot perform accurate FSI predictions without appropriate material properties, and this will constitute the first time these tools have been combined in a unified framework.

We present a novel closed-loop multiscale CABG simulation framework that can accurately predict local hemodynamics and wall mechanics using only non-invasive clinical data. We design a state-of-the-art framework for multiscale patient-specific CABG simulations that includes fluid-solid interaction with appropriate graft material properties. And finally we use this framework to simulate five patient-specific CABG geometries and quantify clinically relevant hemodynamic and wall mechanic properties in the grafts.[40]

2.1.1 Simulation Methodology

The simulation methodology for each patient in the study, following prior patient-specific modeling approaches,[41] consists of the following:

(a) Construction of patient-specific models from CT images, including the aorta with branch vessels, coronary arteries, and grafts.

(b) Formulation of mathematical models to mimic physiology, and tuning to determine model parameters that match clinical and literature data.

(c) Solution of the governing equations of blood and vessel wall biomechanics and their interaction, to obtain primary time and spatially resolved flow and deformation fields in the 3D domain.

(d) Post-processing to compute biologically relevant indices from the primary variables, including WSS, OSI, and wall strain.

Each of these steps is illustrated in Figure 2.1 and is explained in detail in the paragraphs below.

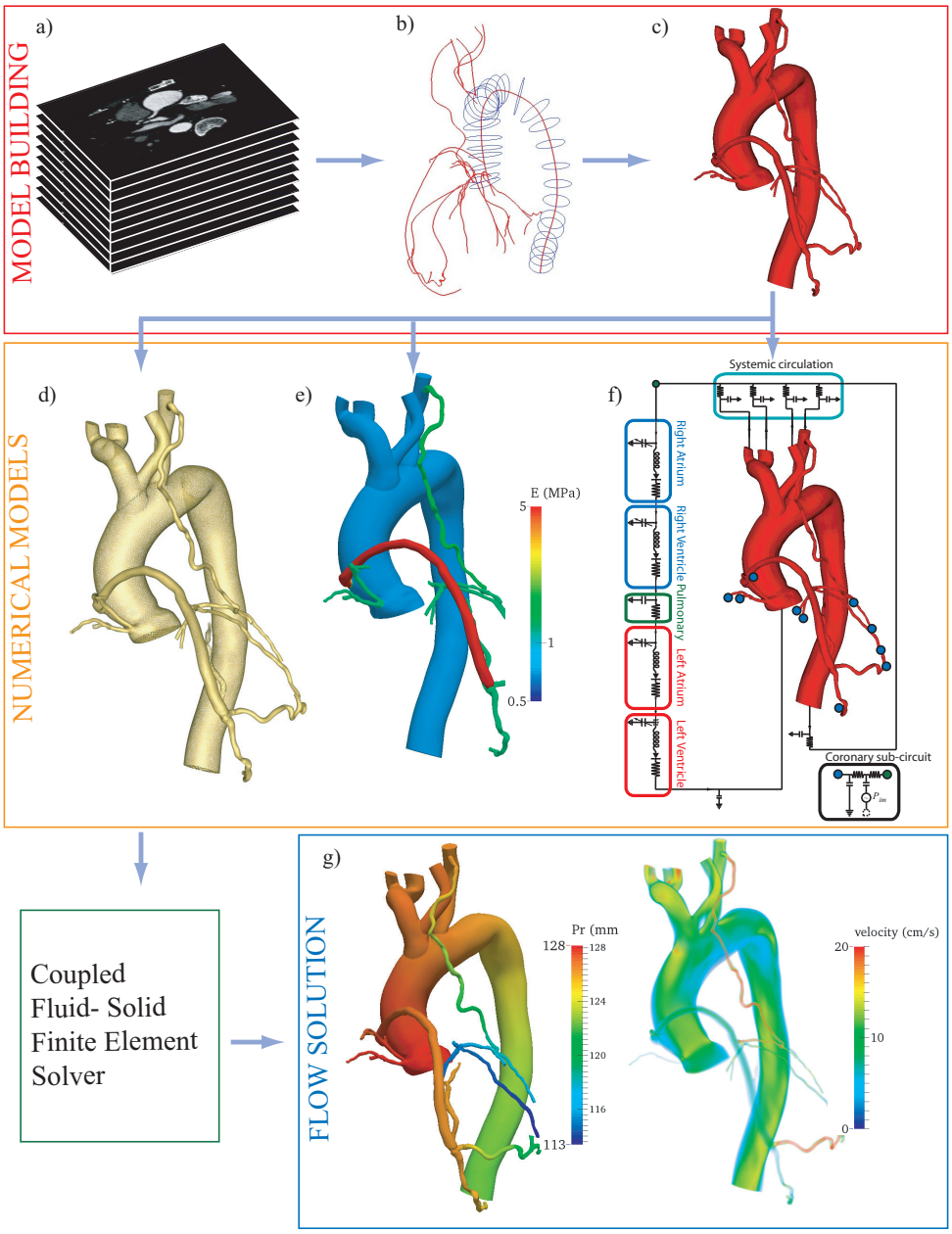

Figure 2.1: Simulation methodology for coronary artery bypass graft (CABG) patients in SimVascular (www.simvascular.org). Major steps in the pipeline are (a) acquire CT image of a CABG patient, (b) create centerline paths and segment the lumen, (c) loft the segmentations to form a 3D model, (d) discretize the 3D model into a finite element mesh, (e) assign material properties, (f) tune lumped parameter network to match clinical and literature targets, (g) solve governing equations on patient-specific models. Analyze and post-process results to determine clinically relevant quantities

Model Construction

The 3D patient-specific anatomic CABG models were segmented from CT axial images using the open source SimVascular software (www.simvascular.org).[42] Models included the coronary arteries, aorta, aortic arch branch vessels, and bypass grafts. Paths were constructed along the vessel centerlines to the limits of CT resolution. Vessel lumens were then segmented on 2D slices perpendicular to the paths. The segmentations were lofted together to produce a patient-specific 3D model (Figure 2.1 – top row).

Numerical Preprocessing

3D patient-specific models require a series of preprocessing steps to render them suitable for simulation. Steps involved in preprocessing are:

(a) discretization (meshing) of the 3D model

(b) assignment of material properties to vessel walls

(c) determination of boundary conditions to mimic the circulatory and coronary physiology.

Meshing

All models were discretized into linear tetrahedral finite elements to make them suitable for finite element simulation using the commercial package MeshSim (Simmetrix Inc., Clifton Park, NY). Mesh independence was guaranteed by successive

mesh adaptation,[43] resulting in meshes of approximately 4 million elements for each model.

Variable Wall Properties

Fluid-structure interaction studies require vessel wall thickness and material properties as inputs, which are usually unattainable by non-invasive CT imaging. While some recent studies have obtained thickness values from intravascular ultrasound (IVUS) or optical coherence tomography (OCT), we chose to restrict this study to data commonly available from standard of care non-invasive clinical measurements.

Clearly the material properties and thickness of the vessel vary across the vasculature,[44–46] and it is the structural stiffness (combined effect of material properties and thickness) that affect deformation of the vessel. It is experimentally impractical to measure material properties at every point in the continuum or at every node on the mesh. Centerline-surface based methods[47] and Laplace equation based methods[48] have been used in the past to assign variable wall properties. Previous work on variable wall properties has been on Fontan,[48] thoracic and cerebral aneurysm,[47] a full body normal circulation[49] but none on a CABG geometry.

Due to its ease of implementation we pursue a Laplace based method. The thickness and material properties are propagated over the patient-specific geometry by solving a homogenous Laplace partial differential equation, with prescribed dirichlet boundary conditions at inlets and outlets, to obtain a distribution of the scalar field. This method accounts for local curvature, vessel branching, change in

vessel properties across branching and anastomosis. The distribution computed this way is smooth, computationally convenient, requires minimum user input. Patient-specific wall thickness and material property information is inaccessible by non invasive imaging. Hence material properties are assigned based on literature values.[44,46,50] Thickness values of the coronary arteries are assigned based on morphometric measurements from the literature.[51] For the aorta, arch branches, and grafts, motivated by a constant homeostatic circumferential stress hypothesis, thickness is calculated from radius-thickness ratios in the literature.[44,52] The thickness and material properties are then propagated over the patient-specific geometry by solving a homogenous Laplace partial differential equation, with prescribed values at the inlets and outlets.[48] This results in a smooth distribution, which is computationally convenient and requires minimal user input (Figure 2.1). When data on thickness is unavailable, motivated by a constant homeostatic circumferential stress hypothesis, its value is calculated from radius-thickness ratios in literature.[52]

Lumped parameter network models of circulation

Existing boundary condition techniques in fluid mechanics, e.g. pressure boundary condition or flow boundary condition, are not suitable for blood flow simulations as they cannot capture the physiological pressure-flow relationships at the outlets.[53] To model the circulation outside of the 3D domain, including the heart, systemic circulation, and microcirculation, we make use of a circuit analogy, in which pressure drop is analogous to voltage and flow is analogous to current, thereby relating

compliance to capacitance, viscous dissipation to resistance, diodes to valves, etc. We use a closed-loop lumped parameter network (LPN), with circuit blocks representing the four chambers of the heart, systemic and coronary circulations (Figure 2.1). The LPN is coupled to the 3D model using an implicit, modular coupling algorithm with excellent stability properties.[34] The algorithm solves the LPN numerically, and pressure and flow data are iteratively passed between the 0D and 3D domains at interface boundaries, resulting in a time-implicit scheme. This method allows for stable 0D/3D coupling with no additional computational cost compared to conventional boundary conditions.

While a standard RCR circuit (Windkessel) is sufficient to model the systemic circulation, the coupling between the myocardium and the coronary arteries poses additional challenges and standard boundary conditions are not sufficient. Ventricular contraction exerts extravascular forces on the coronary arteries, causing increased resistance during ventricular contraction and causing the coronary flow to be out of phase with the systemic mammary circulation. Hence, coronary specific boundary conditions[35,37] coupled to the intramyocardial pressure are used at all coronary artery outlets in the model. Current closed-loop formulation uses an elastance based function to model ventricular pressure-volume relationship[54] and an activation function formulation to model the atria.[55] Intramyocardial pressure scaling was fixed at 0.75[56] and 0.5 times left ventricle for the left and right coronaries, respectively. The governing equations and the details of LPN calculation, except for the modifications mentioned above, are similar to Sankaran et al.[37]

Fluid-Structure Interaction

Fluid-Structure interaction (FSI) simulations require solution of a coupled fluid-solid system of equations to model deformable walls and blood flow. Finite difference, finite volume and finite element methods are the three major approaches to solving fluid problems. Historically, finite element method has had good success with complex patient-specific geometries and coupled boundary conditions.[57] We use finite element methods in our work. Classical Galerkian schemes fail for advection dominated flows. Stabilized finite element formulations overcome this short coming and allow an equal order interpolation of pressure and velocity. Reader is referred to the works of Hughes and colleagues[58–61] for a detailed description of stabilized finite element formulations for fluids.

Previously a range of FSI methods have been applied to cardiovascular flows, including, immersed boundary method, space-time coupling method, coupled momentum method and augmented lagrangian eulerian method (ALE).[33,62,63] Interested reader is referred to works by Bazilevs et al.[57,61] for a detailed description and review of finite element formulations for FSI. Immersed boundary methods model the structure as interconnected elastic boundary points embedded in the fluid domain and are well suited for ventricle simulations. ALE formulation continuously updates the fluid grid to capture the fluid-structure interface accurately and are computationally expensive. We use the coupled momentum method (CMM) with multiscale boundary conditions[34,37] to model flow and wall deformability in the coronary circulation. The CMM method used in this work is based on methods proposed in Figueroa et

al.[33] The governing equations in their strong form and some details of coupling are described briefly in the following section. Interested reader is encouraged to refer Figueroa et al. for a detailed derivation of the method.[64]

Governing Equations

Blood is modeled as a Newtonian fluid, a suitable assumption for flow in large vessels,[65] in the domain $\Omega \in \mathbb{R}^3$. Γ, the boundary of this domain Ω, can be conceptually divided into three different partitions such that $\mathbf{\Gamma} = \mathbf{\Gamma_g} \cup \mathbf{\Gamma_h} \cup \mathbf{\Gamma_s}$ and $\varnothing = \mathbf{\Gamma_g} \cap \mathbf{\Gamma_h} \cap \mathbf{\Gamma_s}$. Subscript g corresponds to a Dirichlet surface and h corresponds to a Neumann surface, unless stated otherwise. The incompressible Navier-Stokes equations for a Newtonian fluid, (in strong form (S)), can be written as:

$$
(S) \begin{cases}
\text{Given } \mathbf{f} : \overline{\mathbf{\Omega}} \times (0,T) \rightarrow \mathbb{R}^3, \text{ find } \mathbf{u}(\mathbf{x},t) \text{ and } p(\mathbf{x},t) : \overline{\mathbf{\Omega}} \rightarrow \mathbb{R}^3, \text{ such that} \\
\rho \mathbf{u}_{,t} + \rho \mathbf{u} \cdot \nabla \mathbf{u} = -\nabla p + \nabla \cdot \mathbf{T} + \mathbf{f} \text{ in } \mathbf{\Omega} \times (0,T) \\
\mathbf{T} = \mu \left(\nabla \mathbf{u} + \nabla \mathbf{u}^T \right) \\
\nabla \cdot \mathbf{u} = 0 \text{ in } \mathbf{\Omega} \times (0,T) \\
\mathbf{u}(\mathbf{x},0) = \mathbf{u}_0(\mathbf{x}) \text{ in } \mathbf{\Omega} \\
\mathbf{u} = \mathbf{g} \text{ in } \mathbf{\Gamma}_g \times (0,T) \\
\mathbf{n} \cdot (-p\mathbf{I} + \mathbf{T}) = \mathbf{h} \text{ in } \mathbf{\Gamma}_h \times (0,T)
\end{cases}
\tag{2.1}
$$

ρ, μ, $\mathbf{u}$, p, $\mathbf{T}$, and f are density, dynamic viscosity, velocity, pressure, deviatoric stress

tensor and body force, respectively. The boundary is divided into $\mathbf{\Gamma}_g$ and $\mathbf{\Gamma}_h$, in which the velocity (Dirichlet condition) and traction (Neumann condition) are prescribed, respectively.

A linearized kinematic approach is used for the elasto-dynamics equations of motion as it enables representation of the solid equations in the fluid Eulerian frame. Since the wavelength of cardiac pulse is much larger than the diameter of the arteries we use a thin wall / membrane formulation for the vessel wall. The strong form of the vessel wall problem can be described as:

$$(S)\begin{cases} \text{Given } \mathbf{b^s} : \overline{\mathbf{\Omega^s}} \times (0,T) \rightarrow \mathbb{R}^3, \text{ find } \mathbf{u^s}(\mathbf{x},t) \text{ and } \mathbf{u^s_{,t}}(\mathbf{x},t)\ \overline{\mathbf{\Omega^s}} \rightarrow \mathbb{R}^3, \text{ such that} \\ \rho^s \mathbf{u^s}_{,tt} = \nabla \cdot \sigma^{\mathbf{s}} + \mathbf{b^s}; \text{in } \mathbf{\Omega^s} \times (0,T) \\ \mathbf{u}(\mathbf{x},0) = \mathbf{u}_0(\mathbf{x}) \text{ in } \mathbf{\Omega^s} \\ \mathbf{u^s} = \mathbf{g^s} \text{ in } \mathbf{\Gamma}^s_g \times (0,T) \\ \mathbf{t_n} = \sigma \mathbf{n} = h^s; \text{in } \mathbf{\Gamma}^s_h \times (0,T) \end{cases} \tag{2.2}$$

where where a superscript s denotes structural domain, $\mathbf{u^s}$ is the displacement field, $\mathbf{b^s}$ is the prescribed body force per unit volume, $\rho^{\mathbf{s}}$ is the density of the vessel, $\sigma^{\mathbf{s}}$ is the wall stress tensor. In our simulations we pick displacement at mean pressure as the initial configuration. A strong kinematic coupling at the fluid solid interface requires the zero-velocity condition (Dirichlet) at the interface be replaced by a traction condition (Neumann). Hence the strong formulation on the fluid domain also needs to accommodate a traction condition, $\mathbf{t^f} = -\mathbf{t^s}$, where the traction exerted by

fluid is equal and opposite to that exerted by a solid. For brevity the derivation and statement of the weak form has been left out of the methods section but can be found in Figueroa et al.[64]

CMM was originally developed for large-scale patient-specific FSI simulations and is computationally less expensive than standard arbitrary Eulerian Lagrangian (ALE) approaches because it relies on a fixed-mesh.[33] This method couples the equations of wall deformation at the variational level as a boundary condition for the fluid domain, keeping the computational mesh fixed during the simulation thus requiring only a modest increase in computational cost compared to the rigid wall case. Because the coupling is monolithic, it retains excellent stability properties. The formulation uses a linear membrane model enhanced with transverse shear. Verification and validation has been performed previously against analytic and in vitro experimental data with excellent agreement.[66]

Quantification of pressure, velocity, and displacement fields require numerical solution of a coupled system of equations to model wall deformation and blood flow. We use SimVascular to solve the time-dependent incompressible Navier-Stokes equations for the fluid domain[32,67] and Cauchys equations of linear elasticity for the vessel wall.[33] An efficient resistance-based preconditioner is used to solve the linear system in the SimVascular flow solver.[68] We use the aforementioned stabilized finite element methods to solve these equations. Blood is modeled as an incompressible Newtonian fluid of density 1.06 g/cm^3 and viscosity 0.04 $dyn/cm^2 s$. Walls are modeled as linear elastic material with Poissons ratio of 0.5. Every vessel is assigned a Young's modulus

based on data from literature.[44,46]

2.1.2 Statistical Analysis

The venous and arterial grafts from the cohort were grouped into two groups for statistical analysis (number of venous grafts =8; number of arterial grafts=5). The graft population was small and statistical distributions were not known a priori; hence, we used a Wilcoxon Rank Sum test, a non-parametric test, from the SciPy library (v0.13.3) in Python[69] to determine statistical significance among the parameters investigated, with p values < 0.05 considered to be statistically significant.

Patients were modeled as random effects and statistics was recomputed using linear mixed effect models[70] to ensure p values were not skewed by variability across patients. Mixed models give structure to the error terms in a statistical model and characterize individual differences due to a random effect (variability across patients in our case). Statistics were rerun using linear mixed effect modules in *lme4* package in R (Douglas Bates, Martin Maechler, Ben Bolker, Steve Walker (2015)).

2.2 Growth and Remodeling Framework

Primary function of cardiovascular system is to provide adequate flow to tissues and organs at particular pressures.[71] The vessels, predominantly in health, are programmed to adapt to acute and chronic changes in hemodynamics such that their function is maintained. For example, they adjust their radius, by modulating the

vascular tone, in response to an acute change in flow[17,72] and they change their thickness, by modulating turnover of wall constituents, in response to a chronic change in pressure.[73] Cells sense mechanical stimuli and trigger biochemical signal cascades that help regulate constituents across organ, tissue and cellular scales and at times change the underlying structure. It has been established that cells are sensitive to mechanical stimuli but it is not clear if its more sensitive to one form of stimuli versus another, eg. stress versus strain. Nonetheless, there is a pressing need for models that can elucidate the underlying mechanisms of adaptation and help identify the gaps in knowledge that will inform future experiments and data collection.

Growth and remodeling are two predominant mechanisms in adaptation and within the realm of vascular mechanics there are myriad definitions of growth and remodeling. In this thesis, similar to a few prior definitions,[74] growth refers to an increase in mass and remodeling refers to a change in structure. The G&R formulation is based on a constrained mixture theory developed for arteries, details of which can be found in prior work.[23,25,74–76] Analyzing a blood vessel in health and disease is challenging due to a host of complexities across spatial and temporal scales including, wall anisotropy, non-linear stress-stretch behaviour, turnover of multiple constituents in multiple layers of the wall, active response to a change in hemodynamic environment, multiaxial loading in the presence of prestress/prestretch, and an inherent intelligence in some vessels to maintain a state of homeostasis. Nonetheless, there is sufficient data to inform a first generation model of vascular G&R.[13,77]

The basic (im)balance laws of continuum mechanics provide a good starting

point to model the wall. Based on in vivo observations we invoke a constancy of total mass density, so $\rho(s) \approx \rho(0)$ where s is the time parameter. The elastodynamics of the vascular wall can be described well quasi-statically, hence one must satisfy the equilibrium equation

$$\nabla.\boldsymbol{\sigma} = \mathbf{0}, \tag{2.3}$$

where $\boldsymbol{\sigma}$ is the overall Cauchy stress, which has contributions from all structurally significant passive (e.g., smooth muscle, collagen, elastin) and active (contraction of the smooth muscle) components of the vessel wall. Within the continuum framework, Cauchy stress can be written as

$$\boldsymbol{\sigma} = \frac{1}{det\mathbf{F}}\mathbf{F}\frac{\partial W}{\partial \mathbf{F}^T} + \sigma_\theta^{act}\boldsymbol{e}_\theta \otimes \boldsymbol{e}_\theta, \tag{2.4}$$

where $\boldsymbol{F}$ is the deformation gradient tensor associated with the passive motions, with $det\boldsymbol{F} \approx \mathbf{1}$, and σ_θ^{act} is the active stress in the circumferential direction.

A point-to-point comparison[78] between 2D and 3D models showed that the 2D models accurately predict adaptive changes in geometry and stiffness and thereby capture salient aspects of G&R sufficient for clinical and fluid-structure interaction studies.[75,79] Hence, here, we briefly describe pertinent aspects for a thin-walled cylindrical tube. Responses to perturbations in pressure or flow rate from homeostatic values occur via changes in (a) lumen geometry, (b) wall thickness and micro-structure, and (c) stiffness by the addition and removal of material in evolving configurations

(Figure 2.2). Optimal G&R responses often involve a combination of vasoconstriction/vasodilation and constituent turnover to achieve homeostatic values of intramural and wall shear stress. While the composition and organization of constituents in the vessel wall might vary to support local structure and function, the vessel wall primarily consists of three structurally significant constituents - elastin, collagen and smooth muscle. Hence, the constrained mixture theory of growth and remodeling models the wall as an (insoluble, isothermal) mixture of structurally significant constituents such as collagen, smooth muscle, and elastin. Each constituent within the mixture is endowed with its own material properties, rates of production and degradation, and natural configuration, but is constrained to deform with the bulk wall, hence a constrained mixture. While it is difficult to distinguish effects of individual constituents from the others, for mathematical convenience, and prompted by prior success with arterial models, we model the elastin as isotropic, smooth muscle along the circumferential direction, and collagen along axial, circumferential, and diagonal $+/-45^0$ directions. Modeling each constituent as hyperelastic, according to a simple rule-of-mixtures, the total energy stored in the wall is given conceptually by $W = \Sigma\phi^k W^k$, where ϕ^k is the mass fraction of constituent k and W^k, its stored energy density.

2.2.1 Active behaviour

Tissues, in their basal state and an altered physiological demand state, undergo a continuous turnover of constituents. To capture turnover of the constituents, mass

density and strain energy density are allowed to evolve according to a 'fading memory' behaviour,[23] namely

$$M^k(s) = M^k(0)Q^k(s) + \int_0^s m^k(\tau)q^k(s,\tau)d\tau, \tag{2.5}$$

$$W^k(s) = \frac{M^k(0)}{\rho(s)}Q^k(s)\widehat{W}^k(\mathbf{C}^k_{n(0)}(s)) + \int_0^s \frac{m^k(\tau)}{\rho(s)}q^k(s,\tau)\widehat{W}^k(\mathbf{C}^k_{n(\tau)}(s))d\tau, \tag{2.6}$$

where $M^k(s)$ and $\widehat{W}^k(s)$ are mass per unit area and energy stored in constituent k per unit volume, respectively, and $\rho(s)$ is the current overall (constant) mass density. $\mathbf{C}^k_{n(\tau)}$ is the right Cauchy-Green tensor for constituent k defined with respect to its individual natural configuration $n(\tau)$.[75] $m^k > 0$ is the true mass density production; $Q^k \in [0,1]$ is the fraction of constituent k produced at or before $\tau = 0$, while $q^k \in [0,1]$ is the fraction of constituent produced at time τ, both surviving until current time s.

2.2.2 Mass production and degradation functions

The constancy of wall density and clinically observed changes to vessel morphometry in the presence of altered shear and intramural stress, motivates a mass production function with contributions from basal production, and shear and intramural stress mediated production of constituents. Mechanical stress-mediated production rates m^k ($k = 1,2,3,4$ for collagen fiber families, $k = m$ for the smooth muscle cell

and $k = e$ for the elastin) are given by

$$m^{k=e} = 0, \quad m^k(\tau) = m_0^k(1 + K_1^k \Delta\sigma(\tau) - K_2^k \Delta\tau_w(\tau)), \tag{2.7}$$

where m_0^k denotes original (basal) values and the normalized deviations from homeostatic stress values (indicated with superscript h) are defined for the intramural stress and wall shear stress, respectively, as

$$\Delta\sigma = \frac{\sigma - \sigma^h}{\sigma^h}, \qquad \Delta\tau_w = \frac{\tau_w - \tau_w^h}{\tau_w^h}, \tag{2.8}$$

with gain parameters K_1^k and K_2^k quantifying the rate of production of constituents in response to perturbations from their homeostatic states. Note that we assume no elastin turnover in the time-frame considered for G&R since it is produced during the perinatal period, cross-linked, and stretched elastically during development, and is biologically stable.[80] At homeostatic load values the mass production function recovers basal production rates and reflects a state of constant geometry and stiffness, assuming other factors such as constituent properties and degradation rates are left unaltered.

Prior mass production and degradation functions were based on a model for a healthy basilar artery.[75] While those mass production functions were adequate for (relatively) moderate perturbations in pressure ($\gamma = P/P_0 = 1.5$), they were

inadequate, that is, did not restore the theoretical homeostatic state within numerical tolerance, for a moderate combined load, defined as a moderate increase in both pressure ($\gamma = 1.5$) and flow ($\epsilon = 1.1$), with $\gamma = P/P_0$ and $\epsilon = Q/Q_0$. Hence, there was a need to modify the mass production constitutive equation for general vein graft responses, especially for altered flow cases. Prior applications of this model to pathological arterial adaptations (e.g. abdominal and cerebral aneurysms[23,81]) required a mass production function that accounted for an increase in cell density in response to severe insults. Because the acute insult from increases in hemodynamic loading experienced by a vein subjected to arterial conditions is more severe, the mass production functions for the vein were similarly modified to handle this increase in cell density,

$$m^k(\tau) = \frac{M^k(\tau)}{M^k(0)} m_0^k (1 + K_1^k \Delta\sigma(\tau) - K_2^k \Delta\tau_w(\tau)). \tag{2.9}$$

The constituent degradation relation was modeled consistent with first order type kinetics, of the form

$$q(s,\tau) = exp(-\int_\tau^s K^k(\tilde{\tau}))d\tilde{\tau}, \tag{2.10}$$

where K^k is a rate-type parameter.[75] The rates of removal depend explicitly on changes in the tension within the fibers; here we consider the specific form[75] $K^k(\tilde{\tau}) =$

$K_h^k + K_h^k \Delta\zeta^k(\tilde{\tau})^2$ where

$$\zeta^{k(\tau)}(s) = \frac{\dfrac{\partial \widehat{W}^k}{\partial \lambda_n^k(\lambda_{n(\tau)}^k(s))}}{\dfrac{\partial \widehat{W}^k}{\partial \lambda_n^k(G_h^k)}} \tag{2.11}$$

is the level of tension on constituent k that was produced at time τ and $\Delta\zeta^k(\tilde{\tau})$ is the difference in fiber tension from its homeostatic value. At homeostasis the vessel wall density is roughly a constant; the mass produced should equal the mass degraded. This was best achieved when smooth muscle was allowed to degrade at basal rates, while collagen degradation had contributions from both basal and tension-dependent degradation.[75,81] Note that these general functional forms, including mass production and degradation, are consistent with biological experiments and prior models of arterial G&R.[75,82]

2.2.3 Active Smooth Muscle

Vasoactive molecules are regulated by the endothelium in response to change in flow and these molecules inturn affect the productions rates of the wall constituents. The short-term response to a change in flow is countered by an adjustment in the smooth muscle vascular tone and this tone is predominantly dependent on two factors, stretch experienced by smooth muscle and the concentration of constrictors and

dilators in the vessel wall. The smooth muscle active stress, σ_θ^{act}, is modeled as,[83]

$$\sigma_\theta^{act}(s) = T_{max}\phi^m(s)\left(1 - exp(-C(s)^2)\right)\lambda_\theta^{m(act)}(s)\left(1 - \left(\frac{\lambda_M - \lambda_\theta^{m(act)}(s)}{\lambda_M - \lambda_0}\right)^2\right), \quad (2.12)$$

where T_{max} (Nm^{-2}) is a (calcium-dependent) scaling parameter, λ_M and λ_0 are circumferential stretches at which the active stress is maximum and zero, respectively. The active behavior is taken with respect to individual unloaded configurations for smooth muscle, not the entire mixture. The values of λ_M and λ_0 are chosen to be consistent with values in the literature for a rat vein, which are different from those of arteries (Table 4.3).[84] $C(s)$ is the net ratio of constrictors to dilators and is shear modulated: $C(s) = C_B - C_s\Delta\tau_w$, where C_B is the basal constrictor to dilator ratio and C_s is a scaling factor for shear stress induced changes in constrictor/dilator concentration. Notice that the proposed constitutive equation captures the experimentally observed inverse parabolic relation with respect to stretch. The vasoactive response of a vessel can evolve over a range of diameters, thus shifting the stretch at which maximum and minimum tone occurs.[85] This shifting behaviour motivates an active circumferential stretch $\lambda_\theta^{m(act)}(s) = a(t)/a^{m(act)}$, that evolves via the first order equation

$$\frac{da^{m(act)}}{dt} = K^{act}(a(t) - a^{m(act)}), \quad (2.13)$$

where $a^{m(act)}(0) = a(0)$ and K^{act} is a rate parameter.[26,75]

In summary, our implemented G&R formulation solves equilibrium of the vessel by accounting for the evolving nature of the wall constituents, including active and passive responses. For simplicity, we keep axial stretch a constant in our simulations. We numerically solve the traction equilibrium equation for radius, at every time step, using the Newton-Raphson method and time advance the radius and mass of constituents using an explicit Euler scheme.

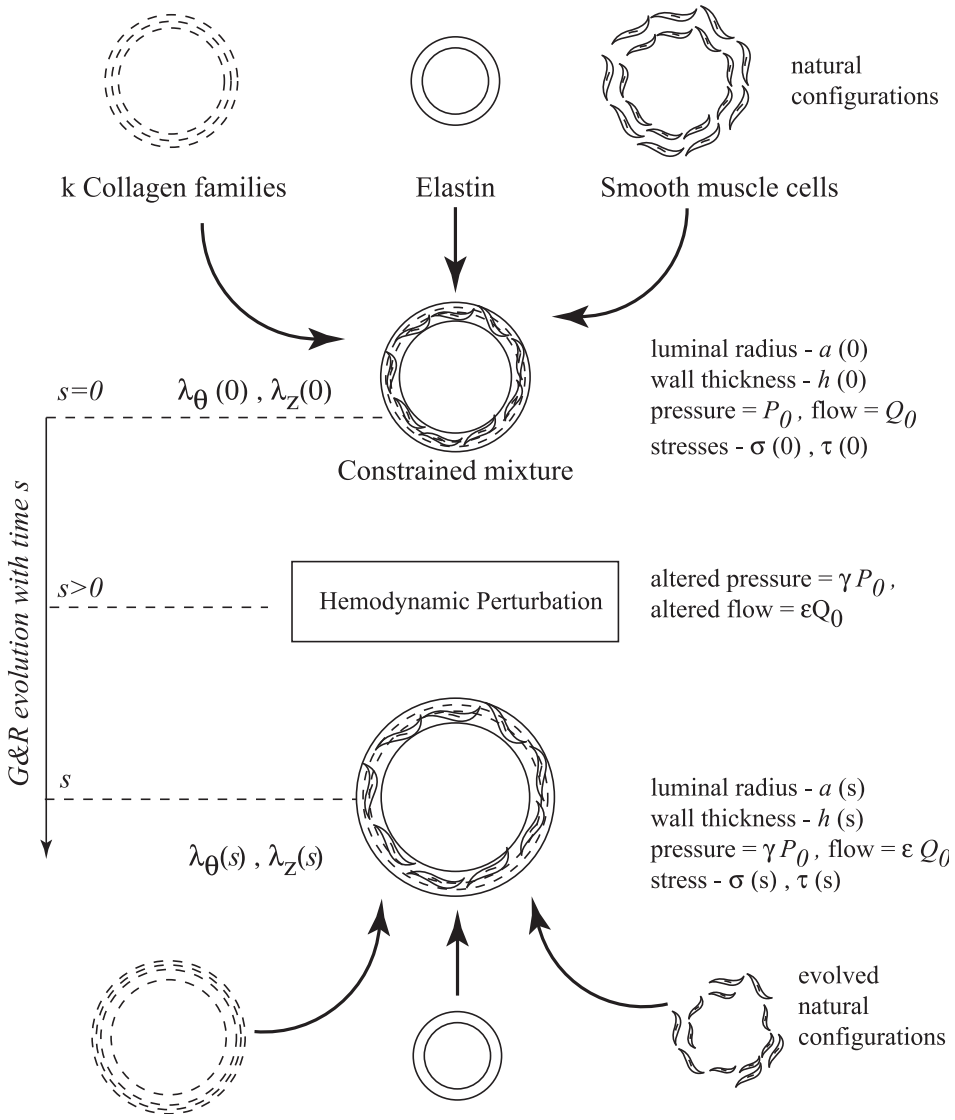

Figure 2.2: Schema of a G&R framework illustrating the configurations of a vessel (i.e., constrained mixture) and its constituents at instant $s = 0$, without hemodynamic perturbations, and at G&R time s, with hemodynamic perturbation. The G&R framework enforces mechanical equilibrium at each instant while accounting for the evolving constituent mass fractions, natural configurations, and strain energy densities as the constituents turn over.

2.2.4 Step and gradual load

We consider changes in stress resulting from either a step increase (jump) or linearly varying (gradual) increase in pressure from a venous towards an arterial

value. Step and gradual changes in load, in the context of a numerical adaptation, are defined as:

- Step change: A step increase is achieved by a change in the load from homeostatic to the new value over one time step (Figure 2.3(a)).
- Gradual change: A gradual increase in loading is characterized by a linear increase in load from homeostatic to the new value over a prescribed period (Figure 2.3(b)).

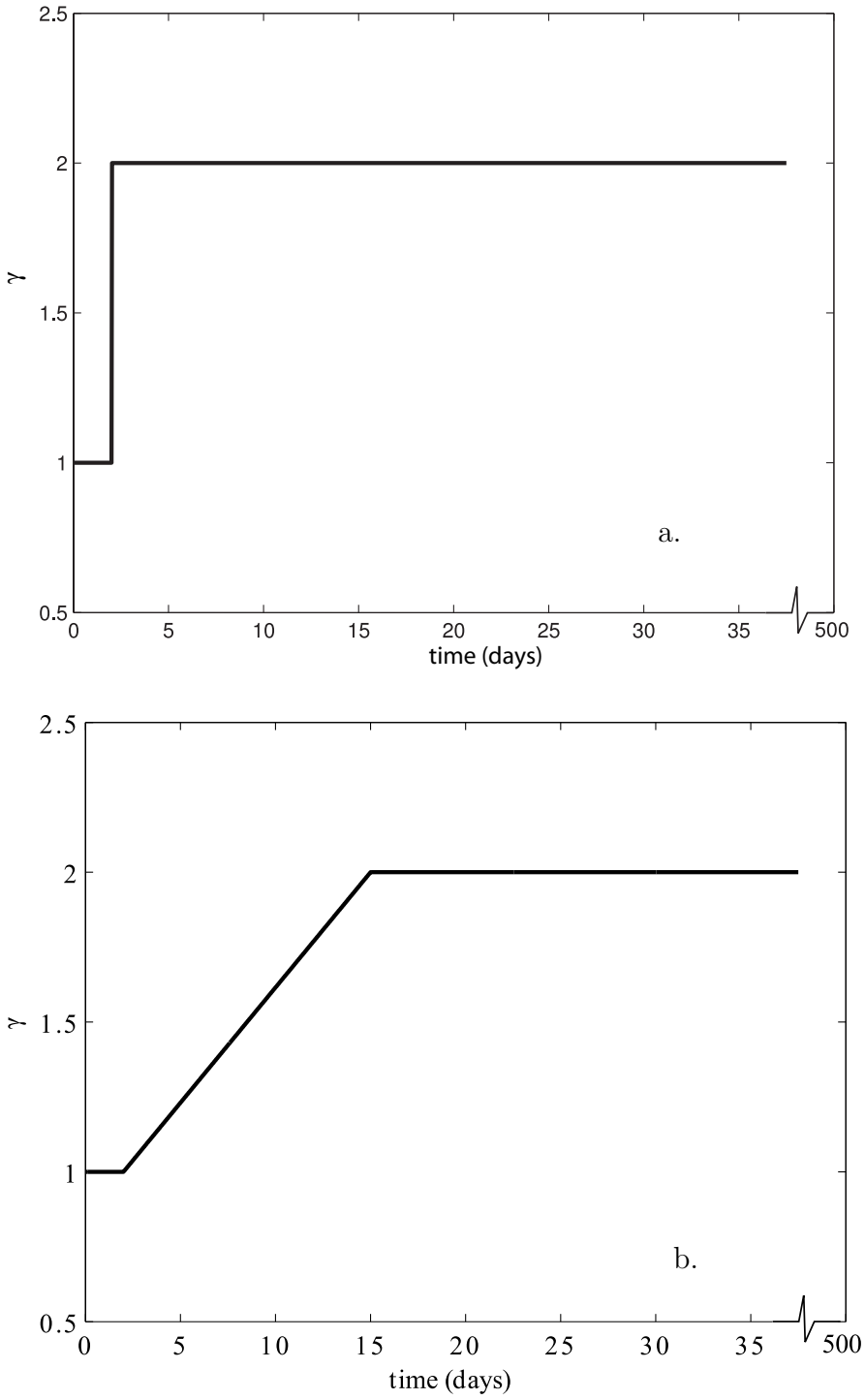

Figure 2.3: Illustration of (a) a step increase in pressure and (b) a gradual increase in pressure, both illustrated for $\gamma = 2$.

2.3 Optimization

2.3.1 The Surrogate Management Framework

The surrogate management framework (SMF) has been used successfully in a variety of complex problems, including unsteady fluid mechanics,[86–88] helicopter rotor blade design,[89,90] quantifying uncertainty in bypass graft models[91] and identifying arterial G&R parameters.[92] The SMF method was originally developed for computationally expensive simulations, and can be applied to discontinuous functions and problems with nonlinear constraints.[93] It requires no information on function gradients and has the advantage that the function can be treated as a black box. Here, linear bound constraints enforce non-negativity of the strain energy function and impose biologically realistic bounds on the parameters of interest.

The SMF has a well-established convergence theory and employs a surrogate function to accelerate convergence. Our implementation of the algorithm starts by running true function evaluations at a set of well-distributed initial points an N-dimensional space using Latin Hypercube Sampling. Then the algorithm moves to a SEARCH step that accelerates convergence by fitting a Kriging surrogate function through evaluated points and finding a candidate point, usually the minima of a Krigged surface, for a true function evaluation. The surrogate is updated with each true function evaluation and this process is repeated until a SEARCH fails to identify an improved design point. When the SEARCH step fails, the algorithm moves to a POLL step. In a POLL step, a positively spanning basis is identified around the

current design point and new trial design points are selected by performing function evaluations along these directions with a specified step size. In our implementation, due to its superior convergence properties, we use a Mesh Adaptive Direct Search (MADS) algorithm to generate POLL sets.[93] When the POLL step also fails to generate a better design point, the grid is refined and the algorithm returns to the SEARCH step. Note that all points evaluated are required to lie on a grid, which can be refined or coarsened, and the algorithm stops when the grid is refined to a preset tolerance. The threshold grid size was set to $1/2^{12}$ in our optimizations. Thus, the algorithm converges to a local minimum using a combination of SEARCH and POLL steps. Note that the SEARCH step is not strictly required for convergence whereas the POLL step is necessary and sufficient for convergence.

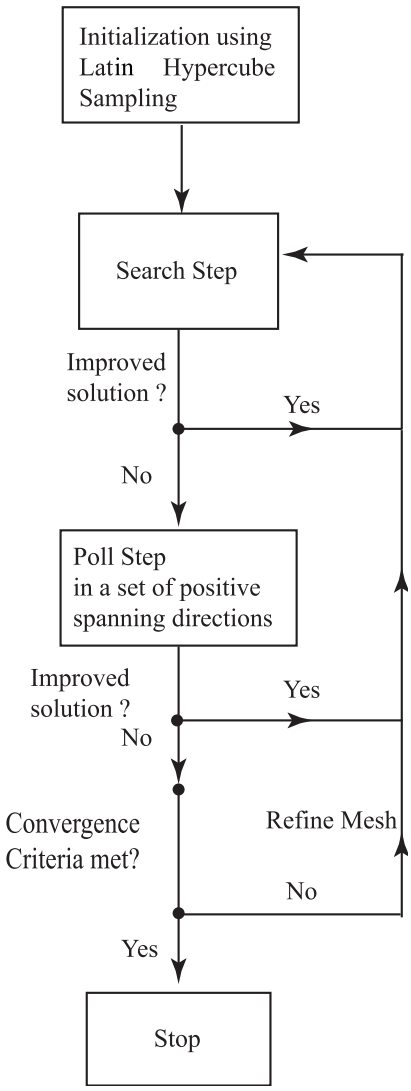

Figure 2.4: Flowchart of the Surrogate Management Framework (SMF) used for identifying the optimal parameter set for vein G&R

2.3.2 Cost function

There are many ways to define a cost function for a multi-objective problem such as G&R; we use a weighted sum of multiple objective functions. One could define an illustrative cost function as a weighted sum of individual geometric and

stress based objective functions. For example,

$$\mathcal{J}_{adapt} = \sqrt{w_1(\frac{\sigma_\theta^h - \sigma_\theta}{\sigma_\theta^h})^2 + w_2(\frac{\tau_w^h - \tau_w}{\tau_w^h})^2 + w_3(\frac{a - a^h}{a^h})^2 + w_4(\frac{h - h^h}{h^h})^2}. \quad (2.14)$$

Weighting of terms plays a vital role in estimating the optima, and consequently the evolution and adaptation of a vessel. Experiments are critical in informing the weight on each of these terms, the lack of which led us to explore different weights. For example, setting $w_3 = 0$ and $w_4 = 0$ produces a stress based cost function, and further setting $w_1 = 1$ and $w_2 = 1$ recovers the cost function used in our work (equation 4.7). On the other hand, setting $w_1 = 0$ and $w_2 = 0$ gives us a pure geometric cost function.

Chapter 3

Patient-Specific Simulations of Coronary Bypass Graft Surgeries

3.1 Patient Population

We identified five patients for this study who had previously undergone coronary artery bypass graft surgery and echocardiography, had no stents in the native coronaries or grafts, had undergone clinically-indicated CT angiography, and were free of graft stenoses.

CT angiography (CTA) was performed using a 64-slice Discovery CT750 HD scanner (GE Healthcare, Milwaukee, Wisconsin) according to clinical protocol. Subjects received beta blocking medication as needed to reduce heart rates to less than 65 beats per minute, and nitroglycerin (0.4 mg sublingual) was administered prior to scanning. All scans were performed using padded prospective gating centered at

Table 3.1: Summary of patients used in study with non-invasive clinical measurements and details of grafts. BP-blood pressure, CO-cardiac output, SV-stroke volume, HR-heart rate, SVG-saphenous vein graft, LIMA-left internal mammary artery, RIMA-right internal mammary artery, OM-obtuse marginal, RCA-right coronary artery, LAD-left anterior descending.

Patient ID	Gender	Age	Interval	Patent grafts
Patient 1	F	48	13	SVG to LAD, SVG to OM
Patient 2	F	69	11	LIMA to OM1, SVG to LAD
Patient 3*	M	72	17	LIMA to OM, SVG to distal RCA
Patient 4	M	61	1	RIMA to LAD, LIMA to OM, SVG Y graft: high diag and PDA
Patient 5	F	43	4	LIMA to LAD, SVG to OM, SVG to RCA

Sample summary – Number of venous grafts =8; Number of arterial grafts=5. * data from the clinic was missing and was calculated based on body mass index (BMI).[95]

75% of the R-R interval with a slice thickness of 0.625 mm. Echocardiograms were performed on four patients in accordance with standard guidelines. Heart rates and blood pressures were measured at the time of echocardiography. Stroke volume was calculated from echocardiographic data as the product of the left ventricular outflow tract (LVOT) area and the velocity-time-integral of the Doppler measurement of flow through the LVOT.[94] Cardiac output was then calculated as the product of stroke volume and heart rate. For one patient (Patient 3) with no available echocardiographic data, a body mass index based population averaged cardiac output was used.[95]

3.2 Preprocessing and Simulations

Methodology outlined in section 2.1.1 was used to obtain patient-specific geometries. Laplace variable property solver was used to assign vessel-specific material

properties and thickness (Figure 3.1).

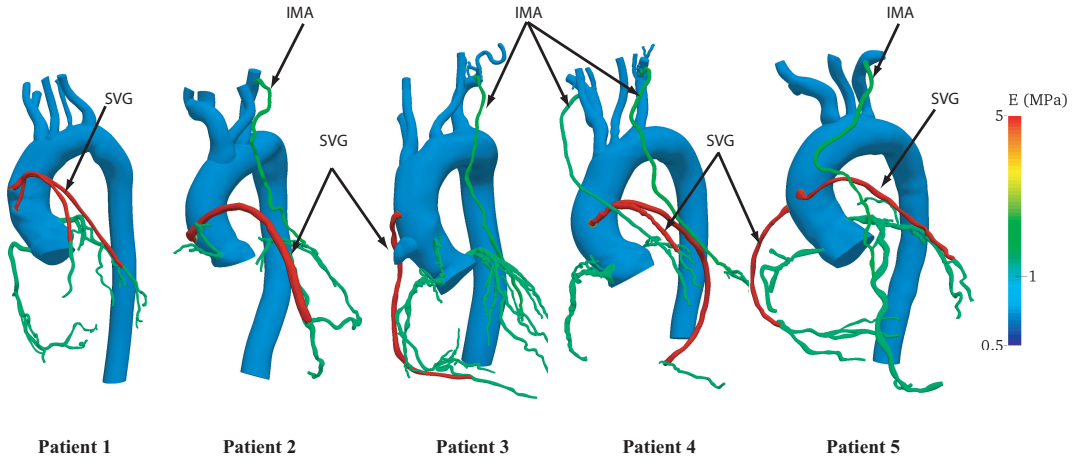

Figure 3.1: Youngs modulus (MPa) distribution in a cohort of patient-specific coronary artery bypass graft (CABG) models. The following material property values were assigned based on literature data: Aorta and the arch walls – 0.7 MPa, left and right coronaries – 1.15 MPa, left internal mammary artery – 1.4 MPa, right internal mammary artery – 1.15 MPa, vein grafts – 5 MPa

The patient-specific geometries were discretized into linear tetrahedral meshes and adapted twice using flow fields.

The LPN parameters were tuned to match standard-of-care non-invasive clinical measurements. The following data were used for tuning: cardiac output (CO), heart rate (HR), systolic and diastolic blood pressure, and literature data to provide additional targets, as summarized in Table 3.2. We assumed 4 % of the total cardiac output was distributed to the coronary arteries.[96] Motivated by Murrays law, a mathematical relationship between vessel size and flow, an area-based approach was used to assign capacitance and resistance values at the outlets. Capacitance values were chosen to be proportional to outlet area, and resistances values were determined according to a modified Murrays law using an exponent of 2.0 for the aortic

branches and 2.6 for the coronary branches.[97,98] The equations governing the LPN, and methods for their solution, follow our previous work.[37]

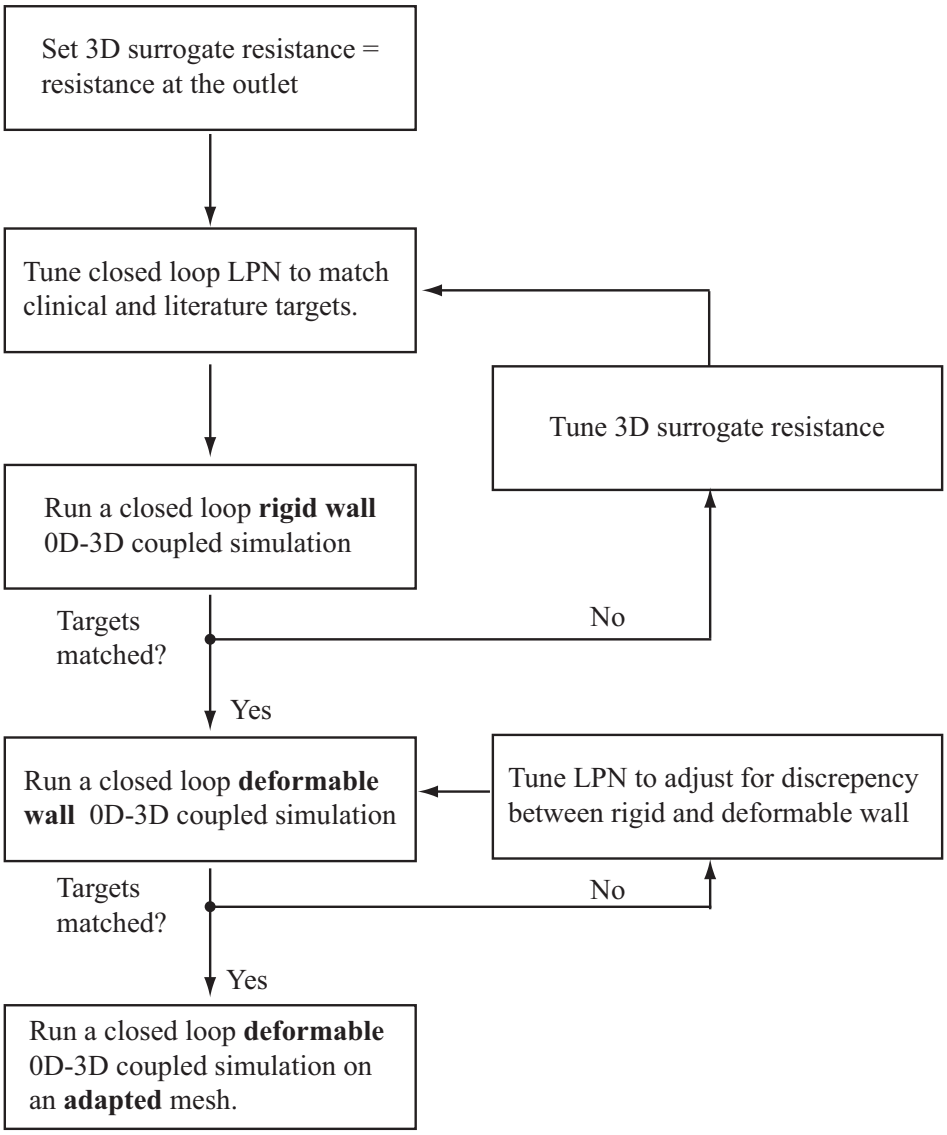

Figure 3.2: CABG simulation tuning pipeline

To accelerate tuning for a variable wall deformable simulation, LPN parameters were tuned in stages to match clinical targets (Figure 3.2). Briefly, 3D patient-specific model was replaced with a corresponding 0D resistance surrogate to model pressure-flow relationship at the outlets. The heart model, RCR and the coronary

circuit parameters were tuned on the 0D surrogate to match clinical targets. This tuned set of parameters were subsequently used in a rigid 3D patient-specific simulation to ensure it matched clinically measured cardiac output, stroke volume and prescribed flow-splits. Finally, capacitances were tuned in a deformable wall simulation to account for compliance of the 3D model and match clinically measured pressure. Note that it is non-trivial to build a 0D surrogate for a deformable model hence, as a workaround, a 0D resistance surrogate for a rigid model was used in this framework.

The simulations were run on XSEDE NICS resource-Darter which is a Cray XC30 system with the compute nodes made of two 2.6 GHz 64 bit Intel 8-Core XEON processors. One cardiac cycle on a mesh of approximately 4 million elements required about 10 h on 96 processors. The entire simulation process, from image data to model construction and deformable simulation on a 4-million-element model, took approximately 3 weeks for each subject.

3.3 Postprocessing and Clinically Relevant Indices

We post-processed simulation results to compute indices of presumed biological relevance, specifically time averaged wall shear stress (TAWSS), OSI, percentage of graft surface area where WSS was less than a pathological value (which we refer to as atheroprone area, A_{athero}), and wall strain quantified through a scalar measure – Green Strain Invariant (GSI1). These quantities were spatially and temporally

averaged over each graft over one cardiac cycle. For statistical analysis, TAWSS in each graft was normalized by the aortic value of TAWSS in the same patient to normalize for patient variability. Every simulation was run for at least six cardiac cycles and these quantities were computed for the final cycle after initial transients had died out. In addition to mechanical stimuli, we also quantified graft diameter and tortuosity and quantified the differences between the two graft types.

The following paragraphs elaborate the computation of mechanical stimuli indices from primary mechanics quantities such as velocity and displacements.

1. Time Averaged Wall Shear Stress (TAWSS)

   Time averaged wall shear stress (TAWSS) is computed as $TAWSS = \frac{|\int_0^{Tcc} \overrightarrow{WSS} dt|}{T_{cc}}$, where $\overrightarrow{WSS}$ is the wall shear stress vector, the tangential traction force produced by blood moving across the endothelial surface, T_{CC} is the duration of one cardiac cycle, and $||$ indicates magnitude. For statistical analysis, TAWSS in each graft was normalized by the aortic value of TAWSS in the same patient to normalize for patient variability.

2. Oscillatory Shear Index (OSI)

   Oscillatory shear index, a measure of oscillatory component of the flow, is computed as $OSI = \frac{1}{2}(1 - \frac{|\int_0^{Tcc} \overrightarrow{WSS} dt|}{\int_0^{Tcc} |\overrightarrow{WSS}| dt})$.

3. Atheroprone area (A_{athero})

   Atheroprone area (A_{athero}), a measure of the area of the graft prone to atherosclerosis, is computed as $A_{\text{athero}} = \frac{\int_{A_{graft}} f dA}{\int_{A_{graft}} dA}$, where $f = 1$ if $\overrightarrow{WSS} < 4\frac{dyn}{cm^{-2}}$ and 0

otherwise, with the threshold for low WSS set to 4 dyn/cm^2 based on literature data.[99]

4. Strain

   Amongst several potential measures of vessel wall strain, we chose to quantify Green Strain Invariant 1 (GSI1), a scalar measure of strain that is insensitive to rigid body motions, measured with respect to diastolic configuration.[100] This is calculated as $GSI1 = \frac{1}{2}(\boldsymbol{F}\boldsymbol{F}^T - \boldsymbol{I})$, where $\boldsymbol{F}$ is the gradient of displacement vector, $\boldsymbol{I}$ is an identity tensor and tr is the matrix trace operator.

5. Geometry

   Diameter was computed from lumen area by approximating the lumen area to be a circle. Lumen area was measured perpendicular to the vessel centerline and averaged across the length of the vessel. Tortuosity was defined as distance between points along the length of centerline divided by the distance between first and last point on the centerline and is a measure of deviation of centerline from a straight line.

Mean values of the following indices were compared for venous vs. arterial grafts: (1) WSS, (2) OSI, (3) A_{athero}, and (4) wall strain. Since WSS and OSI are directional in nature, p values for quantities 1–3 above are reported for one-tailed tests only. For wall strain, two-tailed tests were used. Mean values of diameter and tortuosity were also compared for venous vs. arterial grafts.

Table 3.2: Summary of non-invasive clinical measurements, population averaged targets from literature and respective quantities from simulations. The LPN was tuned to match, within 10 BP blood pressure (mmHg), SV stroke volume (ml/cardiac cycle), coronary flow expressed in percentage, -clinic value from clinic, -sim value from simulation, -lit value from literature

Patient ID	BP-clinic (mmHg)	BP-sim (mmHg)	SV-clinic (ml/cycle)	SV-clinic (ml/cycle)	%CO to Cor-lit	%CO to Cor-sim	L-R flow-sim in %
Patient 1	124/73	118/74.5	60.9	63.5	4.0	4.0	65.7–34.3
Patient 2	133/85	133/85.5	80.4	84.7	4.0	3.9	82.0–18.0
Patient 3*	135/78	133/78	78.1	75.8	4.0	4.0	52.5–47.5
Patient 4	115/74	117/74	115.1	114.8	4.0	4.1	56.4–43.6
Patient 5	113/69	115/68	70.5	70.6	4.0	4.1	74.0–26.0

Sample summary – Number of venous grafts =8 ; Number of arterial grafts=5. * No echocardiogram data for patient, body mass index-based population average was used

3.4 Results

Demographics of patients selected for this study, along with number of grafts and target vessels, are summarized in Table 3.1. We report results for 13 grafts ($n = 5$ arterial, $n = 8$ venous) from five subjects. The LPN was tuned to match clinical and literature targets within 10 % error (Table 3.2).

Contours of wall shear stress and wall displacements from the simulations are shown in Figure 3.3 for all patients. The model captured the expected out of phase behavior of coronary and systemic flow and pressure wave-forms. Representative comparisons of time-dependent quantities in venous and arterial grafts are shown in Figure 3.4 for patient 2. Flow in the grafts was dominant during diastole, while pressure and strain were in phase with the systemic circulation (Figure 3.4) as expected. In line with previous invasive measurements,[96] the tuned LPN produced a high variability in the left-right flow split in coronaries (Table 3.2). TAWSS was sig-

nificantly lower ($7.5 \pm 3.2\ dyn/cm^2$ in venous grafts vs. $23.2 \pm 15.9\ dyn/cm^2$ in arterial grafts, $p = 0.014$), and A_{athero} was significantly higher (0.20 ± 0.21 in venous grafts vs. 0.06 ± 0.07 in arterial grafts, $p = 0.040$) in venous grafts compared to arterial (Figure 3.5). Wall strain was significantly higher in arterial grafts (0.003 ± 0.001 in venous grafts vs. 0.011 ± 0.002 in arterial grafts, $p = 0.003$). No significant difference in OSI was found between arterial and venous grafts (0.022 ± 0.024 in venous grafts vs. 0.013 ± 0.018 in arterial grafts, $p = NS$). Conclusions on significance remained unchanged when statistics were recomputed with log transforms, without aortic WSS normalization, and with patient as a random variable. Uncertainty associated with the value of threshold TAWSS motivated us to quantify the distribution of A_{athero} for different values of TAWSS threshold (Figure 3.6). Regardless of the threshold value for critical wall shear stress, venous grafts consistently had a higher region of atheroprone area than arterial grafts, with the difference increasing and converging towards a constant value at higher threshold values. Mean venous graft diameter was significantly larger than arterial graft diameter (0.31 ± 0.06 in venous grafts vs. 0.23 ± 0.02 in arterial grafts, $p = 0.005$) and there was no significant difference in tortuosity (1.43 ± 0.29 in venous grafts vs. 1.26 ± 0.05 in arterial grafts, $p = ns$) (Figure 3.7).

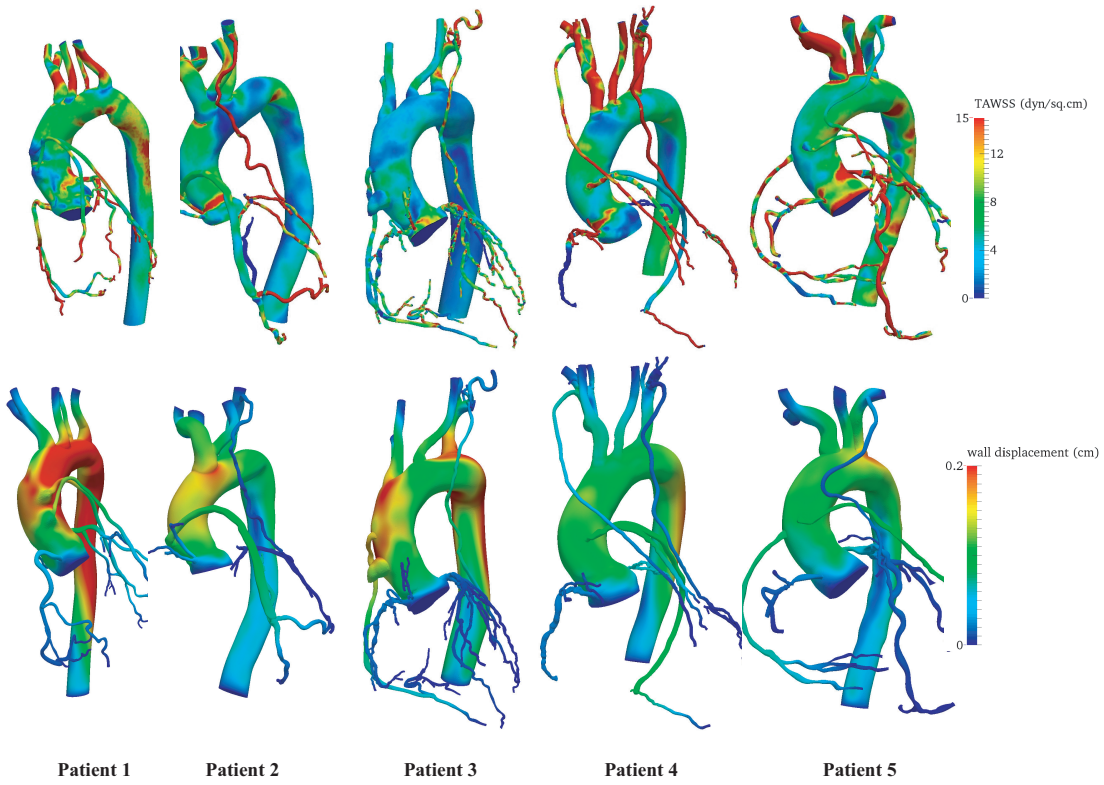

Figure 3.3: Representative solution fields in the patient-specific cohort. Top - time averaged wall shear stress (dyn/cm^2), bottom - displacement (cm) field near peak systole

3.5 Discussion

This study produced several major findings. First, the proposed framework successfully integrates patient-specific image-based models with fluid structure interaction and closed-loop boundary conditions tuned to match non-invasively measured patient-specific clinical targets. Second, simulations predict significant differences in time averaged wall shear stress, area prone to atherosclerosis, wall strain and graft diameter between arterial and venous grafts. Third, there were no significant differences in oscillatory shear index or graft tortuosity between arterial and venous grafts. Finally, we have quantified clinically and biologically relevant mechanical stimuli in

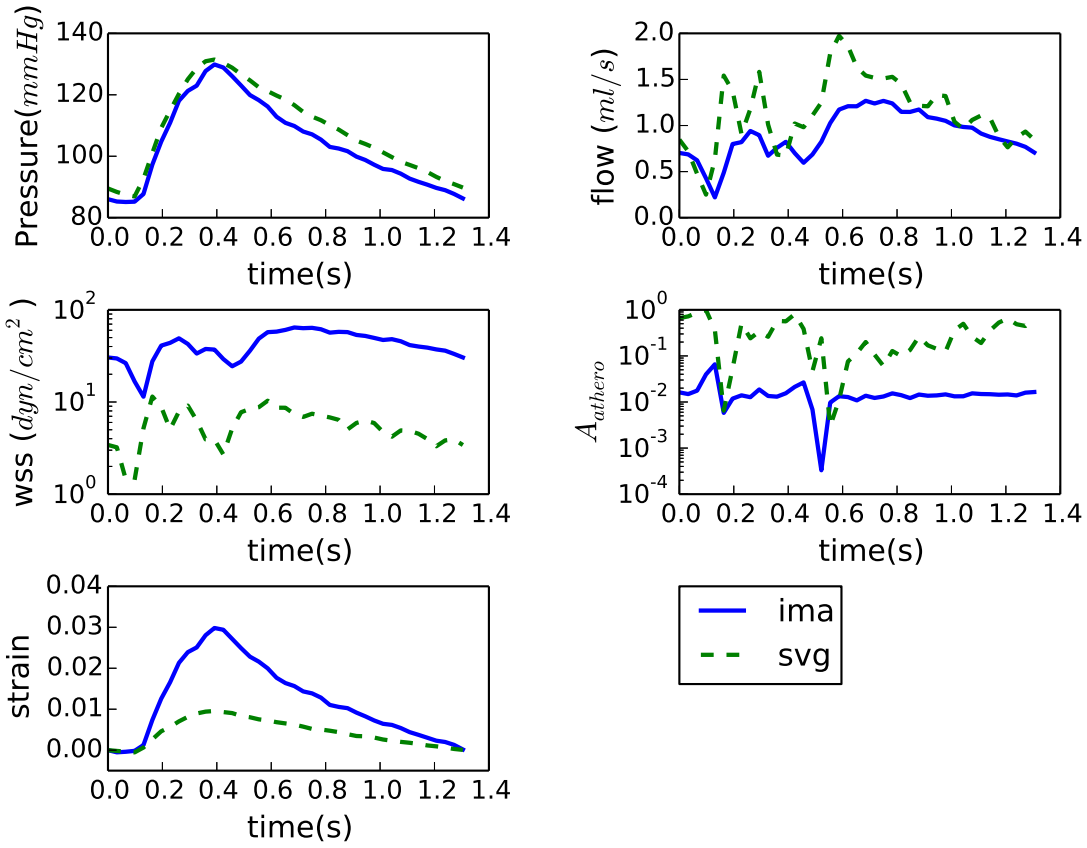

Figure 3.4: Representative pressure, flow, wall shear stress, A_{athero} , and strain values during a cardiac cycle in a venous and an arterial graft from patient 2. Note the flow and wall shear is dominant during diastole in these grafts, primarily because majority of flow in coronary occurs during diastole. Also note the WSS is higher and A_{athero} is lower in the arterial graft

coronary grafts that could guide the design of experiments in vascular biology.

3.5.1 Augmenting clinical practice with non-invasive modeling tools

There is a pressing need for earlier identification of patients at risk for graft failure. While CT imaging provides detailed coronary anatomy, it does not directly provide hemodynamics or biomechanics data. It is therefore likely that imaging alone

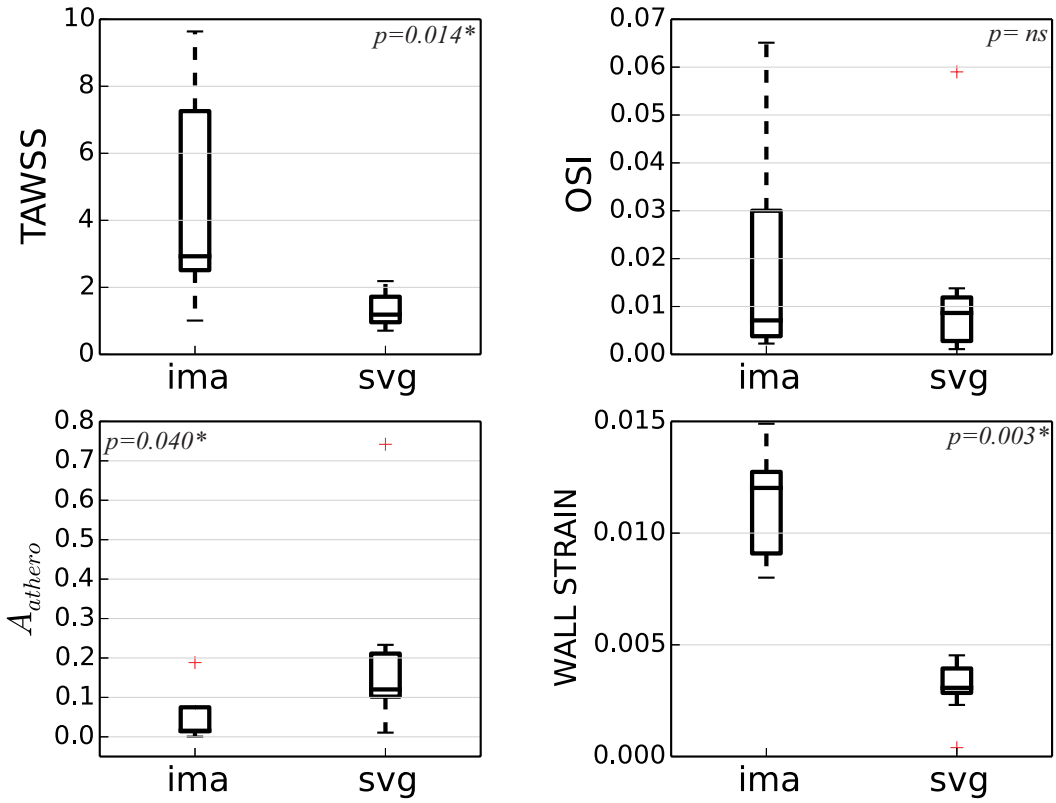

Figure 3.5: Box plot summary of normalized time averaged wall shear stress (TAWSS), oscillatory shear index (OSI), atheroprone area (A_{athero}), and wall strain in the arterial and venous grafts. Differences in TAWSS, A_{athero}, and wall strain between graft types were significant while differences in OSI were not ($p < 0.05$ is significant). Reported statistics are for five patients with a total of 13 grafts

is insufficient for early diagnosis of impending graft failure and patient risk stratification. Quantifying the mechanical stimuli acting on grafts in patient-specific models is a necessary precursor to understanding and predicting the complex mechanobiological process of graft failure.

The links between graft failure and mechanics have been challenging to isolate from myriad influencing factors including patient variability, clinical risk factors, differing clinical and surgical strategies, graft wall compositions and adaptation in

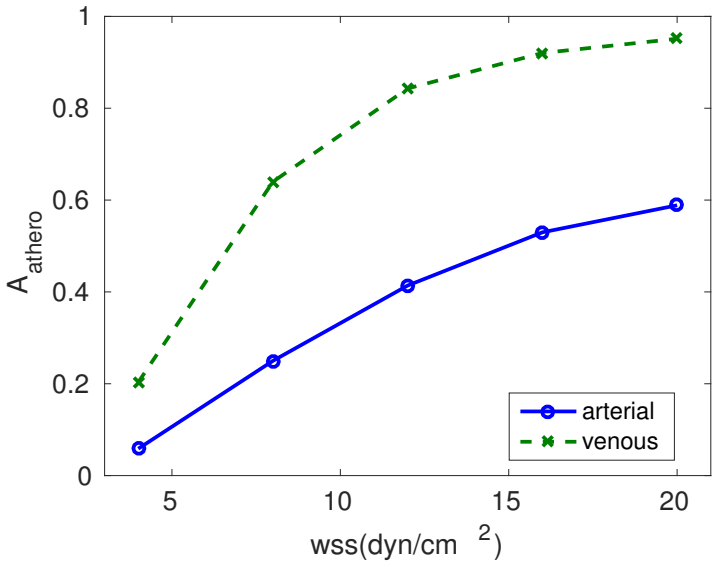

Figure 3.6: Frequency distribution of A_{athero} by different WSS thresholds, averaged across all venous and arterial grafts in the cohort. The averaged A_{athero} regions in arterial grafts are consistently lower than the venous values, regardless of the WSS cutoff value.

health and disease. The primary goal of this study was to quantify differences in mechanical stimuli between venous and arterial grafts with high fidelity patient-specific models of hemodynamics and physiology that account for patient variability and differing graft structural properties. These quantities are necessary inputs for future risk stratification metrics, vascular biology experiments, and growth and remodeling predictions.

3.5.2 Quantification and role of mechanical stimuli

The closed-loop boundary condition formulation we employ enables dynamic prediction of inlet and outlet pressure and flow waveforms, avoiding the need to directly prescribe these as in open-loop simulations. This is important since these data

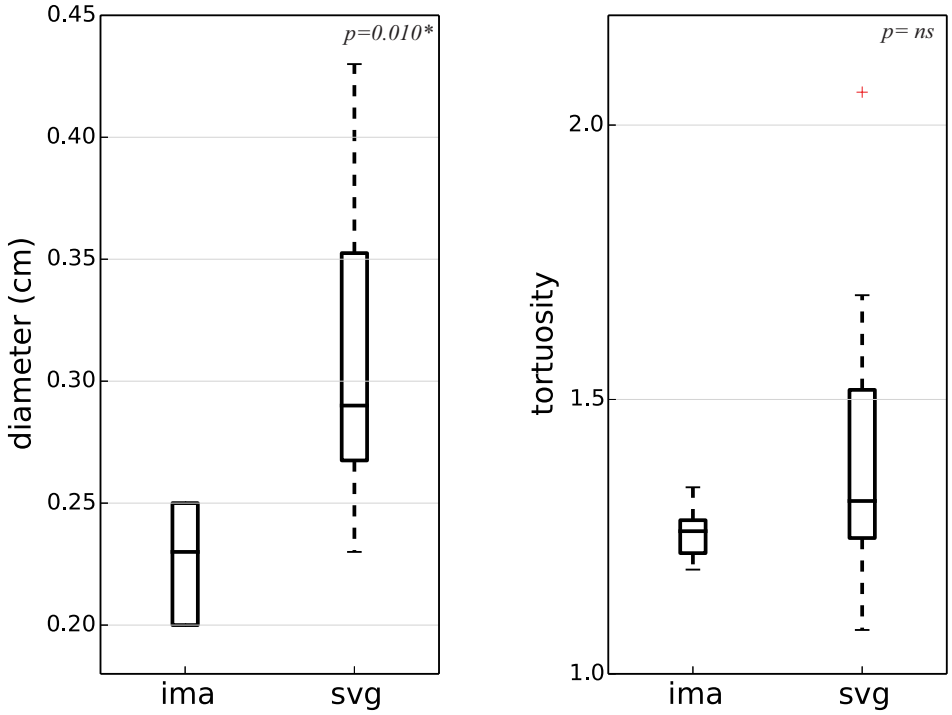

Figure 3.7: Summary of diameter and tortuosity of grafts in the cohort. The venous graft diameters were significantly larger than the arterial graft diameters (p = 0.005*). The differences in tortuosity were not significant (p = ns). SVG – saphenous vein graft, IMA – internal mammary artery

are typically not available from standard-of-care CT measurements. Rigid wall simulations must assume infinite wave propagation speed, which significantly alters flow and pressure waveforms, and over-predicts pressure amplitudes. Hence deformable wall simulations are essential to accurately predict physiologic pressure levels. Also, material properties and wall thickness vary across the vasculature to withstand local loads.[44,46] Integration of closed-loop boundary conditions, appropriate assignment of wall properties, and fluid-structure interaction are necessary for accurate prediction of mechanical stimuli in CABG simulations.

Wall Shear Stress

Wall shear stress in grafts was previously investigated invasively using Doppler flow wire velocimetry, area measurements from angiography, and wall shear computed with a Poiseuille flow assumption.[101] Results confirmed elevated shear stress of $16 \pm 4 dyn/cm^2$ for an IMA compared to $4.8 \pm 1.6 dyn/cm^2$ for an SVG, in patients with low-grade stenosis ($50 - 75\%$) in the native coronary arteries. The respective values for high-grade stenosis ($> 75\%$) were $13.7 \pm 4.9 dyn/cm^2$ for an IMA and $4.6 \pm 2.0 dyn/cm^2$.[101] Mean values of shear stress from our simulations not only mimic the observed qualitative trend of lower shear stress in SVGs compared to IMAs, but are comparable quantitatively. Low wall shear is also known to correlate with atheroprone regions in blood vessels. Our findings agree with these observations, revealing that venous grafts have larger regions (with higher A_{athero}) where the graft is exposed to pathologically low WSS ($< 4 dyn/cm^2$) compared to arterial grafts. This conclusion did not change with different cutoff values for low WSS. Notwithstanding the absence of heart wall motion in our simulations, our findings are consistent with previous invasive measurements, clinical observations, and long-term outcomes on venous grafts. The large difference in WSS between arterial and venous grafts suggests that WSS may be a primary indicator of differential risk for vein graft failure that should be correlated with long-term clinical outcomes in future studies. While there are significant differences in both TAWSS and graft diameter, the increase in diameter alone is not sufficient to predict the difference in TAWSS between arterial and venous grafts. A larger study with outcome data will be necessary to determine any

correlation between graft diameter, flow, material property and measured outcomes.

Oscillatory Shear Index

Oscillatory shear index is a measure of oscillatory component in the flow. Regions of disturbed and recirculating flow, which have high oscillatory flow components, are known to disturb the endothelial lining, upregulate inflammatory pathways, and cause intimal hyperplasia in the vessel wall, which in turn creates conditions conducive to long term atherosclerosis.[8] The venous and arterial grafts in our study did not exhibit significantly different OSI values. This is unsurprising when considering the similarity in curvature in both graft types, and the similarity in imposed pressure differences (systemic minus coronary) driving flow through the graft, which is the primary determinant of oscillatory flow.

Wall Strain

It is known that circumferential stress plays a primary role and WSS plays a secondary role in graft remodeling.[27] Mechanical stress/strain are known to alter the structure and function of wall constituents such as smooth muscle and reprogram gene expression, differentiation, migration, proliferation and apoptosis. Due to its influence on multiple functions, the role of strain and its underlying molecular mechanisms have been hard to elucidate in normal and pathological conditions. Nonetheless, our finding that strain is significantly lower in venous grafts compared to arterial grafts (Figure 3.5) emphasizes the need to probe the role of circumferential strain in

future studies on the long-term adaptation of grafts. We note that it is the structural stiffness (combined effect of Youngs modulus and thickness), and not material stiffness (Youngs modulus) alone, that determines the final strain state and hemodynamics in a vessel.

Furthering models to incorporate biological response

Venous coronary bypass grafts experience pressures of approximately 20 times and flows of 4 times their native environment, often leading to maladaptive response. While CFD tools enable quantification of the mechanical environment, one needs models of growth and remodeling to understand the underlying pathophysiology of maladaptation and correlate directly with clinical outcomes data on graft failure rates. Chapter 2 and 4 describe ways of incorporating cellular level details into mechanics based models to capture growth and remodeling behavior of grafts in the presence of altered hemodynamics.[75,102] Translation of these models requires patient-specific inputs from CFD simulations.

3.6 Limitations

The simulation methodology for coronary simulations has a few limitations. First, coronary wall motion is a superposition of radial motion due to pressure changes and translational motion imposed by the moving heart wall.[103] Effects of translational motion were not considered, and would require more computationally expensive methods, as well as time-resolved CT data with increased radiation doses. Because the

majority of coronary flow occurs during diastole, when wall motion is minimal, we felt justified in this assumption. Second, although the pathophysiological mechanisms of graft failure are not fully understood, it is known that the interplay between local hemodynamics and vascular biology determines long term outcome of the graft. Our CFD models lack the cellular and sub-cellular details required to capture the evolving nature of graft adaptation and subsequent disease progression. As evident in chapter 2 and 4, current efforts are directed towards development of mechanics based models of vascular growth and remodeling.[102] Third, while the boundary conditions were tuned to patient specific data, material properties and blood viscosity were not patient specific. These limitations could potentially be overcome in future work through the incorporation of IVUS or OCT data and patient specific hematocrit measurements. Fourth, the number of subjects and grafts studied in this pilot study was relatively small. This was in large part due to the significant time currently required for model construction and simulation. Current efforts are geared towards accelerating the model building and simulation processes through integration of machine learning and automation algorithms.[104] Finally, the tuning process was manual and did not account for uncertainty in the input parameters or the clinical targets. In addition, manual tuning does not lend itself well to addition of more targets, when more clinical measurements are available, or parameters, when the models are more sophisticated. The tuning pipeline is inconveniently long (Figure 3.2). All these factors impose hurdles to application of these tools to large patient cohorts. An automatic approach (combining parameter identifiability and Bayesian estimation) to

determine optimal LPN parameters for coronary artery simulations from non-invasive clinical targets, and to quantify their variability due to both clinical data uncertainty and the presence of non-identifiable parameter combinations was proposed recently. Recent efforts have also been directed towards systematic parameter estimation and uncertainty quantification, which could streamline the tuning process in CABG simulations.[105]

The LPN used in this work is 'passive' in nature, that is, it does not account for the metabolic feedback and adrenergic feedforward control of coronary blood flow that occur during variations in the cardiac workload. The framework can be extended to include these effects and is much required to model the effects of exercise or disease.[106] In an LPN since geometry is not explicitly defined, wave propagation effects are not incorporated in lumped parameter models. The coupling between LPN and the resistance and compliance of the 3D model could impose hurdles to simulation of patient-specific geometries, especially in disease. Specifically, there could be physiological values of modulus and thickness for which the 3D properties could dominate the flow and pressure solutions and, theoretically, an LPN might struggle / be incapable of hitting the non-invasive targets from clinic. This further emphasizes the need for novel boundary conditions and systematic sensitivity studies with LPN and wall properties. The calcifications on the native coronaries pose challenges to model building and meshing. One could use angio images or non contrast images in conjunction with contrast enhanced CT images to identify calcified regions in the natives. The calcifications and the 'blooming effect' associated with it introduces

uncertainty in image segmentation. Again there is a need for systematic uncertainty quantification in these simulations.

3.7 Acknowledgements

Authors wish to thank Prof. Andrew Kahn for providing clinical inputs to this work. Simvascular open source software was a critical component of this work and we want to thank the Simvascular 2.0 development team - Hongzhi Lan, Adam Updegrove, Daniele Schiavazzi, Nathan Wilson, Prof. Shawn Shadden, and Prof. Alison Marsden for keeping the code functional.

Chapter 3, in full, is a reprint of the material as it appears in " Patient-Specific Simulations Reveal Significant Differences in Mechanical Stimuli in Venous and Arterial Coronary Grafts", *Journal of Cardiovascular Translational Research*, 9:279290, 2016. Authors are Ramachandra, A. B., Kahn, A., & Marsden, A. L.. The dissertation author was the primary investigator and author of this paper.

Chapter 4

Growth and Remodeling Simulations in a Vein Graft

4.1 Material characterization of native vein

Experiments suggest that strain energy functions (W), within the context of pseudo-elasticity, adequately describe the passive behaviour of veins.[77,107] A recent study showed that a four fiber family model for collagen plus a neo-Hookean model for elastin could reasonably describe the full passive experimental dataset and predict the inflation/extension response of porcine veins outside the data range employed for parameter identification.[107] Another study, using uniaxial tension tests on arteries and veins in a rat, speculated that similar constitutive models may be valid for arteries and veins.[9] Motivated by these two studies, the constitutive relations (though not the specific parameter values) used to model structural constituents within venous

wall are similar to those used previously for arterial G&R.[23,24,75] The strain energy function for both collagen and smooth muscle is defined by the well known 'Fung-type' exponential function:

$$\widehat{W}^k = c_1^k \left(e^{(c_2^k((\lambda^k_{n(\tau)})^2-1)^2} - 1 \right), \tag{4.1}$$

where, c_i^k are material constants, the superscript k represents the collagen fiber family or smooth muscle. $\lambda^k_{n(\tau)}(s) = G_h^k \lambda(s)/\lambda(\tau)$ is the stretch of constituent k, that was deposited within the mixture with prestretch G_h^k at instant τ.[23,75] G_h^k represents the stretch at which constituent k is deposited into the mixture and represents one of the major assumptions of the model.

Vascular elastin is assumed to be isotropic and exhibit a neo-Hookean-type response,[75,108] hence

$$\widehat{W}^e = \frac{c^e}{2}(\lambda_\theta^2 + \lambda_z^2 + \lambda_r^2 - 3), \tag{4.2}$$

where c^e is a material constant. These constitutive relations are phenomenological in nature, that is, they describe responses observed in passive mechanical experiments such as biaxial tests. They have successfully captured the passive anisotropic, nonlinear biaxial behavior of a vein.[30,102,107]

Segments of inferior vena-cava of wild-type C57BL/6 mice were previously subjected to pressure-diameter tests at multiple axial stretch values to capture the passive biaxial behaviour.[30] The circumferential (λ_θ) and axial stretches (λ_z) were measured and the radial stretch (λ_r) was computed using the incompressibility con-

straint. The stretch $\lambda^k(\tau)$ experienced by fibers is computed as

$$\lambda^k(\tau) = \sqrt{\lambda_z(\tau)^2 \cos^2 \alpha_0^k + \lambda_\theta(\tau)^2 \sin^2 \alpha_0^k}, \tag{4.3}$$

where α_0^k is the angle between the fiber and the z-axis in a common reference configuration for the mixture; α_0^k is 0° for the axial component and 90° for circumferential components. The angle for the diagonal family of collagen (α_0^{diag}) was determined through parameter estimation.

Assuming the tests were quasi-static and the response was passive, the constitutive equations and equilibrium equations together yield

$$P(s)a(s) = T_\theta(s) = \lambda_\theta \sum \frac{\partial W^k}{\partial \lambda_\theta}, \tag{4.4}$$

and

$$\frac{f(s)}{\pi(2a(s) + h(s))} = T_z(s) = \lambda_z \sum \frac{\partial W^k}{\partial \lambda_z}, \tag{4.5}$$

where $T_i = \sigma_i h$ are the principal intramural tensions in the θ and z directions, P is the transmural pressure and f the applied axial force. These relations are later used to determine the passive constitutive parameters of the murine vena cava.

Contributions of the circumferential collagen family and smooth muscle are physically indistinguishable, hence the material constants representing both these constituent families were modeled together. The coefficients of the two diagonal collagen families were constrained to be the same to impose symmetry and avoid twisting

of the vessel along the longitudinal axis due to pressurization. Hence the proposed constitutive equation for the passive behavior has eight unknown parameters: c_1^z, c_2^z, c_1^θ, c_2^θ, c_1^{diag}, c_2^{diag}, c^e and α_0^{diag}.

A normalized cost function,

$$\mathcal{J} = \sqrt{(\frac{\sigma_z^{exp} - \sigma_z^{mod}}{\sigma_z^{exp}})^2 + (\frac{\sigma_\theta^{exp} - \sigma_\theta^{mod}}{\sigma_\theta^{exp}})^2}, \tag{4.6}$$

was minimized to identify the set of material parameters that best-fit the experimental data (superscripts *exp* and *mod* indicate values calculated from experiment and model, respectively). A pattern search class of derivative-free optimization algorithms, described in Chapter 2, was used to find the optimum set of parameters for the constitutive equations (4.1) and (4.2). The optimal set of material parameters for the normal wall are reported in Table 4.1. The best curve fit ($\mathcal{J} \approx 0.15$) for the passive biaxial experiment is shown in Figure 4.1. The contribution from the circumferential family was relatively small and the contribution of the stiffer diagonal fiber family dominated at high stretch ratios. This trend is consistent with prior results reported in the literature for veins.[9,109] These material parameters were held fixed in all subsequent numerical experiments, described below.

Table 4.1: Material coefficients estimated from the biaxial test, using the SMF algorithm

coefficient	$c_1^z(kPa)$	c_2^z	$c_1^\theta(kPa)$	c_2^θ	$c_1^{diag}(kPa)$	c_2^{diag}	$c^e(kPa)$	α_0^{diag}
value	24.0220	0.1000	1.000	0.0503	0.0712	1.0350	1.0	36.60^o

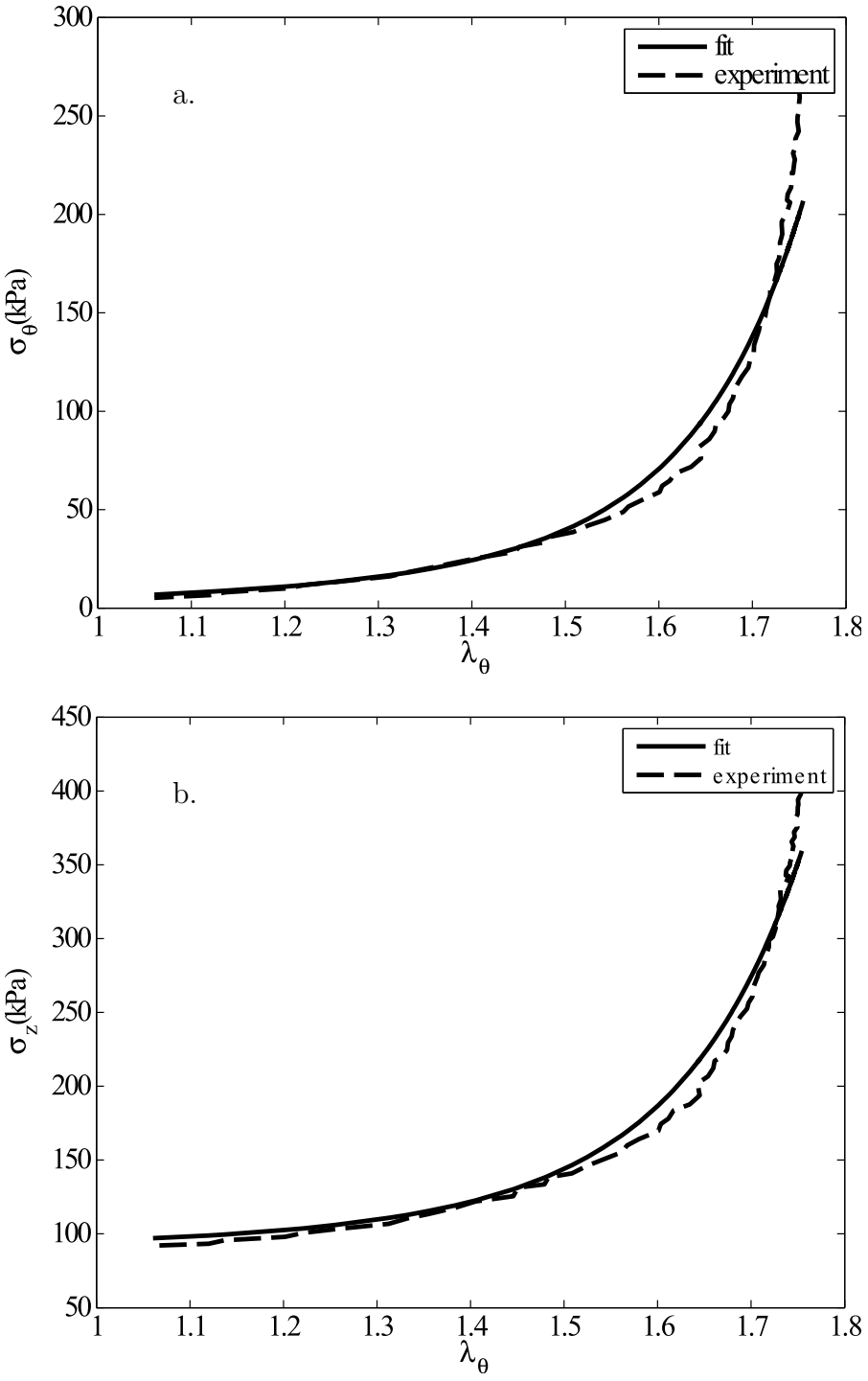

Figure 4.1: Biaxial stress - stretch data (dashed lines) for a mouse vena cava and the associated best-fits achieved in the parameter estimation : (a) $\sigma_\theta - \lambda_\theta$, (b) $\sigma_z - \lambda_\theta$.

4.1.1 Parameter estimation and bounds

Absence of experimental data makes parameter estimation within G&R model challenging. We determine them in stages. We broadly classified parameters into following categories: passive, gain, half life, prestretch, and prescribed. Passive material properties were determined by curve fitting published biaxial experimental data for a murine vena cava[30,102] as outlined in section 4.1. These parameters were then held fixed for subsequent parameter estimations and G&R simulations (Figure 4.2). Some parameters needed to model the G&R can be measured directly (e.g., constituent mass fractions) or inferred (e.g., homeostatic stresses and pressure) from data (Table 4.2) and were prescribed. We used the Surrogate Management Framework (SMF)[89,93] to determine the remaining G&R parameters. Parameter bounds for optimization were chosen consistent with the literature or simply biologically reasonable when data was lacking[75,110,111] (Table 4.2).

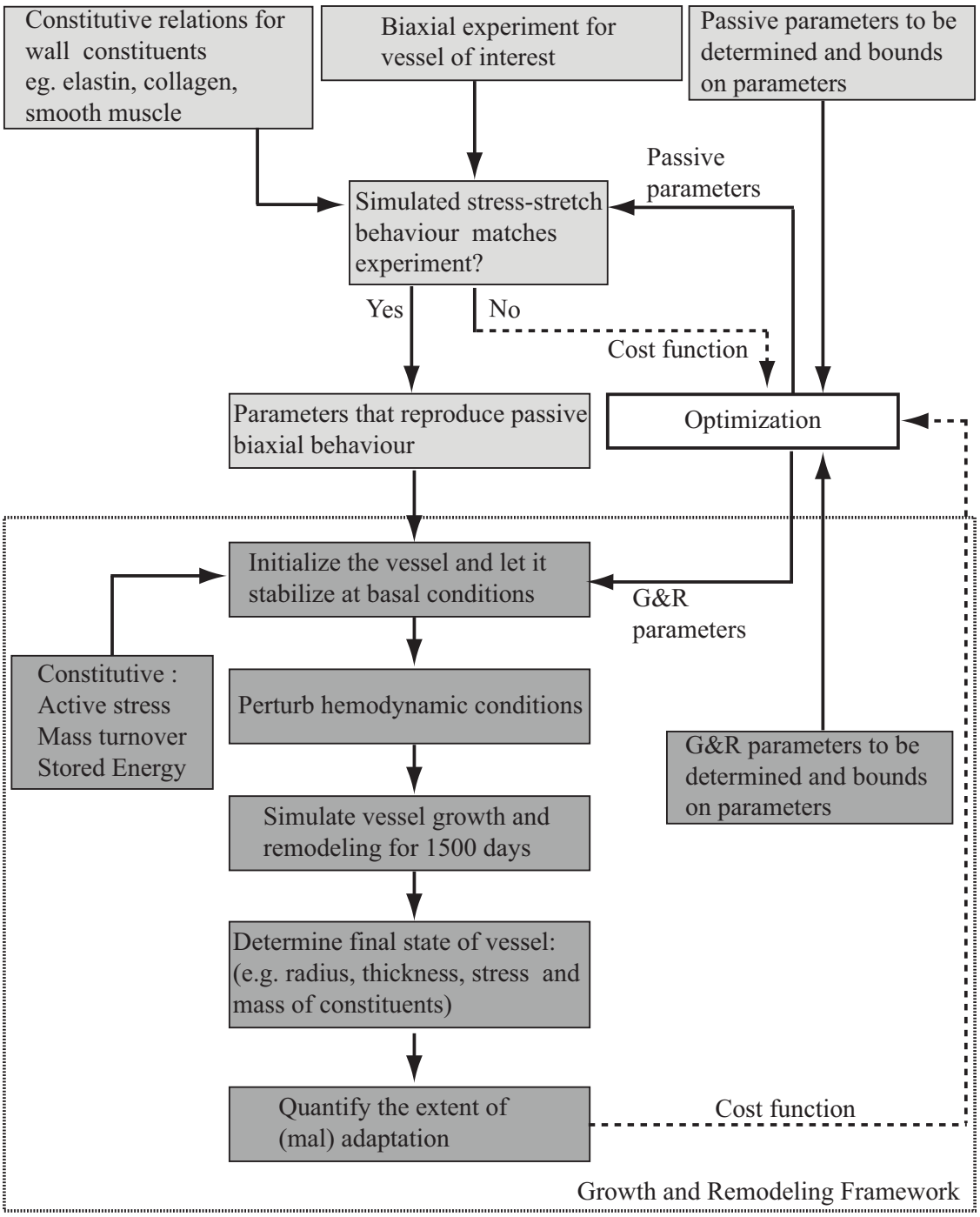

Figure 4.2: Framework demonstrating a general approach for parameter estimation and simulating adaptation in a blood vessel. Parameter estimation is accomplished in several serial steps and optimization is used to accelerate the process.

Table 4.2: Parameters for G&R optimization and their prescribed bounds

Component	Parameter	Lower bound	Upper bound
Collagen gain ($\Delta\sigma_\theta$)	K_1^c	0.1	20
Collagen gain ($\Delta\tau_w$)	K_2^c	0.1	20
SMC gain ($\Delta\sigma_\theta$)	K_1^m	0.1	20
SMC gain ($\Delta\tau_w$)	K_2^m	0.1	20
Collagen half life	$\frac{1}{K_h^c}$ (days)	1	100
SMC half life	$\frac{1}{K_h^m}$ (days)	1	100
Collagen Prestretch	G_h^c	1.01	2
SMC Prestretch	G_h^m	1.1	1.8
Elastin Prestretch - θ direction	$G_{h,\theta}^e$	1.5	2
Elastin prestretch - z direction	$G_{h,z}^e$	1.5	2

4.2 Altered Pressure

The cell-mediated G&R model, explained in methods section, was used to simulate the 1-year evolution of a vein subjected to increased pressure. Note that these simulations were run without the pre-multiplier on the mass production equation and with tension-dependent degradation on collagen and smooth muscle. Biologically, a vessel tries to evolve towards target homeostatic values of stress during adaptation.

To model this behaviour, we minimized a normalized cost function

$$\mathcal{J}_{adapt} = \sqrt{(\frac{\tau_w^h - \tau_w}{\tau_w^h})^2 + (\frac{\sigma_\theta^h - \sigma_\theta}{\sigma_\theta^h})^2} \tag{4.7}$$

using the SMF optimization algorithm to determine the best adaptation to a given pressure perturbation ($\gamma = P/P_0$, where P_0 is the average pressure in the vessel's native environment). The (mal)adaptation of the vein to an increase in hemodynamic load was analyzed systematically using numerical experiments which are elaborated in the paragraphs below.

4.2.1 Numerical Experiment 1

The purpose of numerical experiment 1 was to subject the vein to successively higher pressure perturbations and to identify through optimization the parameter values that allowed best adaptation ($\mathcal{J}_{adapt}$) individually for each level of perturbation. Optimization was re-run for each pressure increase from $\gamma = 1.5$ to $\gamma = 20$. Figure 4.3 shows the resulting evolution of luminal radius and wall thickness for the optimized parameters. The thickness evolution curves (Figure 4.3) revealed increasingly larger deviations from an ideal adaptation with increasingly larger pressure perturbations. Overall, the vein graft response was suboptimal for increases as small as $3P_0$. That the optimal gain parameters were consistently high indicated the need for enhanced mass production to combat the increased wall stress resulting from the increased pressure. At every pressure, the circumferential gain parameter saturated at the upper bound

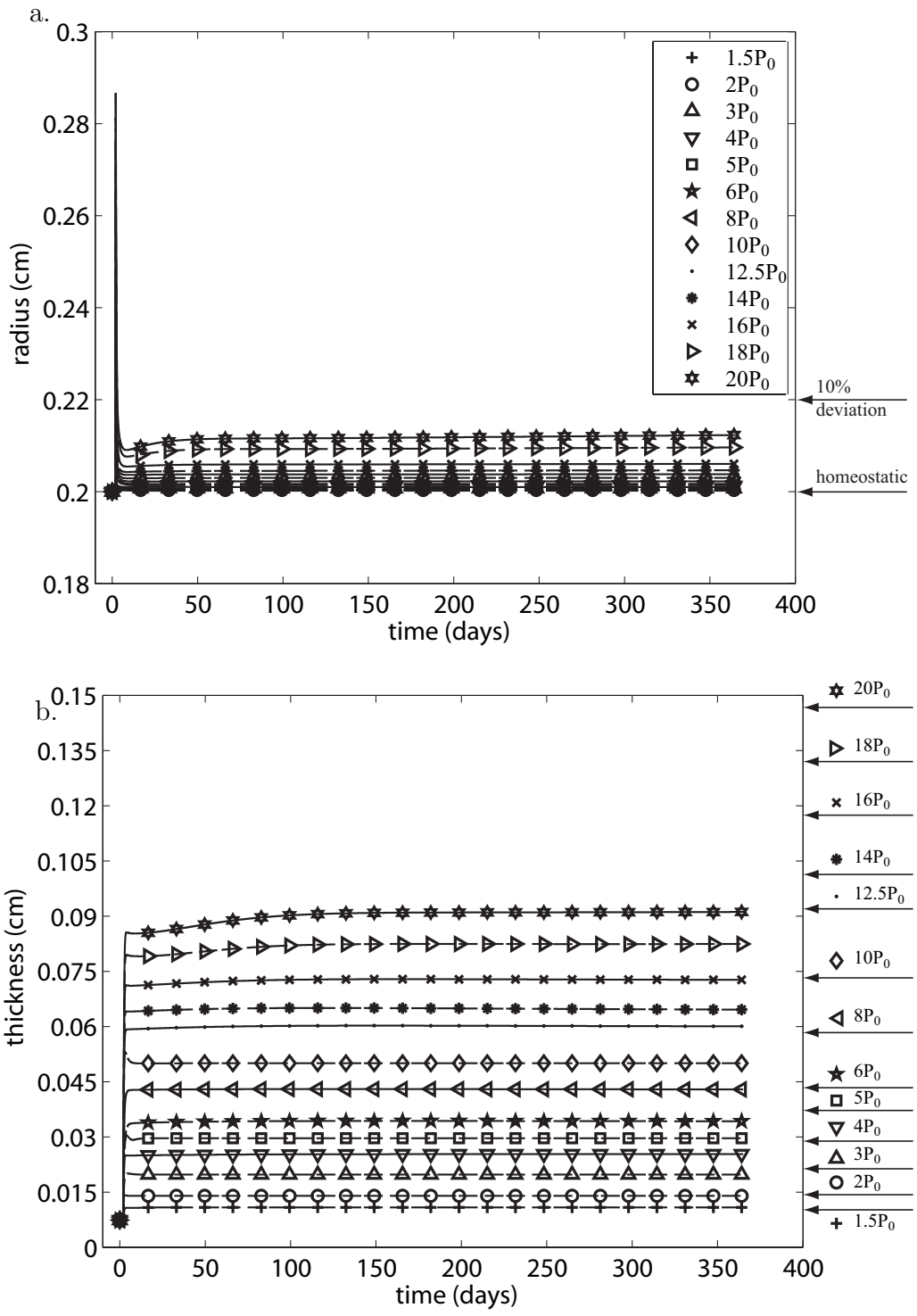

Figure 4.3: Summary of (a) radius and (b) thickness evolution with time for K_1^k & $K_2^k \leq 20$ and $G_h^m \leq 1.8$. The radius curves are within a 10% deviation. The arrows indicate the thickness for an ideal adaptation. Thickness curves exhibit a larger deviation from an ideal adaptation for a larger pressure.

and the half life of the constituents dropped as low as ≈ 1 day for some cases. The half lives affected the evolution of radius and thickness, but did not affect the final state of the vessel. The SMC prestretch values were also consistently high and near the upper bound while the collagen prestretch values were comparable to arteries. The adaptations were most sensitive to the collagen prestretch (G_c^h) followed by the SMC prestretch (G_m^h) and the gain parameters. Elastin prestretch was found to have negligible effect on the adaptation.

4.3 Altered Pressure and Flow

Table 4.3: Parameters used in G&R simulations. Prescribed: Parameters determined from literature, prior G&R models or fixed to biologically reasonable value, when published data was not available. Experimentally-determined (passive): material coefficients estimated, using the SMF algorithm,[102] from published biaxial test on a murine vena cava.[30] Optimization: G&R parameters determined through minimization of $\mathcal{J}_{adapt}$ for moderate perturbations in load ($\gamma = 1.5$ and $\epsilon = 1.1$).

Prescribed:

Muscle activation parameters:[84] $\lambda_m = 1.35$, $\lambda_0 = 0.5$

Vasoactive parameters:[75] C_B=0.68, C_S =20C_B, $\frac{1}{K^{act}} = 20$ days (unless noted otherwise)

Initial Mass fractions:[112] $\phi_0^c = 0.42$, $\phi_0^e = 0.10$, $\phi_0^m = 0.48$

Homeostatic values:$\sigma_\theta^h = 18$ kPa, $\tau_w^h = 0.6$ Pa,[113]$P_0 = 5$ mmHg = 0.67 kPa

Elastin prestretch: G_h^e=1.75

– –

Experimentally Determined:[102]

$c_1^z = 24.0220$ kPa, c_2^z=0.1000, c_1^θ =1.000 kPa,

c_2^θ =0.0503, c_1^{diag}=0.0712 kPa, c_2^{diag}=1.0350, c^e=1 kPa

– –

Optimized:

K_1^c =0.01, K_2^c =8.006, K_1^m =2.009, K_2^m =6.007

G_h^c =1.039, G_h^m=1.31, T_{max} =10.9kPa, $\frac{1}{K_h^c} = 100$ days, $\frac{1}{K_h^m} = 1.11$ days

---

4.3.1 Numerical Experiment 2: Moderate load

We expect a vein to adapt well to modest-to-moderate perturbations in hemodynamic load. Since we were interested in geometric remodeling, not vasoactive changes in geometry, we chose $\gamma = 1.5$ and $\epsilon = 1.1$ as representative upper range values for moderate perturbations. By minimizing the cost function (equation 4.7), we identified G&R parameters that led to an optimal adaptation (Table 4.3) under moderate perturbation. We kept these parameters fixed for the remaining numerical experiments.

Initial optimization results showed that values of radius and thickness at 1500 days were suboptimal using mass constitutive relations derived from a healthy artery,[102] regardless of the choice of parameters for optimization and their bounds. In contrast, optimization identified a near optimal adaptation (Figure 4.4) with a pre-multiplier form of the mass production equation (equation 2.9).[114] Based on these findings, we concluded that an optimal adaptation, even to a moderate perturbation in hemodynamic load, is dominated by the rate of mass turnover of its structural constituents. Thus, the pre-multiplier form of mass production equation (equation 2.9) was used in all subsequent simulations.

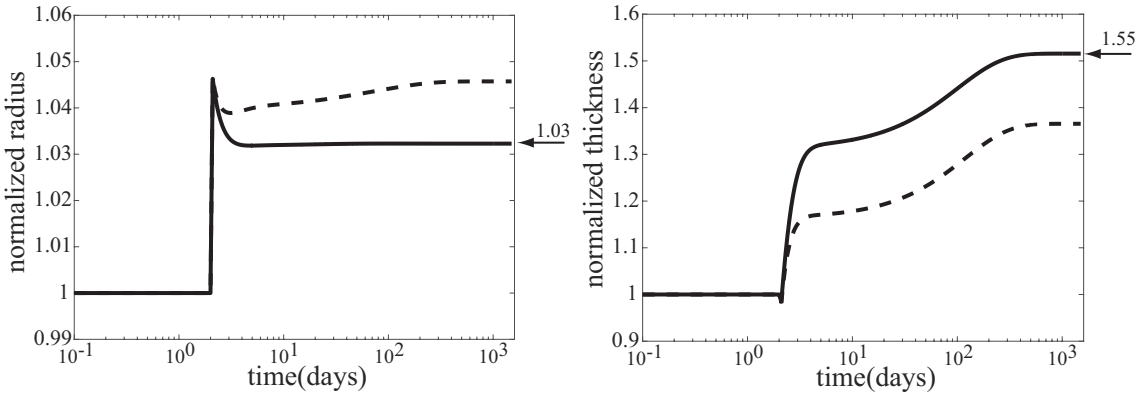

Figure 4.4: Evolution of radius and thickness for a moderate perturbation in load, $\gamma = 1.5$ (fold pressure increase) and $\epsilon = 1.1$ (fold flow increase). Arrows indicate values for an ideal adaptation in a standard thin walled cylindrical geometry: $a = \epsilon^{\frac{1}{3}} a_h$ and $h = \epsilon^{\frac{1}{3}} \gamma h_h$.[115] We classify a converged simulation as optimal if it reaches the theoretical radius and thickness value, or suboptimal otherwise. The adaptation was optimal (solid line) with mass pre-multiplier term and suboptimal (dashed line) otherwise. Radius and thickness are normalized against homeostatic values, a_h and h_h.

4.3.2 Numerical Experiment 3: Combined loads (moderate to severe)

To recapitulate a vascular bypass graft scenario we subjected the numerical vein to a series of increasing combined loads, from venous to arterial conditions: $\gamma \in [1.0, 20.0]$ and $\epsilon \in [1.0, 4.0]$. We sampled 300 points from the $\gamma - \epsilon$ space, with approximately 75 points in each quadrant (with origin at $\epsilon = 2.0$ and $\gamma = 10.0$), and simulated adaptations for up to 1500 days at each of the load combinations (Figure 4.5). Failed simulations clustered in the upper right corner of the $\gamma - \epsilon$ space, with failure defined as an inability to satisfy the equilibrium equation at every time step in the simulation.

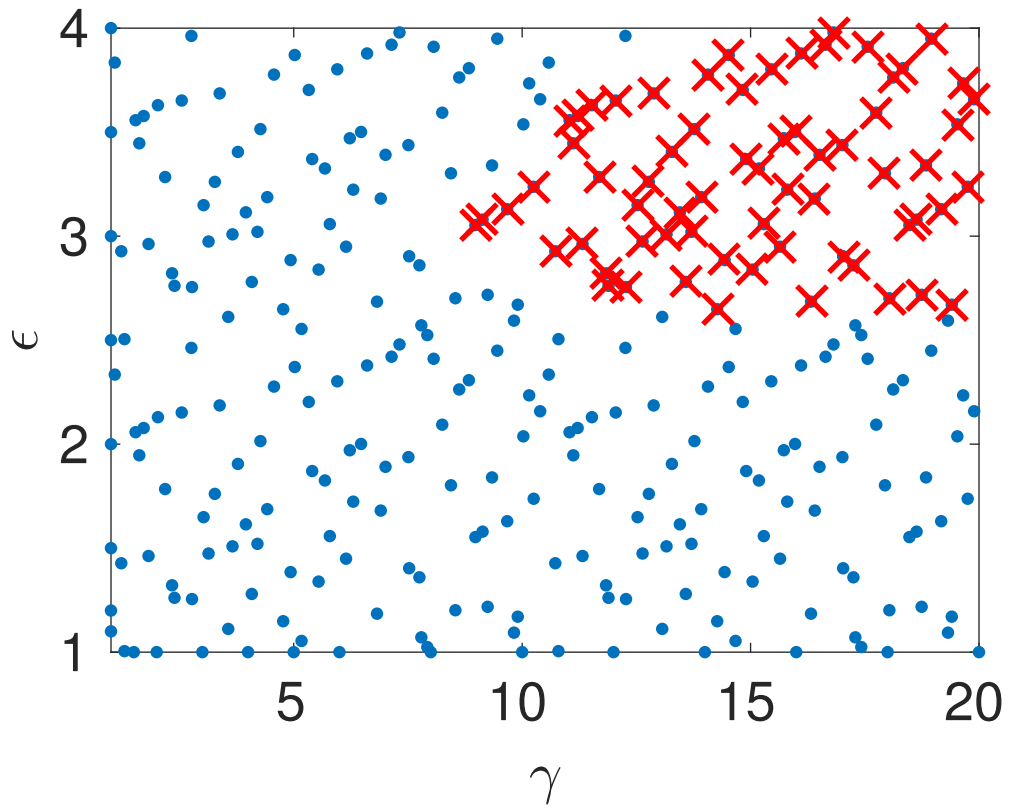

Figure 4.5: Failed points in $\gamma - \epsilon$ load space, where γ is the fold increase in pressure above homeostatic and ϵ is fold increase in flow. 'X'- indicates a failed simulation and '.' indicates a simulation that successfully converged. Failed simulation is defined as failure to satisfy the traction equilibrium equation. Note the clustering of failed points in the top right corner of $\gamma - \epsilon$ load space.

Veins typically failed during the first few days after hemodynamic perturbation, which motivated us to probe vasoactive changes since they can be immediate. While exploring possible mechanisms of failure, an altered rate of tonic adjustment (K^{act}) enabled successful adaptations, that is, equilibrium was successfully established at every time step in the simulation (Figure 4.6). All simulations on the $\gamma - \epsilon$ grid converged for values of $K^{act} > 1/3day^{-1}$. The cost function distribution in $\gamma - \epsilon$ space for $K^{act} = 1/3day^{-1}$ is depicted in Figure 4.7; it represents the deviation of stress from a homeostatic value. This figure reveals that adaptations are flow limited.

Juxtaposing $K^{act} = 1/3day^{-1}$ with values for two cerebral arteries ($1/20day^{-1}$ and $1/6day^{-1}$),[26,75] we infer that venous adaptation at severe loads is impaired by the vein's ability to maintain or rapidly evolve the smooth muscle tone.

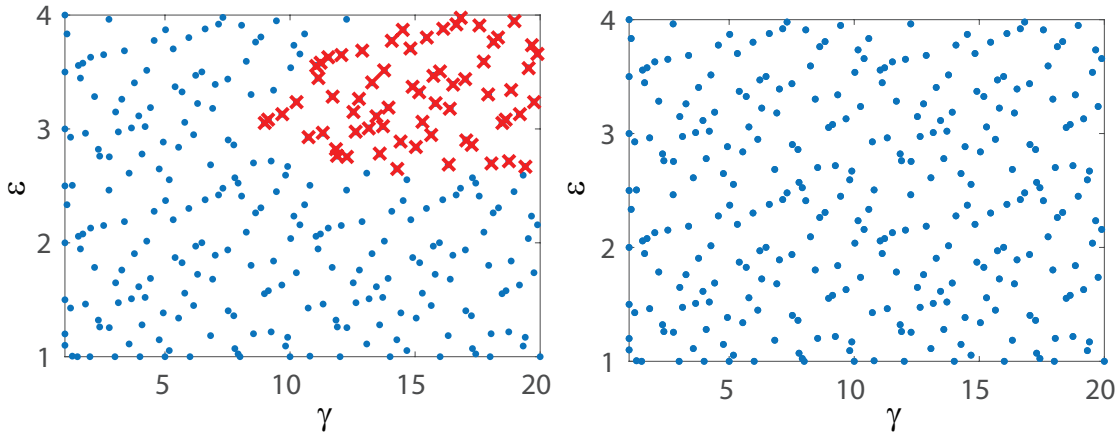

Figure 4.6: Changes in adaptive capacity with different values of smooth muscle tone - $K^{act} = 1/20day^{-1}$ (control, left panel) and $K^{act} = 1/3day^{-1}$ (right panel). An altered rate of tonic adjustment ($K^{act} = 1/3day^{-1}$) enabled successful adaptations in the entire $\gamma - \epsilon$ load space. 'X'- indicates a failed simulation and '.' indicates a simulation that converged successfully.

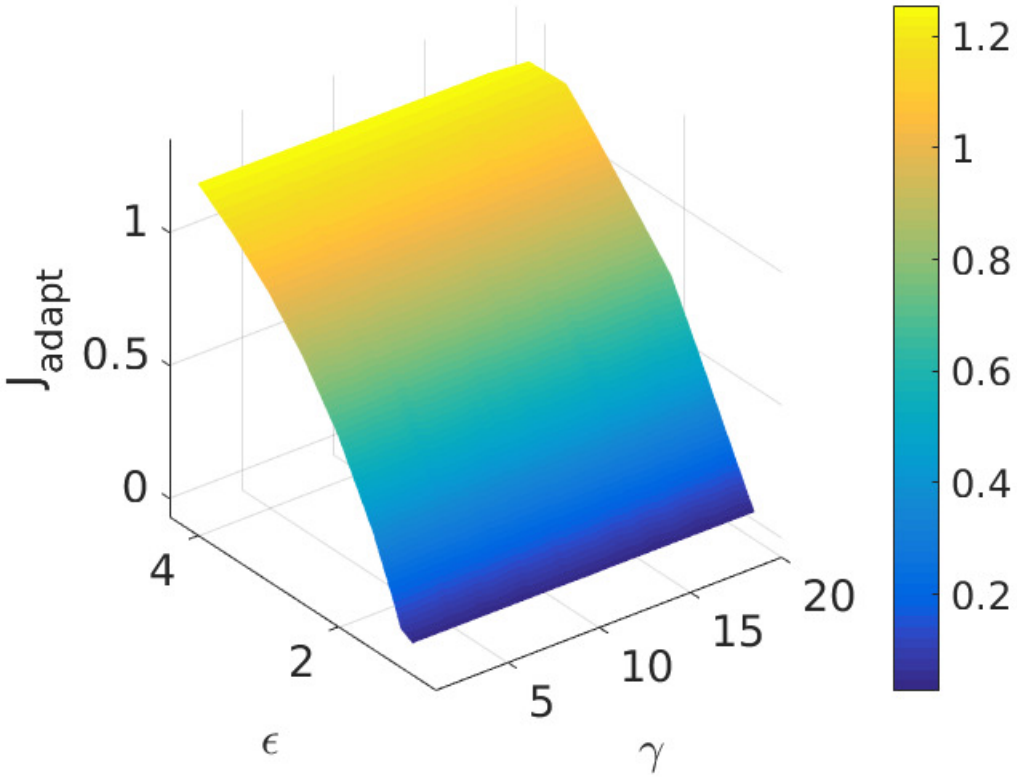

Figure 4.7: Interpolated surface plot of cost function as a function of $\gamma - \epsilon$ loads, with a modified vasomotor evolution rate of $K^{act} = 1/3day^{-1}$. Cost function (J_{adapt}) is a measure of deviation from venous homeostatic value. Adaptation is predominantly flow limited.

In summary, results from this numerical experiment led us to conclude that endowing a vein with enhanced mass production and vasomotor capabilities can ameliorate maladaptation, even at severe loads.

4.3.3 Step versus Gradual loading

The purpose of step versus gradual load experiments were to test the hypothesis that a gradual, compared with a step, change in load would extend the adaptive capacity of the vein. To evaluate potential benefits of a gradual change in load and to

understand the interplay between different factors affecting adaptation, we performed simulations at the same 300 sampled (γ,ϵ) combinations for the following conditions:

(a) gradual change in pressure over 3 days, but a step change in flow

(b) step change in pressure, but a gradual change in flow over 3 days

(c) gradual change in pressure and flow over 3 days

(d) gradual change in pressure and flow over 8 days

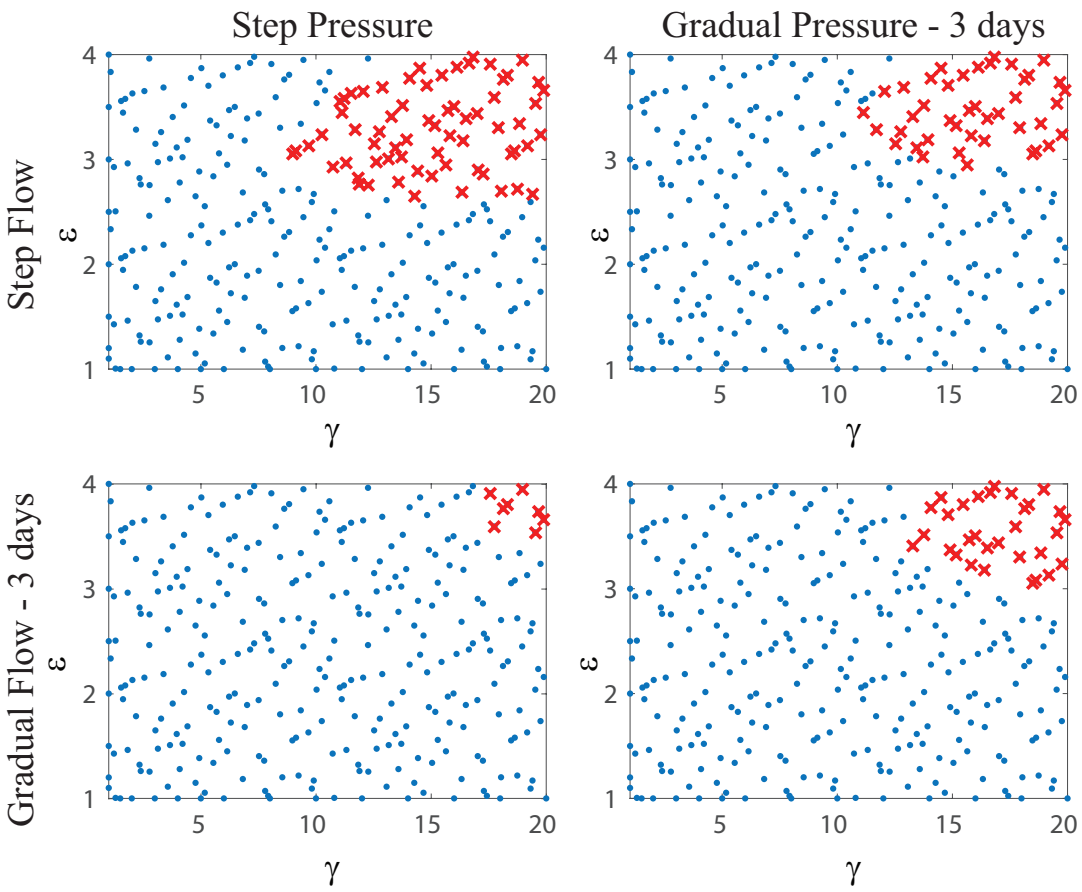

Figure 4.8: Failed simulations in the $\gamma - \epsilon$ load space for four scenarios of loading- a) step pressure and flow (control), b) step pressure and gradual flow, c) gradual pressure and step flow, and d) gradual pressure and gradual flow. Gradual load was applied as a linear ramp in load over 3 days. Note that a gradual change in flow and a step change in pressure had fewer failed points than other scenarios. 'X'- indicates a failed simulation and '.' indicates a simulation that successfully converged.

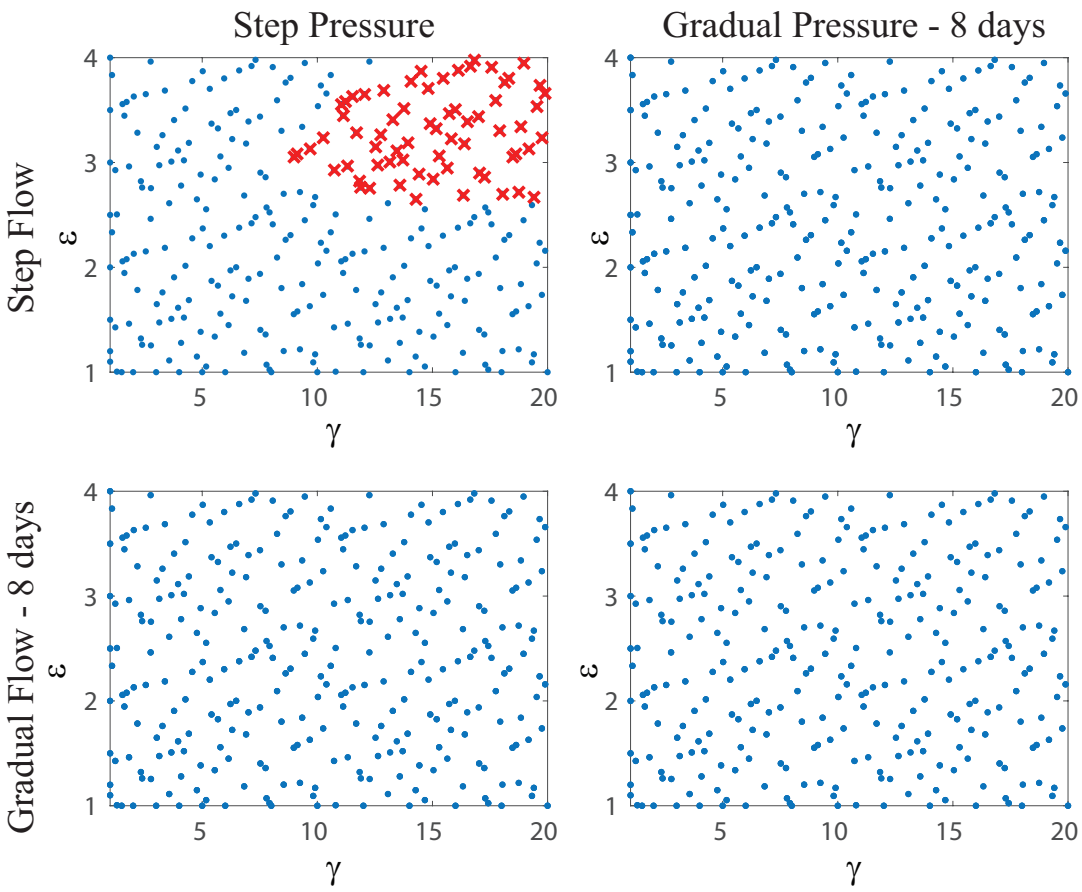

Figure 4.9: Failed simulations in the $\gamma - \epsilon$ load space for four scenarios of loading- a) step pressure and flow (control), b) step pressure and gradual flow, c) gradual pressure and step flow, and d) gradual pressure and gradual flow. Gradual load was applied as a linear ramp in load over 8 days. The gradual change cases had no failed simulations. 'X'- indicates a failed simulation and '.' indicates a simulation that successfully converged.

Note that the pre-multiplier form of mass production (equation 2.9) but $K^{act} = 1/20 day^{-1}$ (more conservative) were used for these simulations. Results for cases (a), (b) and (c) are summarized in Figure 4.8 together with results from a step change in pressure and flow (as used for Figures 2-6). Overall, the gradual load cases have fewer failed points than a combined step change in load (Experiment 2). Counter-intuitively, gradual flow accompanied by a step change in pressure (case (b)) had the

lowest number of failed points, fewer than the gradual change in flow and pressure (case (c)). All simulations fully converged when the gradual load was applied over 8 days (case (d), Figure 4.9). Results from this numerical experiment led us to conclude that a gradual change in load can mitigate maladaptation, even with a non-optimal evolution of active properties.

4.4 Discussion

Blood vessels respond to sustained changes in hemodynamic loads by modulating the turnover of their wall constituents to restore the homeostatic mechanical environment, often represented in terms of stresses.[13,80,110,116] It is well known that blood vessels change their caliber in response to changes in flow and increase their wall thickness in response to increased pressure.[75,117] Recall that the wall shear and circumferential stress in a cylindrical vessel are given by $\tau_w = 4\mu Q/\pi a^3$ and $\sigma_\theta = Pa/h$, respectively, where a is the inner radius and h the thickness. Hence, for changes in flow ($Q = \epsilon Q_h$) and pressure ($P = \gamma P_h$), if homeostatic stress values are restored, we expect $a \to \epsilon^{\frac{1}{3}} a_h$ and $h \to \epsilon^{\frac{1}{3}} \gamma h_h$.[115] Thickness and radius are clinically observable quantities and probably the most useful indicators of adaptivity, so, although our optimization used stress-based cost functions to determine the best parameters, we used radius and thickness as indirect measures of adaptation in our simulations.

In cases where homeostasis is achieved, the vessel reaches a new equilibrium state in which production balances removal. In other cases, however, such changes

may be maladaptive. Our results for altered pressure with no pre-multiplier on mass production function suggest that a vein can adapt to modest changes in blood pressure, but its adaptive capacity appears limited (Figure 4.3). Because of its elasticity, the vein distends upon pressurization, which decreases wall shear stress and increases mean circumferential stress. Both changes in stress should thus initiate a mechanobiologically driven G&R process, provided that the endothelial and smooth muscle cells/fibroblasts remain functional. Due to an early adjustment in vascular tone, the radius was quickly restored to its homeostatic value. A simple force balance indicates, in an ideal adaptation, that the increase in thickness should be proportional to the increase in pressure. The venous adaptation (Figures 4.3) was found to be suboptimal, without pre-multiplier term in mass production equation, for pressure perturbations as small as $\gamma = 3$, well below the $\gamma > 20$ expected in a typical vein graft procedure. Since the parameter bounds for optimization were biologically motivated and the target values for adaptation were for a venous system, these results suggest that the venous wall has a limited capacity to respond adequately to a dramatic increase in pressure. In other words, clinical observations of maladaptation should not be surprising.

We evaluated possible venous adaptations to perturbed hemodynamic conditions, ranging from venous (modest) to arterial (severe) loads, in the presence of altered pressure and flow. We uncovered two plausible mechanisms leading to maladaptation: a) an impaired mass production of constituents and b) an inability of smooth muscle to maintain or rapidly evolve its tone. Both findings are intuitive

particularly given previous experimental[117] and computational[75] studies that show complementary roles of vasoactivity and matrix turnover. Nevertheless, this is the first study to confirm this representation based on vein-specific parameters. The finding that mass production must be augmented (via the pre-multiplier in equation 2.9) further shows the importance of heightened turnover in the severe case of vein grafting, hence requiring either proliferation of resident intramural cells or recruitment of inflammatory cells that promote matrix synthesis.

We also found ways to mitigate maladaptation. Venous adaptations to a gradual change in flow over 3 days plus an initial step change in pressure were shown to have fewer maladaptations compared to step changes in pressure and flow or even a gradual change in pressure and flow over 3 days. In addition, a gradual change in flow and pressure over 8 days enabled a successful venous adaptation for loads as severe as the arterial loads. This finding is intuitive and emphasizes that vessels have tremendous potential for adaptation, but there are limitations on how fast and how much.

Qualitative comparison with experimental data

While knowledge of the homeostatic state can suggest the final state of an adaptation,[115] cell-mediated G&R models can shed light on mechanisms of these adaptations. Some previous attempts at modeling vein graft adaptations have prescribed changes in geometry as functions of time and stress.[28,118] In contrast, the current model makes changes in geometry, structure, and composition of the vessel

a consequence of the cell mediated G&R that tries to restore homeostatic stresses; that is, the results of the present model are "emergent". The model captured salient features of pressure and flow-induced adaptation in a vein graft, including an increase in constituent mass production. Recent histological results show an ≈ 3 fold increase in collagen content in the walls of veins subjected to a pressure and flow overload.[109] A 15-fold increase in SMC proliferation has also been reported for arteries in hypertensive rats.[111] The pressure perturbations in the current work are higher than the hypertensive case in arteries and the aforementioned observations qualitatively support the optimization algorithm's prediction of an enhanced mass production. The passive properties imply that the vein is initially stiff in the axial direction but compliant in the circumferential direction. The high mass production predicted in the circumferential direction in numerical experiments can be interpreted as a mechanism by which the vein negotiates an increase in circumferential stress due to an increased pressure.

Many G&R parameters are difficult to measure in vivo and have not yet been reported. Experimental data reported on (mal)adaptations of vein grafts do not yet provide sufficient details to make quantitative longitudinal validations with the current model. The few available studies concentrate on short term responses.[27,28,109,119] Nonetheless, parallels can be drawn between the current results and observed trends in arterial G&R in hypertension (which is a modest pressure perturbation relative to that considered here). Nissen et al.[110] showed that the half life of collagen in a rat aorta reduced from 60-70 days under normotension to 17 days in hypertension

($\approx 1.5P_0$). The pressure perturbations herein are an order of magnitude higher than the systemic hypertension that leads to an exuberant turnover of matrix. The value of ≈ 1 day for collagen half life, as predicted by the optimization for a few cases, thus seems reasonable, if biologically possible. Monos et al.[120] reported the active stress generated by smooth muscle in a canine femoral vein to be 5.1 ± 1.5 kPa at a stretch of 1.36. The active stress for the vein deduced from Table 4.3, for a murine vena cava, is approximately 3.2 kPa at a smooth muscle prestretch of 1.31. In contrast, the active stress of smooth muscle in the arterial circulation is of the order of 100 kPa, and the range on T_{max} during optimization was chosen to reflect the disparity in active stress between an artery and a vein.

Venous adaptations are flow limited

Smooth muscle cells and fibroblasts can turnover constituents within evolving configurations at homeostatic values to counter increases in load. Their turnover rates depend on at least two mechanical stimuli, intramural stress and wall shear stress (equation 2.7). In an increased pressure scenario these two stimuli work in unison; the pressure increases wall stress-mediated production and decreases shear-stress inhibition of production. In contrast, in an increased flow scenario, the dilatory response (mediated by increased NO production) slows production while the increased wall stress hastens it.[22] Our results (Figure 4.7) suggest that the ability to normalize stress in the wall is impaired more by a flow perturbation than a pressure perturbation, which suggests that venous adaptations are predominantly flow lim-

ited, given the assumption that there is no cellular damage. The dynamic interaction between pressure-induced and flow-induced changes makes the resulting adaptations non-intuitive. For example, a gradual change in flow over 3 days accompanied by a step change in pressure had fewer maladapted points than a gradual change in pressure and flow over 3 days (Figure 4.8). Such findings remind us that the G&R framework is well suited both to generate and test hypotheses and to gain insights that are otherwise hard to intuit due to interactions between dynamic components of adaptation.

Acute response and long term adaptation

Vascular adaptations are known to be biphasic, with acute adaptations dominated by adjustments to vasomotor tone and chronic adaptations governed by the turnover of structural constituents in evolving configurations. Our results in Figure 4.7 allude to the subtle relationship between acute responses and long term adaptations, a relatively underexplored topic in G&R. Our simulations, together with prior studies, suggest a link through endothelial dependent smooth muscle responses.[116,121] An inability of smooth muscle to counter an increase in load with a contractile force may result in a switch to a synthetic phenotype,[14] similar to mechanisms in hypertension.[122] A focused set of experiments examining time courses of changes in SMC activity and matrix production could be carried out to confirm this hypothesis.

Optimization to accelerate parameter estimation

The current work also demonstrates utility of a modular optimization tool to accelerate parameter estimation and numerically test competing hypotheses in vascular G&R. The proposed methods are non-intrusive and scalable. Each level of the algorithm is parallelizable and can be run as a multi-processor job. By formulating the parameter identification problem as an optimization problem with an objective function measuring differences from homeostatic targets, parameter sets were efficiently identified without the need for expensive brute force trial and error approaches.

Choice of cost function is non-trivial

Response to flow-induced wall shear stress, and hence modulations in radius, depends on the location of the vessel within the vascular tree. Unfortunately little information is available for a vein. Hence, although the choice of cost function used in our work is illustrative and the results look reasonable, it needs further probing. For example, setting $w_3 = 0$ and $w_4 = 0$ in equation 2.14 produces a stress based cost function, and further setting $w_1 = 1$ and $w_2 = 1$ recovers the cost function used in our work (equation 4.7). On the other hand, setting $w_1 = 0$ and $w_2 = 0$ gives us a pure geometric cost function. Figure 4.10 illustrates the predicted evolution of radius and thickness for the optimal solution for a modest hemodynamic perturbation ($\gamma = 1, \epsilon = 1.1$) with a geometric cost function ($w_3 = 1$ and $w_4 = 1$). A 10% increase in flow, in an incompressible vessel, should lead to a quick increase in radius and a decrease in thickness. The geometric cost function based optimization predicted a

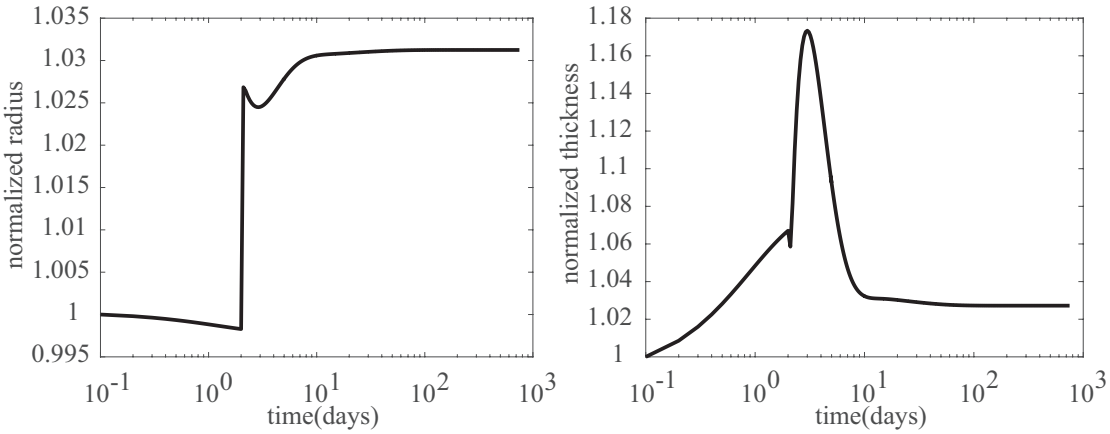

Figure 4.10: Predicted evolution of radius and thickness for an optimized set of parameters from a geometric cost function based optimization for a modest hemodynamic perturbation ($\gamma = 1, \epsilon = 1.1$) - notice the non-physiological immediate increase in thickness.

non-physiological evolution of thickness, however, in which incompressible behaviour was absent. Thus, a cost function inconsistent with constitutive relations can predict non-physiological behaviour. Our use of a stress-based optimization was, in contrast, consistent with most mass production and survival functions. Hence the choice of parameters and cost function for problems with little experimental data is a non-trivial exercise in parameter estimation but we managed to address it for a vein in this work. The cost functions were stress based to keep them consistent with constitutive relations for constituent mass production and we wanted the model to retain the "emergent" behaviour, where evolving radius and thickness emerge naturally from the equilibrium equation.

Numerical Challenges

In the past, constrained mixture theory has typically been employed for modest-to-moderate perturbations in hemodynamics, making this study perhaps the first when the theory has been applied in severe hemodynamic loading scenarios. The consistent clinical observation of maladaptation in vein grafts would lead one to expect that simulations should fail at higher loads. Because greater perturbations from homeostatic also pose challenges to numerical schemes, it is hard to differentiate a numerical failure from an adaptation failure. In the G&R framework a failed simulation could be due to a failure in the root finding Newton-Raphson scheme, the time marching explicit scheme, or due to a failure in theory. In Newton-Raphson schemes, high gradients can lead to a bad initial guess and hence push the algorithm outside the range of guaranteed convergence. This issue was resolved in our simulations using a bound check condition on the roots at every iteration. In addition, cost function values were confirmed with 4^{th} order Runge-Kutta time advancement schemes and tested to ensure time step convergence. Thus, none of the failed simulations reported in this work could be attributed to lack of convergence or failures in numerical algorithms.

Numerical vein - a useful tool to understand G&R in a vein graft

A typical goal of a computational model is to capture experimental observations, as, for example, the time course of changes in geometry, composition, and mechanical properties of an implanted vein graft. In the case of these grafts, it is

known that such changes often reflect a maladaptive rather than an adaptive response to the higher pressures and flows experienced in the arterial system. The goal of our work was very different, however. We sought to identify upper and lower bounds on the adaptive capacity of a vein as a means to understand better why vein grafts often maladapt. Towards this end, we first assumed that veins can adapt well to modest changes in hemodynamics and identified associated "homeostatic" G&R parameters that enabled such adaptations. These parameters were then used to assess responses to increases in pressure and flow that would be experienced by a vein graft. Next, we identified different sets of G&R parameters that numerically enabled adaptations to increasingly higher loads, from venous to arterial levels; there was no constraint on this parameter identification regarding whether or not an actual vein could achieve such adaptions in vivo. Interestingly, neither the homeostatic nor the numerically optimized values of G&R parameters enabled venous adaptations to loads actually experienced in the arterial circulation, in the absence of an enhanced mass production. Hence, our numerical results are consistent with the preponderance of the experimental and clinical observations that veins maladapt. Given this finding, and motivated by some prior empirical (e.g., El-Kurdi et al.[123]) and computational (e.g., Karsaj et al.;[124] Sankaran et al.[92]) studies, we then explored possible advantages of increasing the load gradually rather than abruptly, as occurs during surgical procedures when the arterial clamps are released. The simulations suggested that gradual increases in loads, and thus vascular wall stress, may allow a more favorable adaptation. Indeed, noting that we did not include potential cellular damage due to

the abrupt increase in pressure, these results are thus likely conservative. We submit, therefore, that first, computational G&R models can play an important role in understanding mechanobiological mechanisms of vascular (mal)adaptation and, second, a gradual loading of vein grafts may provide a means to improve mural adaptations and hence outcomes.

In conclusion, continuum-based constrained mixture models are well suited for simulating vein graft (mal)adaptations as well as hypothesis generation and testing. We have demonstrated the utility of one such framework in eliciting mechanisms leading to vein graft maladaptation and ways to mitigate it in a numerical vein.

4.5 Limitations

The proposed model for venous G&R has several assumptions and simplifications, many of which are due to the lack of experimental and/or clinical data. The structure and properties of a vein vary with age, location in the body, and species.[125] Although the prescribed single layer model is based on a healthy murine inferior vena cava, a three-layer G&R model would obviously provide more detail on the (mal)adaptations, perhaps elucidating salient aspects of vein graft G&R such as clinically observed medial versus neointimal thickening. Lack of a clear distinction between intima and media in a mouse vein, and challenges of dissecting layers without damaging the wall, impose practical constraints on obtaining biaxial data for the different layers.[119] There is also recent histological evidence challenging the assumption

of elastin isotropy in veins.[109] In the light of more experimental evidence, anisotropic models for elastin can be easily incorporated into the current framework, including the use of anisotropic elastin pre-stretch.

There is uncertainty associated with the target homeostatic circumferential and wall shear stress in the current study. Data on potential differences in homeostatic wall shear stress across species is lacking, hence the current target values of stress were chosen to reasonably represent existing experiments on veins independent of species.[84,107,113] Experiments looking at venous and arterial markers suggest that the venous identity is lost but an arterial identity is not fully gained during a vein graft adaptation.[126] There is a need for more experimental data to answer questions on arterialization of a vein graft. The homeostatic stress values in arteries are larger than veins,[75] hence the current study will serve as an upper bound for optimal adaptation. A similar study, where the target homeostatic values are for an artery, should serve as a lower bound. The question of target homeostatic stress is one of the many instances where computational models become useful in testing hypotheses in vein graft remodeling, thus pointing out the gaps in knowledge and setting directions for future experiments.

It is still not clear if the manifestations of G&R in a vein graft are an adaptation or an injury response.[13] Endothelial cell functionality is likely compromised after bypass graft surgery, hence the vein could lose its ability to sense and restore wall shear stress.[13,15] The current work disregards possible effects of compromised endothelial function; subsequent studies will need to take this effect into account once

additional data are available. An endothelial injury response function similar to the one used by Baek et al.[26] could be incorporated into the current model to capture such an injury response, noting that normal veins are more sensitive to vasoconstrictors and less sensitive to vasodilators than arteries.[8] Nitric oxide and prostacyclin, which are potent vasodilators and inhibitors of platelet adhesion and aggregation, are released in greater amounts in arterial than venous coronary bypass vessels.[127] Since the mechanobiology of vasodilation/vasocontraction is not completely understood, it poses challenges when modeling the response of veins to altered flow and needs to be considered in future work. With the absence of endothelial injury and a venous value for homeostatic stress, the current representation is a best-case scenario for a vein graft adaptation.

The absence of simulated changes in axial stretch and cell damage are two major assumptions in our model. Axial stresses play fundamental roles in compensatory adaptations.[128] A vein, when transposed from its native environment to an arterial environment, undergoes changes in axial stretch. It is not yet understood how and if this change in stretch affects venous adaptation. Adaptive responses to flow and pressure, for the most part, are achieved without independent altering of vessel length.[85,128] Also, lack of clinical evidence on maladaptation due to axial loading, such as kinking or twisting of grafts, justified our choice to neglect axial stretch changes. While there is evidence of cell damage in vein grafts placed in an arterial environment,[129] such data are currently too limited to inform models of damage or the inflammation that accompanies cell damage. Again, there is need for more focused

experimental data.

Despite several simplifications and assumptions, the present patient-specific framework and G&R framework produced results consistent with general observations in the literature. Perhaps most importantly, however, the current work illustrates that these frameworks can provide a platform to quickly test multiple hypotheses and gain insights into consequences of changes in hemodynamics. There is, however, a pressing need for more data and focused experiments to motivate better constitutive relations and make quantitative comparisons and validations.

4.6 Acknowledgements

Authors wish to thank Prof. Jay Humphrey and Sethuraman Sankaran for lending their expertise with the G&R models and parameter estimation, respectively, to this work.

Chapter 4, in part, is a reprint of the material as it appears in " Computational simulation of the adaptive capacity of vein grafts in response to increased pressure", *Journal of Biomechanical Engineering*, 137(3), 2015. Authors are Ramachandra, A. B., Sankaran, S., Humphrey, J. D., & Marsden, A. L. The dissertation author was the primary investigator and author of this paper.

Chapter 4, in part, has been submitted for publication of the material as it may appear in " Gradual loading ameliorates maladaptation in computational simulations of vein graft growth and remodeling", *submitted* and is under review. Authors are

Ramachandra, A. B., Humphrey, J. D., & Marsden, A. L. The dissertation author was the primary investigator and author of this paper.

Chapter 5

Future work

Most clinical manifestations of remodeling and adaptation are at a macroscale whereas the underlying mechanisms are at a microscale. Thanks to advances in experimental and computational methods past several decades has seen tremendous advances in our understanding of vein graft failure, yet glaring gaps in knowledge of vein graft failure demand we further extend our understanding of (mal)adaptations in a vein graft, especially from a mechnobiological viewpoint. Here we discuss a few aspects of the computational models, their usefulness in informing experiments and hurdles to translation into the clinic.

5.1 Translational Outlook

5.1.1 Patient-Specific Simulations

Computational simulations of coronary flow have gained recent attention with the FDA approval of HeartFlows FFR CT (fractional flow reserve derived from CT) technology, with recent clinical trials demonstrating that simulations can reliably provide data previously only available via invasive catheterization procedures. In addition, simulations have led to clinical translation of novel surgical methods in congenital heart disease with promising results.[130,131] Development of simulation tools to predict venous graft failure poses additional challenges of incorporating long-term mechanobiological responses, and correlation with intermediate-long-term clinical outcomes. Validation against clinical data is one of the major challenges in translation. Our solvers and boundary conditions have been validated against in vitro experiments, and against in vivo data in other clinical scenarios, but direct comparisons to patient-specific in vivo data in coronary arteries are still underway. These validations require in vivo measurements of flow, pressure, and wall displacements. However, these efforts are limited by challenges of small size, cardiac motion, and risks associated with invasive measurements in the coronary arteries. The mechanical stimuli quantified in our study are motivated by biological experiments and are surrogates of cellular mechanobiologic response. Demonstration of the clinical utility of these indices will require larger patient cohorts and longitudinal data.

Surgical Revascularization Planning Tool

Methods developed for patient-specific CABG simulations could serve as valuable tools for surgical planning in patients who are scheduled to undergo CABG surgery. Surgeons are faced with a choice of several different revascularization techniques for venous grafts, including Y-shaped, sequential, or single grafts, with varying long term outcomes. Decisions regarding the spatial arrangement of grafts, and the locations of anastomoses on target native vessels, rely on retrospective studies, limited geometric guidelines, surgeons intuition and experience. Prior studies on the efficacy and superiority of each of these techniques[132,133] report varied results.

As a pilot study we built patient-specific 3D models of CABG geometries from CT images of a patient who had undergone bypass surgery using simulation methodology outlined in section 2.1.1. With input from surgeons on our team, we virtually modified the venous graft geometric configurations to mimic the commonly performed revascularization techniques (Figure 5.1). In this study, we compared the Y-configuration, sequential anastomosis, and single graft approach, while keeping rest of the simulation parameters, including boundary conditions, material properties, and remaining anatomy, the same. Patients in this study act as their own control, as only the graft geometry is altered virtually keeping all other parameters fixed. This allows for a controlled comparison of surgical methods that is not possible in the clinical setting.

The mechanical stimuli correlated with atherogenesis and graft failure were quantified in each of these virtual surgical configurations. Figure 5.2 is an illustrative

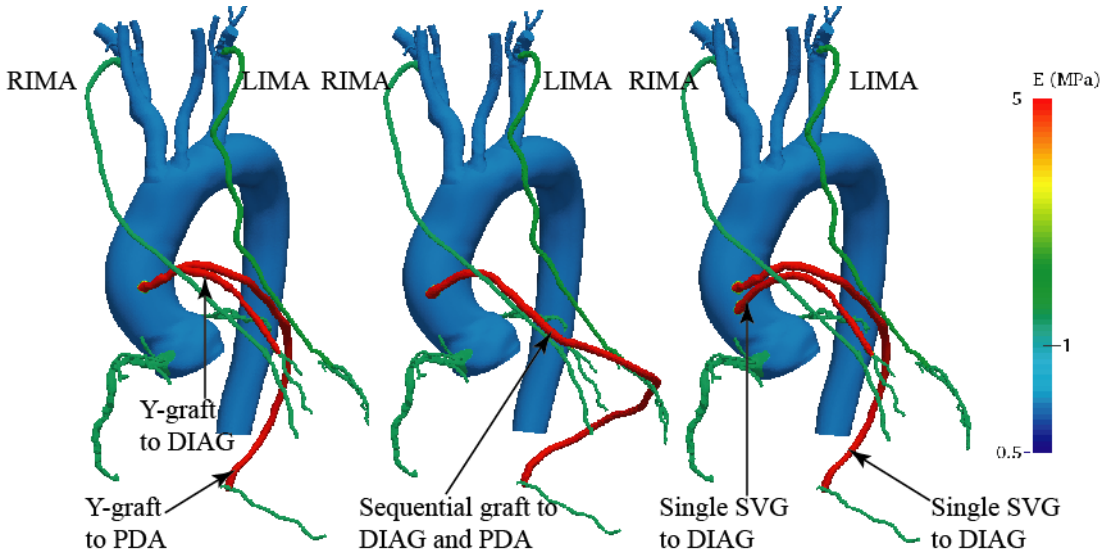

Figure 5.1: Patient-specific model from CT scan of a patient who had undergone CABG surgery with venous grafts in Y configuration (left); Sequential (middle) and 2 single graft (right) - virtual modifications of the graft geometry. Vessels are colored by their Youngs Modulus values. PDA-posterior descending artery, SVG- Saphenous vein graft, IMA-internal mammary artery, DIAG- Left Diagonal branch

result showing the TAWSS distribution in these geometries. The graft regions at potential risk for restenosis or failure can be identified.

Additional patients need to be added to the study cohort before further conclusions regarding clinical application can be drawn. Myriad factors, such as varying local geometry, wall properties and dynamic distal demand, make surgical design decisions non-intuitive, necessitating the use of computational tools, such as those proposed here, to aid in clinical decisions. This pilot study demonstrates that virtual surgery studies with patient-specific simulation tools developed in this dissertation could provide a means to perform a controlled experiment in which patient variability can be controlled for, and the mechanics can be examined independent of other factors.

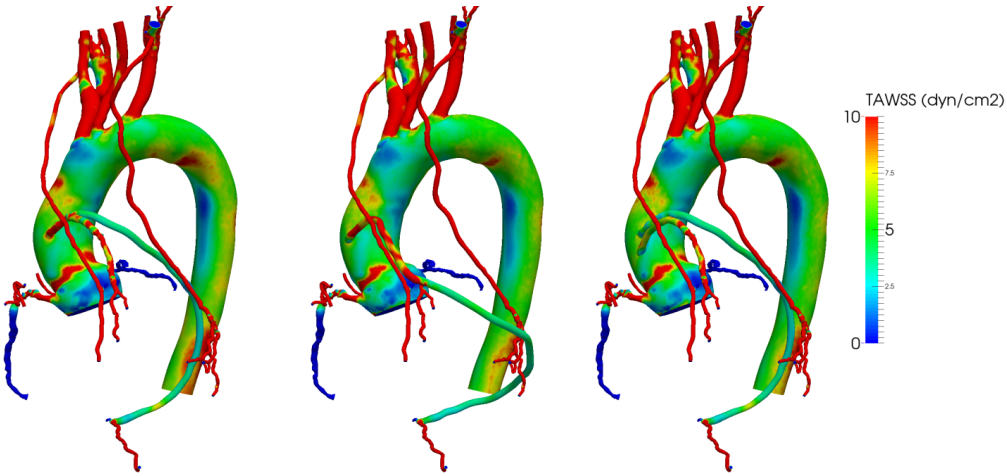

Figure 5.2: Illustrative result showing the TAWSS distribution in the original geometry (left) and the modified geometries (middle and right).

5.1.2 Growth and Remodeling

Some of our findings from G&R work have translational potential as a pharmacological therapy or medical device. For example, a pharmacological therapy that upregulates constituent mass production, alters active muscle properties or thresholds for phenotypic modulation could hold promise as an avenue to prevent vein maladaptation. Increased matrix production can be achieved with certain antagomiRs, for example,[134] and various agonists can increase smooth muscle contractility. There is a need to understand what modulates smooth muscle adaptation in veins, however. Also a step change in load, as occurs during surgical procedures when the arterial clamps are released, can lead to a graft failure at arterial conditions. The differences

in response to step and gradual changes in pressure demonstrate the ability of numerical models to compare and contrast potential clinical treatment strategies. A gradual change in load, possibly achieved using a polymer wrap or an external biodegradable sheath or stent,[135] holds promise in preventing venous graft maladaptation. Towards that end, we explored the effect of the duration of the gradual loading, which we found need not be that long (≤ 8 days). We hope this will inform design considerations and specifications. Of course, many other issues such as foreign body response, uncertainties associated with parameter values,[92] and sensitivity analysis to loads would need to be addressed prior to translation. The proposed framework is, however, general enough to provide a good starting point for each of these considerations. In vivo models of vein graft failure[136,137] and ex vivo setups,[138] coupled with histochemical and biaxial studies, are natural pathways for validation and translation of these results.

5.2 Frameworks are general enough for multiple clinical applications

Our current patient-specific framework is targeted at post-CABG coronary anatomy with SVGs, including a comprehensive model of the coronary circulation that includes patient-specific anatomy, FSI, and closed-loop boundary conditions. Hence, the proposed simulation tools will be applicable to numerous other coronary pathologies including native coronary artery disease, congenital and aortic root abnormalities, anomalous coronary origins, Kawasaki disease, and tissue engineered graft

design. With validation, these tools will permit accurate non-invasive determination of the hemodynamic significance of stenoses, and anatomic conditions that increase local risk of atherosclerosis and thrombosis.

Vein graft maladaptation and failure are ubiquitous in vascular surgeries, including coronary artery bypass graft (CABG) surgery, peripheral vascular surgery, and arteriovenous fistula (AVF) procedures for hemodialysis access. The failure rate is as high as 50% at 10 years for CABG grafts,[5] 25-55% at 5 years for infragenicular bypass grafts,[139,140] and 40% for the primary failure of AVF.[141] Although the primary mode of long term failure differs across each of these pathologies, for example, atherosclerosis for CABG venous grafts[8] and intimal hyperplasia for AVF,[142] the altered mechanical environment remains a common theme. There are important differences, however. While CABG grafts experience relatively uniform pressure conditions and largely laminar flow, flow in AVFs is highly complex, perhaps turbulent, with large pressure drops from systemic to venous levels. The failure in venous segments of the AVF is associated with intimal hyperplasia and associated thickening of the intima[143] (in contrast to thickening of the media in vein grafts). Hence, one needs to look at the combined effects of non-uniform alterations in pressure and flow to understand the failure of veins in AVF. With appropriate modifications, the models and the methods presented in this thesis could be used to study venous growth and remodeling in AVFs, and peripheral bypass grafts which is of significant importance in a relatively large and high-risk population. We note that optimization would also be useful in this context to identify appropriate parameter changes.

5.3 Coupled Fluid-Structure-Growth (FSG) models to risk stratify patients

Most vascular diseases manifest over a time span of weeks, months and years, whereas most efforts in patient-specific modeling has focused on responses during a cardiac cycle. There is a pressing need for multiscale models that span multiple temporal and spatial scales and captures essential physics and biology, from a cellular to an organ scale. The existence of multiple scales raise issues with respect to coupling, both computational and experimental, and impose hurdles to translation and scalability to large cohorts. A high fidelity simulation might be computationally expensive while a low fidelity simulation may not capture essential physics or biology to answer questions of translational interest. The challenge is in finding the right scales to couple, to generate a computationally useful and tractable problem.

In vascular adaptations the time scales for fluids and solids are very different. Hence it might be sufficient to solve a loosely coupled problem. A few applications in an arterial setting have managed to achieve this with reasonable success.[21,144] Out of these approaches the theory of small on large, which has its origins in some of the classical works on continuum mechanics[145] holds promise for vein graft application. Small deformations of blood vessel during the cardiac cycle when superimposed on large can exploit methods in linearized elasticity without compromising the nonlinear description of the wall. This approach allows incorporation of nonlinear mechanical behaviour, anisotropy, active smooth muscle contractility and constituent turnover

while recovering equations relevant to cardiac cycle that can be solved using methods in linearized elasticity.[23]

A plausible mechanism for coupling could be:

(a) Simulate blood flow and wall deformation in a patient-specific geometry

(b) Pass information on pressure, flow and deformation fields to the G&R model

(c) Simulate vein G&R until a predefined instant in simulation is reached

(d) Use the new, predicted G&R geometry to modify the patient-specific geometry

(e) Repeat the above steps until a criterion for termination is reached (e.g. predefined set of iterations, steady state)

(f) Classify the adaptation as optimal, suboptimal, maladaptive or failure

This algorithm provides a loose coupling between the models and might be enough to gain several insights into remodeling process. Of course, details on passing of information between models, criterion for convergence, validation etc. need due consideration before translation. Figure 5.3 is an illustration of one such FSG framework. While the G&R theory has been coupled with fluid-structure solvers in the past,[21] lack of quantitative data on venous endothelial responses to oscillatory flow makes extensions to pulsatile flow premature and likely non-trivial.

In the near term we envision an integrated fluid-structure-growth model spanning scales from the cellular to vessel level, which would enable prediction of graft mechanics together with long-term adaptive response in individual patients. These

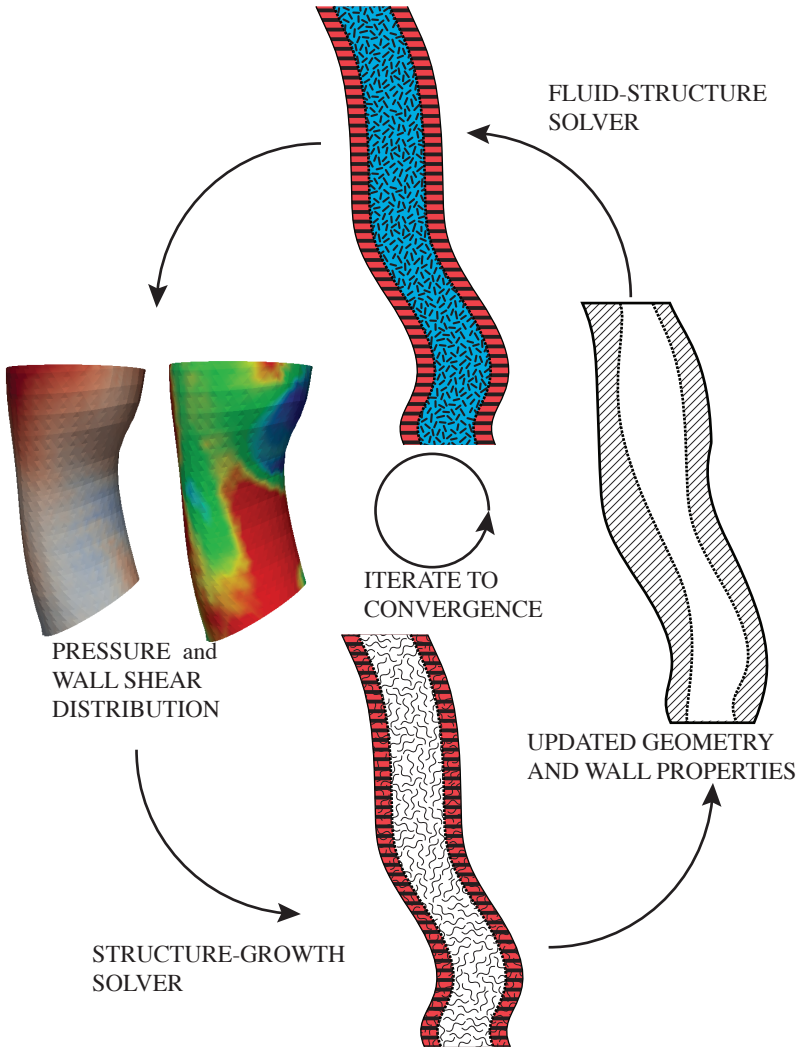

Figure 5.3: FSI simulations and models coupled with models of Growth and Remodeling can inform risk stratification guidelines in CABG models.

combined models could also inform future vascular biology experiments, guide clinical data collection and outcomes correlations, and ultimately aid clinical decision-making. Future efforts should be directed towards extending the formulation to a 3-D vein accounting for injury responses. The modeling community should begin to move towards an all encompassing model coupling G&R to patient-specific fluid-structure simulations and furthering the feasibility of personalized treatments employing vein

grafts.

5.4 Acknowledgements

Chapter 5, in part is currently being prepared for submission for publication of the material. Authors are Ramachandra, A. B., Jensen, C. W., Chu, C., Boyd, J., Kahn, A. M. & Marsden, A. L. The dissertation author was the primary investigator and author of this paper.

Bibliography

[1] Peter Libby and Pierre Theroux. Pathophysiology of coronary artery disease. *Circulation*, 111(25):3481–3488, 2005.

[2] Ilke Sipahi, M Hakan Akay, Sinan Dagdelen, Arie Blitz, and Cem Alhan. Coronary artery bypass grafting vs percutaneous coronary intervention and long-term mortality and morbidity in multivessel disease: meta-analysis of randomized clinical trials of the arterial grafting and stenting era. *JAMA internal medicine*, 174(2):223–230, 2014.

[3] Edward L Hannan, Michael J Racz, Gary Walford, Robert H Jones, Thomas J Ryan, Edward Bennett, Alfred T Culliford, O Wayne Isom, Jeffrey P Gold, and Eric A Rose. Long-term outcomes of coronary-artery bypass grafting versus stent implantation. *New England Journal of Medicine*, 352(21):2174–2183, 2005.

[4] David P Taggart. Coronary artery bypass grafting is still the best treatment for multivessel and left main disease, but patients need to know. *The Annals of Thoracic Surgery*, 82(6):1966–1975, 2006.

[5] Joseph G Motwani and Eric J Topol. Aortocoronary saphenous vein graft disease pathogenesis, predisposition, and prevention. *Circulation*, 97(9):916–931, 1998.

[6] Abdul R Halabi, John H Alexander, Linda K Shaw, Todd J Lorenz, Lawrence Liao, David F Kong, Carmelo A Milano, Robert A Harrington, and Peter K Smith. Relation of early saphenous vein graft failure to outcomes following coronary artery bypass surgery. *The American journal of cardiology*, 96(9):1254–1259, 2005.

[7] William S Weintraub, Ellis L Jones, Douglas C Morris, Spencer B King, Robert A Guyton, and Joseph M Craver. Outcome of reoperative coronary bypass surgery versus coronary angioplasty after previous bypass surgery. *Circulation*, 95(4):868–877, 1997.

[8] J. L. Cox, D. A. Chiasson, and A. I. Gotlieb. Stranger in a strange land: The pathogenesis of saphenous vein graft stenosis with emphasis on structural and

functional differences between veins and arteries. *Progress in cardiovascular diseases*, 34:45–68, 1991.

[9] D. P. Sokolis. Passive mechanical properties and constitutive modeling of blood vessels in relation to microstructure. *Medical & biological engineering & computing*, 46:1187–1199, 2008.

[10] M. E. Shelton, M. E. Forman, R. Virmani, A. Bajaj, W. S. Stoney, and J. B. Atkinson. A comparison of morphologic and angiographic findings in long-term internal mammary artery and saphenous vein bypass grafts. *Journal of the American College of Cardiology*, 11:297–307, 1988.

[11] Christopher D Owens, Warren J Gasper, Amreen S Rahman, and Michael S Conte. Vein graft failure. *Journal of vascular surgery*, 61(1):203–216, 2015.

[12] Ralf E Harskamp, Renato D Lopes, Clinton E Baisden, Robbert J de Winter, and John H Alexander. Saphenous vein graft failure after coronary artery bypass surgery: pathophysiology, management, and future directions. *Annals of surgery*, 257(5):824–833, 2013.

[13] J. D. Humphrey. *Cardiovascular solid mechanics: cells, tissues, and organs*. Springer, 2002.

[14] Benjamin Klein, Anthony Destephens, Leanne Dumeny, Qiongyao Hu, Yong He, Kerri OMalley, Zhihua Jiang, Roger Tran-Son-Tay, and Scott Berceli. Hemodynamic influence on smooth muscle cell kinetics and phenotype during early vein graft adaptation. *Annals of Biomedical Engineering*, pages 1–12, 2016.

[15] S. Q. Liu and Y. C. Fung. Changes in the organization of the smooth muscle cells in rat vein grafts. *Annals of Biomedical Engineering*, 26:86–95, 1998.

[16] S. Q. Liu. Influence of tensile strain on smooth muscle cell orientation in rat blood vessels. *Journal of Biomechanical Engineering*, 120:313–320, 1998.

[17] S. W. Galt, R. W. Zwolak, R. J. Wagner, and J. J. Gilbertson. Differential response of arteries and vein grafts to blood flow reduction. *Journal of vascular surgery*, 17:563–570, 1993.

[18] M.F. Fillinger, J. L. Cronenwett, S. Besso, D. B. Walsh, and R. M. Zwolak. Vein adaptation to the hemodynamic environment of infrainguinal grafts. *Journal of vascular surgery*, 19:970–979, 1994.

[19] Philip B Dobrin. Mechanical factors associated with the development of intimal and medial thickening in vein grafts subjected to arterial pressure a model of arteries exposed to hypertension. *Hypertension*, 26(1):38–43, 1995.

[20] S Glagov, C Zarins, DP Giddens, and DN Ku. Hemodynamics and atherosclerosis. insights and perspectives gained from studies of human arteries. *Archives of pathology & laboratory medicine*, 112(10):1018–1031, 1988.

[21] C Alberto Figueroa, Seungik Baek, Charles A Taylor, and Jay D Humphrey. A computational framework for fluid–solid-growth modeling in cardiovascular simulations. *Computer methods in applied mechanics and engineering*, 198(45):3583–3602, 2009.

[22] A Valentin and JD Humphrey. Evaluation of fundamental hypotheses underlying constrained mixture models of arterial growth and remodelling. *Philosophical Transactions of the Royal Society of London A: Mathematical, Physical and Engineering Sciences*, 367(1902):3585–3606, 2009.

[23] S. Baek, K. R. Rajagopal, and J. D. Humphrey. A theoretical model of enlarging intracranial fusiform aneurysms. *Journal of biomechanical engineering*, 128:142–149, 2006.

[24] J. F. Eberth, L. Cardamone, and J. D. Humphrey. Evolving biaxial mechanical properties of mouse carotid arteries in hypertension. *Journal of biomechanics*, 21:460–471, 1995.

[25] J. D. Humphrey, S. Baek, and L. E. Niklason. Biochemomechanics of cerebral vasospasm and its resolution: I. A new hypothesis and theoretical framework. *Annals of biomedical engineering*, 35:1485–1497, 2007.

[26] S. Baek, A. Valentin, and J. D. Humphrey. Biochemomechanics of cerebral vasospasm and its resolution: II. Constitutive relations and model simulations. *Annals of biomedical engineering*, 35:1498–1509, 2007.

[27] P. Dobrin, F. N. Littooy, and E. D. Endean. Mechanical factors predisposing to intimal hyperplasia and medial thickening in autogenous vein grafts. *Surgery*, 105:393–400, 1989.

[28] R. Tran-Son-Tay, M. Hwang, M. Garbey, Z. Jiang, C. K. Ozaki, and S.A. Berceli. An experiment-based model of vein graft remodeling induced by shear stress. *Annals of biomedical engineering*, 36:1083–1091, 2008.

[29] Richard D Brown Lee and B Lowell Langille. Arterial adaptations to altered blood flow. *Canadian journal of physiology and pharmacology*, 69(7):978–983, 1991.

[30] Y. U. Lee, Y. Naito, H. Kurobe, C. K. Breuer, and J. D. Humphrey. Biaxial mechanical properties of the inferior vena cava in c57bl/6 and cb-17 scid/bg mice. *Journal of biomechanics*, 46:2277–2282, 2013.

[31] Alison L Marsden and Mahdi Esmaily-Moghadam. Multiscale modeling of cardiovascular flows for clinical decision support. *Applied Mechanics Reviews*, 67(3):030804, 2015.

[32] Charles A Taylor, Thomas JR Hughes, and Christopher K Zarins. Finite element modeling of blood flow in arteries. *Computer methods in applied mechanics and engineering*, 158(1):155–196, 1998.

[33] C Alberto Figueroa, Irene E Vignon-Clementel, Kenneth E Jansen, Thomas JR Hughes, and Charles A Taylor. A coupled momentum method for modeling blood flow in three-dimensional deformable arteries. *Computer methods in applied mechanics and engineering*, 195(41):5685–5706, 2006.

[34] Mahdi Esmaily Moghadam, Irene E Vignon-Clementel, Richard Figliola, Alison L Marsden, and Modeling Of Congenital Hearts Alliance (mocha) Investigators. A modular numerical method for implicit 0d/3d coupling in cardiovascular finite element simulations. *Journal of Computational Physics*, 244:63–79, 2013.

[35] H.J. Kim, I. E. Vignon-Clementel, J.S. Coogan, C.A. Figueroa, K.E. Jansen, and C.A. Taylor. Patient-specific modeling of blood flow and pressure in human coronary arteries. *Annals of Biomedical Engineering*, 38(10):3195–3209, 2010.

[36] Mahdi Esmaily Moghadam, Yuri Bazilevs, Tain-Yen Hsia, Irene E Vignon-Clementel, Alison L Marsden, and Modeling Of Congenital Hearts Alliance (mocha) Investigators. A comparison of outlet boundary treatments for prevention of backflow divergence with relevance to blood flow simulations. *Computational Mechanics*, 48(3):277–291, 2011.

[37] Sethuraman Sankaran, Mahdi Esmaily Moghadam, Andrew M Kahn, Elaine E Tseng, Julius M Guccione, and Alison L Marsden. Patient-specific multiscale modeling of blood flow for coronary artery bypass graft surgery. *Annals of biomedical engineering*, 40(10):2228–2242, 2012.

[38] Dibyendu Sengupta, Andrew M Kahn, Jane C Burns, Sethuraman Sankaran, Shawn C Shadden, and Alison L Marsden. Image-based modeling of hemodynamics in coronary artery aneurysms caused by kawasaki disease. *Biomechanics and modeling in mechanobiology*, 11(6):915–932, 2012.

[39] Dibyendu Sengupta, Andrew M Kahn, Ethan Kung, Mahdi Esmaily Moghadam, Olga Shirinsky, Galina A Lyskina, Jane C Burns, and Alison L Marsden. Thrombotic risk stratification using computational modeling in patients with coronary artery aneurysms following kawasaki disease. *Biomechanics and modeling in mechanobiology*, 13(6):1261–1276, 2014.

[40] Abhay B Ramachandra, Andrew M Kahn, and Alison L Marsden. Patient-specific simulations reveal significant differences in mechanical stimuli in venous

and arterial coronary grafts. *Journal of Cardiovascular Translational Research*, 9(4):279–290, 2016.

[41] Charles A Taylor, Timothy A Fonte, and James K Min. Computational fluid dynamics applied to cardiac computed tomography for noninvasive quantification of fractional flow reserve: scientific basis. *Journal of the American College of Cardiology*, 61(22):2233–2241, 2013.

[42] Adam Updegrove, Nathan M Wilson, Jameson Merkow, Hongzhi Lan, Alison L Marsden, and Shawn C Shadden. Simvascular: An open source pipeline for cardiovascular simulation. *Annals of Biomedical Engineering*, pages 1–17, 2016.

[43] Onkar Sahni, Jens Müller, Kenneth E Jansen, Mark S Shephard, and Charles A Taylor. Efficient anisotropic adaptive discretization of the cardiovascular system. *Computer Methods in Applied Mechanics and Engineering*, 195(41):5634–5655, 2006.

[44] Jessica S Coogan, Jay D Humphrey, and C Alberto Figueroa. Computational simulations of hemodynamic changes within thoracic, coronary, and cerebral arteries following early wall remodeling in response to distal aortic coarctation. *Biomechanics and modeling in mechanobiology*, pages 1–15, 2013.

[45] Joseph T Keyes, Danielle R Lockwood, Bruce R Simon, and Jonathan P Vande Geest. Deformationally dependent fluid transport properties of porcine coronary arteries based on location in the coronary vasculature. *Journal of the mechanical behavior of biomedical materials*, 17:296–306, 2013.

[46] S Roccabianca, CA Figueroa, G Tellides, and JD Humphrey. Quantification of regional differences in aortic stiffness in the aging human. *Journal of the mechanical behavior of biomedical materials*, 29:618–634, 2014.

[47] Guanglei Xiong, C Alberto Figueroa, Nan Xiao, and Charles A Taylor. Simulation of blood flow in deformable vessels using subject-specific geometry and spatially varying wall properties. *International journal for numerical methods in biomedical engineering*, 27(7):1000–1016, 2011.

[48] Yuri Bazilevs, M-C Hsu, DJ Benson, S Sankaran, and AL Marsden. Computational fluid–structure interaction: methods and application to a total cavopulmonary connection. *Computational Mechanics*, 45(1):77–89, 2009.

[49] Nan Xiao, Jay D Humphrey, and C Alberto Figueroa. Multi-scale computational model of three-dimensional hemodynamics within a deformable full-body arterial network. *Journal of computational physics*, 244:22–40, 2013.

[50] Dong-Wook Han, Young Hwan Park, Jeong Koo Kim, Tae Gon Jung, Kwon-Yong Lee, Suong-Hyu Hyon, and Jong-Chul Park. Long-term preservation of human saphenous vein by green tea polyphenol under physiological conditions. *Tissue engineering*, 11(7-8):1054–1064, 2005.

[51] BK Podesser, F Neumann, M Neumann, W Schreiner, G Wollenek, and R Mallinger. Outer radius-wall thickness ratio, a postmortem quantitative histology in human coronary arteries. *Cells Tissues Organs*, 163(2):63–68, 1998.

[52] Emil Monos and József Csengődy. Does hemodynamic adaptation take place in the vein grafted into an artery? *Pfluegers Archiv*, 384(2):177–182, 1980.

[53] Irene E Vignon-Clementel, C Alberto Figueroa, Kenneth E Jansen, and Charles A Taylor. Outflow boundary conditions for three-dimensional finite element modeling of blood flow and pressure in arteries. *Computer methods in applied mechanics and engineering*, 195(29):3776–3796, 2006.

[54] Hideaki Senzaki, Chen-Huan Chen, and David A Kass. Single-beat estimation of end-systolic pressure-volume relation in humans a new method with the potential for noninvasive application. *Circulation*, 94(10):2497–2506, 1996.

[55] Chiara Corsini, Catriona Baker, Ethan Kung, Silvia Schievano, Gregory Arbia, Alessia Baretta, Giovanni Biglino, Francesco Migliavacca, Gabriele Dubini, Giancarlo Pennati, Alison Marsden, Irene Vignon-Clementel, Tain-Yen Taylor, Andrew Hsia, and Adam Dorfman. An integrated approach to patient-specific predictive modeling for single ventricle heart palliation. *Computer methods in biomechanics and biomedical engineering*, 17(14):1572–1589, 2014.

[56] Soon-Sung Kwon, Eui-Chul Chung, Jin-Seo Park, Gook-Tae Kim, Jun-Woo Kim, Keun-Hong Kim, Eun-Seok Shin, and Eun Bo Shim. A novel patient-specific model to compute coronary fractional flow reserve. *Progress in biophysics and molecular biology*, 116(1):48–55, 2014.

[57] Yuri Bazilevs, Kenji Takizawa, and Tayfun E Tezduyar. *Computational fluid-structure interaction: methods and applications*. John Wiley & Sons, 2013.

[58] Alexander N Brooks and Thomas JR Hughes. Streamline upwind/petrov-galerkin formulations for convection dominated flows with particular emphasis on the incompressible navier-stokes equations. *Computer methods in applied mechanics and engineering*, 32(1-3):199–259, 1982.

[59] Charles A Taylor, Thomas JR Hughes, and Christopher K Zarins. Finite element modeling of blood flow in arteries. *Computer methods in applied mechanics and engineering*, 158(1-2):155–196, 1998.

[60] Thomas JR Hughes. *The finite element method: linear static and dynamic finite element analysis*. Courier Corporation, 2012.

[61] Y Bazilevs, VM Calo, JA Cottrell, TJR Hughes, A Reali, and G Scovazzi. Variational multiscale residual-based turbulence modeling for large eddy simulation of incompressible flows. *Computer Methods in Applied Mechanics and Engineering*, 197(1):173–201, 2007.

[62] Ryo Torii, Marie Oshima, Toshio Kobayashi, Kiyoshi Takagi, and Tayfun E Tezduyar. Computer modeling of cardiovascular fluid–structure interactions with the deforming-spatial-domain/stabilized space–time formulation. *Computer Methods in Applied Mechanics and Engineering*, 195(13):1885–1895, 2006.

[63] Kenji Takizawa, Yuri Bazilevs, and Tayfun E Tezduyar. Space–time and ale-vms techniques for patient-specific cardiovascular fluid–structure interaction modeling. *Archives of Computational Methods in Engineering*, 19(2):171–225, 2012.

[64] C Alberto Figueroa. *A coupled-momentum method to model blood flow and vessel deformation in human arteries: applications in disease research and simulation-based medical planning*. PhD thesis, Stanford University, 2006.

[65] Wilmer Nichols, Michael O'Rourke, and Charalambos Vlachopoulos. *McDonald's blood flow in arteries: theoretical, experimental and clinical principles*. CRC press, 2011.

[66] Ethan O Kung, Andrea S Les, C Alberto Figueroa, Francisco Medina, Karina Arcaute, Ryan B Wicker, Michael V McConnell, and Charles A Taylor. In vitro validation of finite element analysis of blood flow in deformable models. *Annals of biomedical engineering*, 39(7):1947–1960, 2011.

[67] Christian H Whiting and Kenneth E Jansen. A stabilized finite element method for the incompressible navier-stokes equations using a hierarchical basis. *International Journal for Numerical Methods in Fluids*, 35(1):93–116, 2001.

[68] Mahdi Esmaily-Moghadam, Yuri Bazilevs, and Alison L Marsden. A new preconditioning technique for implicitly coupled multidomain simulations with applications to hemodynamics. *Computational Mechanics*, 52(5):1141–1152, 2013.

[69] Eric Jones, Travis Oliphant, and P Peterson. Open source scientific tools for python, 2001.

[70] Bodo Winter. Linear models and linear mixed effects models in r with linguistic applications. *arXiv preprint arXiv:1308.5499*, 2013.

[71] Charles A Taylor and Mary T Draney. Experimental and computational methods in cardiovascular fluid mechanics. *Annu. Rev. Fluid Mech.*, 36:197–231, 2004.

[72] Christopher K Zarins, Michael A Zatina, Don P Giddens, David N Ku, and Seymour Glagov. Shear stress regulation of artery lumen diameter in experimental atherogenesis. *Journal of Vascular Surgery*, 5(3):413–420, 1987.

[73] SQ Liu and YC Fung. Relationship between hypertension, hypertrophy, and opening angle of zero-stress state of arteries following aortic constriction. *ASME J. Biomech. Eng*, 111(4):325–335, 1989.

[74] J. D. Humphrey and K. R. Rajagopal. A constrained mixture model for growth and remodeling of soft tissues. *Mathematical models and methods in applied sciences*, 12:407–430, 2002.

[75] A. Valentin, L. Cardamone, S. Baek, and J. D. Humphrey. Complementary vasoactivity and matrix remodelling in arterial adaptations to altered flow and pressure. *Journal of The Royal Society Interface*, 6:293–306, 2009.

[76] R. L. Gleason and J. D. Humphrey. A mixture model of arterial growth and remodeling in hypertension: altered muscle tone and tissue turnover. *Journal of vascular research*, 41:352–363, 2004.

[77] Y. C. Fung. *Biomechanics: Mechanical Properties of Living Tissues*. Springer-Verlag, 1993.

[78] I. Karšaj and J. D. Humphrey. A multilayered wall model of arterial growth and remodeling. *Mechanics of materials*, 44:110–119, 2012.

[79] J. D. Humphrey and C. A. Taylor. Intracranial and abdominal aortic aneurysms: similarities, differences, and need for a new class of computational models. *Annual review of biomedical engineering*, 10:221–246, 2008.

[80] B. L. Langille. Arterial remodeling: relation to hemodynamics. *Canadian journal of physiology and pharmacology*, 74:834–841, 1996.

[81] JS Wilson, S Baek, and JD Humphrey. Importance of initial aortic properties on the evolving regional anisotropy, stiffness and wall thickness of human abdominal aortic aneurysms. *Journal of The Royal Society Interface*, 9(74):2047–2058, 2012.

[82] CJ Cyron and JD Humphrey. Growth and remodeling of load-bearing biological soft tissues. *Meccanica*, pages 1–20, 2016.

[83] A. Rachev and K. Hayashi. Theoretical study of the effects of vascular smooth muscle contraction on strain and stress distributions in arteries. *Annals of biomedical engineering*, 27:459–468, 1999.

[84] R. Zhang, A. A. Gashev, D. C. Zawieja, and M. J. Davis. Length-tension relationships of small arteries, veins, and lymphatics from the rat mesenteric microcirculation. *American Journal of Physiology-Heart and Circulatory Physiology*, 292:H1943–H1952, 2007.

[85] B Lowell Langille, Michelle P Bendeck, and Fred W Keeley. Adaptations of carotid arteries of young and mature rabbits to reduced carotid blood flow. *The American journal of physiology*, 256(4 Pt 2):H931–9, 1989.

[86] A. L. Marsden, M. Wang, J. E. Dennis, and P. Moin. Trailing-edge noise reduction using derivative-free optimization and large-eddy simulation. *Journal of Fluid Mechanics*, 572:13–36, 2007.

[87] A. L. Marsden, M. Wang, J. E. Dennis Jr, and P. Moin. Suppression of vortex-shedding noise via derivative-free shape optimization. *Physics of fluids*, 16:L83–L86, 2004.

[88] W. Yang, J. A. Feinstein, and A. L. Marsden. Constrained optimization of an idealized y-shaped baffle for the fontan surgery at rest and exercise. *Computer methods in applied mechanics and engineering*, 199:2135–2149, 2010.

[89] A. J. Booker, J. E. Dennis Jr., P. D. Frank, D. B. Serafini, V. Torczon, and M. W. Trosset. A rigorous framework for optimization of expensive functions by surrogates. *Structural optimization*, 17:1–13, 1999.

[90] A. L. Marsden, M. Wang, J. E. Dennis Jr., and P. Moin. Optimal aeroacoustic shape design using the surrogate management framework. *Optimization and Engineering*, 5:235–262, 2004.

[91] S. Sankaran and A. L. Marsden. The impact of uncertainty on shape optimization of idealized bypass graft models in unsteady flow. *Physics of Fluids*, 22:121902–1 – 121902–16, 2010.

[92] S. Sankaran, J. D. Humphrey, and A. L. Marsden. An efficient framework for optimization and parameter sensitivity analysis in arterial growth and remodeling computations. *Computer methods in applied mechanics and engineering*, 256:200–210, 2013.

[93] C. Audet and J. E. Dennis Jr. Mesh adaptive direct search algorithms for constrained optimization. *SIAM Journal on optimization*, 17:188–217, 2006.

[94] Miguel A Quiñones, Catherine M Otto, Marcus Stoddard, Alan Waggoner, and William A Zoghbi. Recommendations for quantification of doppler echocardiography: a report from the doppler quantification task force of the nomenclature and standards committee of the american society of echocardiography. *Journal of the American Society of Echocardiography*, 15(2):167–184, 2002.

[95] Henry T Stelfox, Sofia B Ahmed, Rodrigo A Ribeiro, Elise M Gettings, Eugene Pomerantsev, and Ulrich Schmidt. Hemodynamic monitoring in obese patients: The impact of body mass index on cardiac output and stroke volume*. *Critical care medicine*, 34(4):1243–1246, 2006.

[96] Hugo G Bogren, Richard H Klipstein, David N Firmin, Raad H Mohiaddin, S Richard Underwood, R Simon O Rees, and Donald B Longmore. Quantitation of antegrade and retrograde blood flow in the human aorta by magnetic resonance velocity mapping. *American heart journal*, 117(6):1214–1222, 1989.

[97] Mark A Changizi and Christopher Cherniak. Modeling the large-scale geometry of human coronary arteries. *Canadian journal of physiology and pharmacology*, 78(8):603–611, 2000.

[98] Mair Zamir, Paula Sinclair, and Thomas H Wonnacott. Relation between diameter and flow in major branches of the arch of the aorta. *Journal of biomechanics*, 25(11):1303–1310, 1992.

[99] John F LaDisa Jr, Ismail Guler, Lars E Olson, Douglas A Hettrick, Judy R Kersten, David C Warltier, and Paul S Pagel. Three-dimensional computational fluid dynamics modeling of alterations in coronary wall shear stress produced by stent implantation. *Annals of biomedical engineering*, 31(8):972–980, 2003.

[100] Paolo Di Achille and Jay D Humphrey. Toward large-scale computational fluid-solid-growth models of intracranial aneurysms. *The Yale journal of biology and medicine*, 85(2):217, 2012.

[101] Tsuyoshi Shimizu, Shigeki Ito, Yujiro Kikuchi, Masaharu Misaka, Tetsuzo Hirayama, Shin Ishimaru, and Akira Yamashina. Arterial conduit shear stress following bypass grafting for intermediate coronary artery stenosis: a comparative study with saphenous vein grafts. *European journal of cardio-thoracic surgery*, 25(4):578–584, 2004.

[102] Abhay B Ramachandra, Sethuraman Sankaran, Jay D Humphrey, and Alison L Marsden. Computational simulation of the adaptive capacity of vein grafts in response to increased pressure. *Journal of biomechanical engineering*, 137(3):031009, 2015.

[103] Dehong Zeng, Zhaohua Ding, Morton H Friedman, and C Ross Ethier. Effects of cardiac motion on right coronary artery hemodynamics. *Annals of biomedical engineering*, 31(4):420–429, 2003.

[104] Jameson Merkow, Zhuowen Tu, David Kriegman, and Alison Marsden. Structural edge detection for cardiovascular modeling. In *International Conference on Medical Image Computing and Computer-Assisted Intervention*, pages 735–742. Springer, 2015.

[105] Justin Tran, Daniele Schiavazzi, Abhay Ramachandra, Andrew Kahn, and Alison Marsden. Automated tuning for parameter identification in multiscale coronary simulations. *Computers and Fluids*, 2016.

[106] Christopher J Arthurs, Kevin D Lau, Kaleab N Asrress, Simon R Redwood, and C Alberto Figueroa. A mathematical model of coronary blood flow control: simulation of patient-specific three-dimensional hemodynamics during exercise. *American Journal of Physiology-Heart and Circulatory Physiology*, 310(9):H1242–H1258, 2016.

[107] D. P. Sokolis. Experimental investigation and constitutive modeling of the 3D histomechanical properties of vein tissue. *Biomechanics and modeling in mechanobiology*, 12:431–451, 2013.

[108] G. A. Holzapfel, T. C. Gasser, and R. W. Ogden. A new constitutive framework for arterial wall mechanics and a comparative study of material models. *Journal of elasticity and the physical science of solids*, 61:1–48, 2000.

[109] S. G. Sassani, A. Theofani, T. Sokrates, and D. P. Sokolis. Time-course of venous wall biomechanical adaptation in pressure and flow-overload: Assessment by a microstructure-based material model. *Journal of biomechanics*, 46:2451–2462, 2013.

[110] R. Nissen, G. J. Cardinale, and S. Udenfriend. Increased turnover of arterial collagen in hypertensive rats. *Proceedings of the National Academy of Sciences*, 75:451–453, 1978.

[111] C. Xu, S. Lee, T. M. Singh, E. Sho, X. Li, M. Sho, H. Masuda, , and C. K. Zarins. Molecular mechanisms of aortic wall remodeling in response to hypertension. *Journal of vascular surgery*, 33:570–578, 2001.

[112] J. Švejcar, I. Přerovskỳ, J. Linhart, and J. Kruml. Content of collagen, elastin, and water in walls of the internal saphenous vein in man. *Circulation research*, 2:296–300, 1962.

[113] A. Kamiya, R. Bukhari, and T. Togawa. Adaptive regulation of wall shear stress optimizing vascular tree function. *Bulletin of mathematical biology*, 46:127–137, 1984.

[114] Abhay B Ramachandra, Jay D Humphrey, and Alison L Marsden. Computational simulation of the adaptive capacity of vein grafts in response to increased pressure. *submitted*.

[115] J. D. Humphrey. Mechanisms of arterial remodeling in hypertension coupled roles of wall shear and intramural stress. *Hypertension*, 52:195–200, 2008.

[116] Peter F Davies. Flow-mediated endothelial mechanotransduction. *Physiological reviews*, 75(3):519–560, 1995.

[117] D. Dajnowiec and B. Langille. Arterial adaptations to chronic changes in haemodynamic function: coupling vasomotor tone to structural remodelling. *Clinical Science*, 113:15–23, 2007.

[118] M. Hwang, S. A. Berceli, M. Garbey, N. H. Kim, and R. Tran-Son-Tay. The dynamics of vein graft remodeling induced by hemodynamic forces: a mathematical model. *Biomechanics and modeling in mechanobiology*, 11:411–423, 2012.

[119] E. P. Kritharis, J. D. Kakisis, A. T. Giagini, T. Manos, N. Stergiopulos, S. Tsangaris, and D. P. Sokolis. Biomechanical, morphological and zero-stress state characterization of jugular vein remodeling in arteriovenous fistulas for hemodialysis. *Biorheology*, 47:297–319, 2010.

[120] Emil Monos and József Csengődy. Does hemodynamic adaptation take place in the vein grafted into an artery? *Pfluegers Archiv*, 384(2):177–182, 1980.

[121] Lowell B Langille. Remodeling of developing and mature arteries: endothelium, smooth muscle, and matrix. *Journal of cardiovascular pharmacology*, 21:S11–S17, 1993.

[122] Jin-Jia Hu, Andy Ambrus, Theresa W Fossum, Matthew W Miller, Jay D Humphrey, and Emily Wilson. Time courses of growth and remodeling of porcine aortic media during hypertension: a quantitative immunohistochemical examination. *Journal of Histochemistry & Cytochemistry*, 56(4):359–370, 2008.

[123] M. S. El-Kurdi, Y. I. Hong, J. J. Stankus, L. Soletti, W. R. Wagner, and D. A. Vorp. Transient elastic support for vein grafts using a constricting microfibrillar polymer wrap. *Biomaterials*, 29:3213–3220, 2008.

[124] I. Karšaj, J Sorić, and J. D. Humphrey. A 3-D framework for arterial growth and remodeling in response to altered hemodynamics. *International journal of engineering science*, 48:1357–1372, 2010.

[125] J. A. G. Rhodin. Architecture of the vessel wall. *Comprehensive Physiology*, pages 1–31, 2011.

[126] F. A. Kudo, A. Muto, S.P. Maloney, J. M. Pimiento, S. Bergaya, T. N. Fitzgerald, T. S. Westvik, J.C. Frattini, C.K. Breuer, C.H. Cha, T. Nishibe, G. Tellides, W. C. Sessa, and A. Dardik. Venous identity is lost but arterial identity is not gained during vein graft adaptation. *Arteriosclerosis*, 27:1562–1571, 2007.

[127] T. F. Lüscher. Vascular biology of coronary bypass grafts. *Current opinion in cardiology*, 6:868–876, 1991.

[128] JD Humphrey, JF Eberth, WW Dye, and RL Gleason. Fundamental role of axial stress in compensatory adaptations by arteries. *Journal of biomechanics*, 42(1):1–8, 2009.

[129] S. Q. Liu, M. M. Moore, and C. Yap. Prevention of mechanical stretch-induced endothelial and smooth muscle cell injury in experimental vein grafts. *Journal of biomechanical engineering*, 122:31–38, 2000.

[130] Weiguang Yang, Frandics P Chan, V Mohan Reddy, Alison L Marsden, and Jeffrey A Feinstein. Flow simulations and validation for the first cohort of

patients undergoing the y-graft fontan procedure. *The Journal of thoracic and cardiovascular surgery*, 149(1):247–255, 2015.

[131] Mahdi Esmaily-Moghadam, Tain-Yen Hsia, Alison L Marsden, and Modeling of Congenital Hearts Alliance (MOCHA) Investigators. The assisted bidirectional glenn: A novel surgical approach for first-stage single-ventricle heart palliation. *The Journal of thoracic and cardiovascular surgery*, 149(3):699–705, 2015.

[132] Rajendra H Mehta, T Bruce Ferguson, Renato D Lopes, Gail E Hafley, Michael J Mack, Nicholas T Kouchoukos, C Michael Gibson, Robert A Harrington, Robert M Califf, Eric D Peterson, and John H. Alexander. Saphenous vein grafts with multiple versus single distal targets in patients undergoing coronary artery bypass surgeryclinical perspective. *Circulation*, 124(3):280–288, 2011.

[133] Jianrong Li, Yongmin Liu, Jun Zheng, Tao Bai, Yuyong Liu, Xiaolong Wang, Ningning Liu, Lijian Cheng, Yu Chen, and Hongjia Zhang. The patency of sequential and individual vein coronary bypass grafts: a systematic review. *The Annals of thoracic surgery*, 92(4):1292–1298, 2011.

[134] Pei Zhang, Angela Huang, Jacopo Ferruzzi, Robert P Mecham, Barry C Starcher, George Tellides, Jay D Humphrey, Frank J Giordano, Laura E Niklason, and William C Sessa. Inhibition of microrna-29 enhances elastin levels in cells haploinsufficient for elastin and in bioengineered vesselsbrief report. *Arteriosclerosis, thrombosis, and vascular biology*, 32(3):756–759, 2012.

[135] V Vijayan, FCT Smith, GD Angelini, RA Bulbulia, and JY Jeremy. External supports and the prevention of neointima formation in vein grafts. *European journal of vascular and endovascular surgery*, 24(1):13–22, 2002.

[136] Anita C Thomas. Animal models for studying vein graft failure and therapeutic interventions. *Current opinion in pharmacology*, 12(2):121–126, 2012.

[137] Thomas Schachner, Günther Laufer, and Johannes Bonatti. In vivo (animal) models of vein graft disease. *European journal of cardio-thoracic surgery*, 30(3):451–463, 2006.

[138] Marco Piola, Francesca Prandi, Nina Bono, Monica Soncini, Eleonora Penza, Marco Agrifoglio, Gianluca Polvani, Maurizio Pesce, and Gianfranco Beniamino Fiore. A compact and automated ex vivo vessel culture system for the pulsatile pressure conditioning of human saphenous veins. *Journal of tissue engineering and regenerative medicine*, 2013.

[139] RD Sayers, S Raptis, M Berce, and JH Miller. Long-term results of femorotibial bypass with vein or polytetrafluoroethylene. *British journal of surgery*, 85(7):934–938, 1998.

[140] Michael Belkin, James Knox, Magruder C Donaldson, John A Mannick, and Anthony D Whittemore. Infrainguinal arterial reconstruction with nonreversed greater saphenous vein. *Journal of vascular surgery*, 24(6):957–962, 1996.

[141] Carrie A Schinstock, Robert C Albright, Amy W Williams, John J Dillon, Eric J Bergstralh, Bernice M Jenson, James T McCarthy, and Karl A Nath. Outcomes of arteriovenous fistula creation after the fistula first initiative. *Clinical Journal of the American Society of Nephrology*, 6(8):1996–2002, 2011.

[142] Prabir Roy-Chaudhury, Burnett S Kelly, Mary Ann Miller, Anita Reaves, Janice Armstrong, Nuwan Nanayakkara, and Sue C Heffelfinger. Venous neointimal hyperplasia in polytetrafluoroethylene dialysis grafts. *Kidney international*, 59(6):2325–2334, 2001.

[143] T. A. Manos, D. P. Sokolis, A. T. Giagini, C. H. Davos, J. D. Kakisis, E. P. Kritharis, N. Stergiopulos, P. E. Karayannacos, and S. Tsangaris. Local hemodynamics and intimal hyperplasia at the venous side of a porcine arteriovenous shunt. *Information Technology in Biomedicine, IEEE Transactions*, 14:681–690, 2010.

[144] Andrii Grytsan, Paul N Watton, and Gerhard A Holzapfel. A thick-walled fluid–solid-growth model of abdominal aortic aneurysm evolution: Application to a patient-specific geometry. *Journal of biomechanical engineering*, 137(3):031008, 2015.

[145] Clifford Truesdell and Walter Noll. The non-linear field theories of mechanics. In *The non-linear field theories of mechanics*, pages 1–579. Springer, 2004.